The Effects of mTOR Inhibition in Ischemic Stroke

UNIVERSITY OF
OXFORD

Anna Maria Schneider

St John's College

A thesis submitted for the degree of

Doctor of Philosophy

May 2022

Abstract

With a global incidence of 9.5 million cases annually and 56 million disability-adjusted life-years, ischemic stroke is the primary cause of adult disability in developed countries. However, the significant successes in stroke trials have been in the field of reperfusion therapies for ischemic stroke, whereas clinical trials focusing on amplifying the brain's intrinsic neuroprotective pathways have so far been unsuccessful for numerous reasons. One neuroprotective target that has been shown to play an essential role in cell death after stroke is the mammalian target of rapamycin complex 1 (mTORC1), a key regulator of the cells' energy supply, which can be modulated pharmacologically through rapamycin and non-pharmacologically through dietary intervention. The overarching aim of this thesis was to investigate the therapeutic potential of mTOR inhibition in ischemia. I found that post-stroke rapamycin treatment improves cerebral perfusion in the hyperacute phase, decreases lesion volume, and improves functional outcomes at three days in a rat model of focal stroke using magnetic resonance imaging. I then showed that rapamycin application after oxygen-glucose deprivation improves the function of pericytes and endothelial cells *in vitro* but does not prevent cell death. Finally, I found that fasting following ischemia might be an alternative strategy to improve stroke outcomes by decreasing inflammation, stabilizing the BBB, and reducing stroke volume. Together, these data highlight the potential of therapeutic options beyond reperfusion therapies and suggest that targeting metabolic regulators such as the mTOR pathway using pharmacology or dietary modulation might be effective adjunct therapy options alongside reperfusion for patients suffering from an ischemic stroke.

Acknowledgments

No words will come to do justice to describe how grateful I am for having had the opportunity to commence this research journey and experience so much professional and personal growth over the last four years. My supervisors, Yvonne Couch and Alastair Buchan, were powerful and brilliant mentors introducing me to the wonderful world of science. They very patiently guided me through this journey (while also navigating our team through the COVID-19 pandemic), encouraging me to pay close attention to detail yet never lose sight of the big picture, skillfully balancing the art of teaching with encouraging my own deep thinking and independent working. Thank you for letting me learn so much from you.

Our cerebral ischemia lab team, with all its precious members, created a welcoming and joyful environment, and I am beyond thankful for having spent time with every one of them. From the bottom of my heart, thank you, Daniel Beard, Paul Holloway, Ain Neuhaus, Gina Hadley, Christina Simoglou Karagli, James Larkin, and James Grist, for letting me work alongside and learn from you. I am also profoundly grateful for the continuous support and generous smiles of Pramodi Majithia and Rachel Teal. It has been a great privilege to work in the Medical Sciences Department, with brilliant and helpful people all around, including colleagues from the research group next door, the laboratory management team, and the team taking such good care of our animals.

With deep gratitude for discovering my deep passion for stroke research and having had the last four years to devote my attention to it, I am beyond excited to take the knowledge, skills, and experiences with me and marry it with my future endeavors in clinical Neurology.

I dedicate this thesis to my parents and Leander Heldring for all their love, support, and unwavering faith in me. This thesis would not have been possible without them.

Table of contents

List of figures

List of tables

List of abbreviations

ACA	Anterior cerebral artery
ACoA	Anterior communicating artery
ADC	Apparent diffusion coefficient
AICA	Anterior inferior cerebellar artery
AIS	Acute ischemic stroke
AJ	Adherens junction
AMP	Adenoside monophosphase
AMPA	Amino methyl isoxazolepropionic acid
AMPK	AMP-activated protein kinase
Ang-1	Angiopoetin-1
ASA	Anterior spinal artery
ATP	Adenosine triphosphate
BA	Basilar artery
BBB	Blood brain barrier
BCA	Bicinchoninic acid
BDNF	Brain-derived neurotrophic factor
BM	Basement membrane
BMEC	Brain microvascular endothelial cell
BSA	Bovine serum albumin
CBF	Cerebral blood flow
CCA	Common carotid artery
CL	Contralateral
CNS	Central nervous system
CRP	C-reactive protein
CT	Computed tomography
CTA	Computed tomography angiography
DAG	Diacylglycerol
DALY	Disability adjusted life year
DAMP	Damage associated molecular pattern

DkS	Donkey serum
DSA	Digital subtraction angiography
DTI	Diffusion tensor imaging
DTT	Dithiothreitol
DWI	Diffusion weighted imaging
ECA	External carotid artery
ECASS	European cooperative acute stroke study
ECM	Extracellular matrix
EDTA	Ethylenediaminetetraacetic acid
EES	Extracellular extravascular space
eNOS	Endothelial nitric oxide synthase
EPI	Echo planar imaging
ESP	Echo spacing
EVT	Endovascular thrombectomy
FCS	Fetal calf serum
FDA	Food and drug administration
fMRI	Functional magnetic resonance imaging
FOV	Field of view
FSEMS	Fast spin echo multi slice
GABA	Gamma aminobutyric acid
GBCA	Gadolinium-based contrast agent
Gd	Gadolinium
GFAP	Glial fibrillary acidic protein
GJ	Gap junction
HBVP	Human brain vascular pericytes
hCMEC	Human cerebral microvascular endothelial cells
HIF	Hypoxia-inducible factor
HRP	Horseradish peroxidase
HT	Hemorrhagic transformation
I/R	Ischemic reperfusion
Iba-1	Ionized calcium binding adaptor molecule 1

ICA	Internal carotid artery
ICAM-1	Intercellular adhesion molecule 1
IGF	Insulin growth factor
IGF-1	Insulin-like growth factor 1
IgG	Immunoglobulin G
IHC	Immunohistochemistry
IL	Ipsilateral
IL1β	Interleukin-1β
IP3	Inositol triphosphate
IVT	Intravenous thrombolysis
LDF	Laser doppler flowmetry
LDH	Lactate dehydrogenase
MCA	Middle cerebral artery
MCAo	Middle cerebral artery occlusion
MLC	Myosin light chain
MLCK	Myosin light chain phosphatase
MMP	Matrix metalloproteinases
MRI	Magnetic resonance imaging
mTOR	Mammalian target of rapamycin
mTORC1	Mammalian target of rapamycin complex 1
mTORC2	Mammalian target of rapamycin complex 2
MW	Molecular weight
N/L ratio	Neutrophil/lymphocyte ratio
NINDS	Neurological disorders and stroke scale
NK cells	Natural killer cells
NMDA	N-methyl-D-aspartate
nNOS	Neuronal nitric oxide synthase
NOX4	NADPH oxidase 4
NVU	Neurovascular unit
OD	Optical density
OGD	Oxygen glucose deprivation

OGD/R	Oxygen glucose deprivation and reperfusion
PICA	Posterior inferior cerebellar artery
p-mTOR	Phosphorylated mammalian target of rapamycin
PBS	Phosphate buffered saline
PCA	Posterior cerebral artery
PCoA	Posterior communicating artery
PDGFR	Platelet-derived growth factor receptor
PDM	Perfusion diffusion mismatch
PET	Positron emission tomography
PFA	Perfluoroalkoxy alkane
PIP2	Phosphoatidylinositol-4,5-biphosphate
PKC	Protein kinase c
pMCAo	Permanent middle cerebral artery occlusion
PPA	Pterygopalatine artery
PVDF	Polyvinylidene difluoride
PWI	Perfusion weighted imaging
RCT	Randomized controlled trial
rhEGF	Recombinant human epidermal growth factor
rhFGF	Recombinant human fibroblast growth factor
RM	Repeated-mesures
ROI	Region of interest
RT	Room temperature
SCA	Superior cerebellar artery
SCD	Small vessel disease
SEM	Standard error of the mean
SHSRP	Stroke-prone spontaneously hypertensive rat
SIRT1	Sirtuin-1
SPECT	Single photon emission computed tomography
T1w	T1-weighted
T2w	T2-weighted
TE	Echo time

TJ	Tight junction
tMCAo	Transient middle cerebral artery occlusion
TNFα	Tumor necrosis factor-α
TR	Repetition time
TSC	Tuberous sclerosis complex
VA	Vertebral artery
VEGF	Vascular endothelial growth factor
WB	Western blotting

Chapter 1: Introduction

1.1 Stroke

1.1.1 History

The history of stroke goes back more than 2,400 years when the father of medicine, Hippocrates, first mentioned "apoplexia", an ancient Greek word ἀποπληξία that means to be struck down by sudden violence (Caplan, 2016, Fields, 1989). Galen (131-201), who is nowadays famous for his theory that attributes disease to a disequilibrium between body humours and secretions, was the first to describe the brain's anatomy and blood vessels based on observations from dissecting animals (Nuland, 1995). Andreas Vesalius (1514-1564) challenged not only Galen's humour theory but also his anatomical descriptions and published his drawings from human dissections in the famous volume *De Humani Corpis Fabrica*, which contained 15 diagrams of the brain that were the most detailed neuroanatomical studies up to that time (Vesalius, 1543). In the 17th century, Johann Jakob Wepfer (1620-1695) and Thomas Willis (1621-1675) significantly contributed to what was known about the anatomy of the brain vasculature and hypothesized on the causes of apoplexy (Tubbs, Mortazavi et al., 2011). To test these hypotheses, Wepfer meticulously performed anatomical dissections on patients who died of a stroke, and he was the first to show that bleeding into the brain was a leading cause of apoplexy (Wepfer, 1658). Thomas Willis, an astute observer, neuroanatomist, and physician, recognized embolism as another leading cause of stroke and described the phenomena of transient ischemic attack (TIA) and the permanent occlusion of the carotid artery (Zimmer, 2005).

After the clinicopathological method (correlating anatomical findings of deceased patients with their symptoms) that was introduced by Giovanni Battista Morgagni (1682-1771) and John Cheyne (1777-1863), John Abercrombie published a detailed classification of apoplexy in 1828,

which also included speculations of etiological mechanisms of stroke such as spasm or rupture of brain vessels. Knowledge about stroke was significantly increased after the publication of four atlases containing drawings of brains and vascular lesions by Hooper, Cruveilher, Carsell, and Bright (Bright, 1827, Cruveilhier, 1829, Hollman, 1995, Hooper, 1828).

During the latter half of the nineteenth century, Rudolf Virchow (1821-1902) disproved the prevailing theory that not inflammation but thrombosis and embolism were the leading causes of brain infarction and described his well-known triad of vascular thrombosis: (1) stasis of blood flow, (2) injury to the vessel wall and (3) hypercoagulability (Caplan, 2016). At the same time, texts by Osler, Gowers, and Wilson described clinical findings and prognosis of many stroke syndromes. This era was also marked by novel detailed anatomical observations of the brain by Düret and Foix (Caplan, 2016).

In the twentieth century, C. Miller Fisher (1913-2012) was a Canadian pathologist and stroke neurologist practicing in Boston whose notable contributions include the identification of TIAs as stroke precursors, detailed descriptions of lacunar strokes, and linking carotid atherosclerosis to stroke. Fisher developed the first stroke fellowship in the US and mentored many now senior stroke neurologists, such as Louis R. Caplan (1936). The last quarter of the twentieth century saw a significant growth of interest in and knowledge about stroke, whereby the predominance of anecdotal cases and sparse data on incidence and frequency of clinical findings were replaced by databases and large registries of well-studied stroke patients. Advances in technology that improved visualization of the anatomy allowed stroke neurologists to cease their reliance on fatal cases for diagnosis, and, importantly, therapeutic trials began to systematically evaluate the safety and effectiveness of treatment options (Caplan, 2016).

1.1.2 Epidemiology

Stroke is defined as interrupted or reduced blood flow to parts of the brain or spinal cord, preventing a sufficient supply of oxygen and nutrients (Sacco, Kasner et al., 2013). In the last 15 years, the treatment of stroke patients has been revolutionized. Yet, despite these advances, stroke with its clinical consequences remains foremost among the leading health issues worldwide. 13.7 million people suffer from a stroke each year, of which 5,5 million die, making it the second leading cause of death in the world (Virani, Alonso et al., 2021). Of those surviving, the years lost due to disability (DALYs) are 116 million (Owens Johnson, Nguyen et al., 2019). 52% of all strokes occur in men, 48% in women and the average median age of a patient suffering from their first stroke is 73 years. Only a fraction of people regain full functional recovery, and stroke survivors are often unable to re-integrate into work. One stroke case costs the US economy roughly $140,084 - accounting for health care costs and loss of workforce - and annual stroke-related expenses are estimated to be $40.1 billion in the US alone (Virani, Alonso et al., 2021).

1.1.3 Diagnosis

The initial presentation of an ischemic stroke event depends on the function of the brain region supplied by the vessel that has been occluded or has ruptured (**Table 1.1**). Clinical examination with neurological testing is essential. In light of many stroke mimics, including blood-glucose disturbances, seizures, and migraines, the mainstay for definite stroke diagnosis is brain imaging (Campbell, De Silva et al., 2019). Computed tomography (CT) imaging, a relatively cheap and readily available imaging modality in the Westernized world, is the most widely used imaging tool for diagnosing stroke and allows for reliable identification of intracranial hemorrhage, which is critical for management decisions (Campbell, De Silva et al., 2019). Alternative imaging modalities to CT that are widely available are CT angiography (CTA) or digital subtraction angiography (DSA), which will provide more insight into the stroke etiology by reproducing an image of the brain vasculature, including atherosclerotic changes or stenosis, for example. Magnetic resonance imaging (MRI) offers multiple sequences that aid in stroke diagnosis and treatment decision making: Diffusion-weighted imaging (DWI) is highly sensitive for displaying the infarcted area within minutes after the onset of occlusion, while T2-weighted MRI is more helpful around 2-3 hours after stroke onset when the injury has become more consolidated, and edema has formed (Campbell, De Silva et al., 2019).

Table 1.1 Signs and symptoms of ischemic stroke based on the occluded vessel. Adapted from Hurford et al. (Hurford, Sekhar et al., 2020).

Vascular territory	**Signs and symptoms**
Internal carotid artery	Combined anterior cerebral artery/middle cerebral artery syndromes; ipsilateral monocular visual loss secondary to transient central retinal artery occlusion (amaurosis fugax); branch retinal artery occlusions may present as ipsilesional altitudinal field cuts.
Anterior cerebral artery	Contralateral leg numbness and weakness, possibly ipsilateral ('sympathetic') or contralateral ideomotor apraxia, (L) transcortical motor aphasia, (R) motor neglect. Occasionally urinary incontinence (medial micturition centre), ipsilateral eye deviation, and paratonic rigidity.
Middle cerebral artery	Superior division (lateral frontal and superior parietal lobes): contralateral face/arm (more than leg) numbness and weakness, contralateral homonymous hemianopia (lower fields), cortical hand syndrome*, ipsilateral gaze preference, [dom] expressive aphasia, [non-dom] contralateral hemispatial neglect, agraphaesthesia, astereognosis. Inferior division (lateral temporal and inferior parietal lobes): contralateral homonymous hemianopia (upper fields), [dom] receptive aphasia, [non-dom] constructional apraxia.
Posterior cerebral artery	Complete or partial contralateral homonymous hemianopia, if midbrain involvement ipsilateral third nerve palsy with mydriasis and contralateral hemiparesis (Weber syndrome), (L with splenium of corpus callosum) alexia without agraphia.
Superior cerebellar artery	Ipsilateral limb and gait ataxia.
Anterior inferior cerebellar artery	Vertigo and ipsilateral deafness, possibly also ipsilateral facial weakness and ataxia.
Vertebral/posterior inferior cerebellar artery	Ipsilateral limb and gait ataxia; if lateral medullary involvement, may have ipsilateral fifth cranial nerve, cerebellar, nucleus ambiguous (hoarseness and dysphagia), vestibular nucleus dysfunction, Horner's syndrome and contralateral hemisensory loss to pain and temperature (Wallenberg syndrome).
Basilar artery	Pontine localisation with impaired lateral gaze, horizontal diplopia and dysconjugate gaze, non-localised hemiparesis, dysarthria; 'locked-in syndrome' with bilateral pontine infarction (intact vertical eye movements, anarthria, quadriplegia).

1.1.4 Treatment

Management decisions are dependent on various factors and include the type of stroke, i.e., ischemic or hemorrhagic, the area affected, the duration since symptom onset, patient age, and co-morbidities, such as hypertension, cancer, and atrial fibrillation (Campbell, De Silva et al., 2019). The two available treatment options, intravenous thrombolysis (IVT) and endovascular thrombectomy (EVT), focus on restoring cerebral blood flow (CBF) to salvageable ischemic brain tissue. The clinical evidence of IVT for acute ischemic stroke (AIS) was derived from randomized controlled trials (RCTs) and pooled analysis of IVT studies (Brott, Broderick et al., 1995, Emberson, Lees et al., 2014, Lees, Emberson et al., 2016). It has been now 25 years since the publication of the first RCT investigating the safety and effectiveness of IVT treatment. Thanks to the National Institute of Neurological Disorders and Stroke (NINDS) recombinant tissue plasminogen activator (rtPA) trial, there was a paradigm shift in the management of ischemic stroke (Brott, Broderick et al., 1995). Before 1995, stroke patients were not considered an emergency in clinical management, and brain imaging was not considered urgent because not even the fundamental differentiation of intracerebral hemorrhage and ischemic stroke would change patient management. The NINDS trial then showed that patients treated with rtPA, compared to those given placebo, were at least 30% more likely to have minimal or no disability at three months (Brott, Broderick et al., 1995).

Hemorrhagic transformation (HT), a threatening side effect of thrombolysis causing severe neurological deterioration, occurred in 6.4% of rtPA-treated patients but only in 0.6% of patients given placebo (Brott, Broderick et al., 1995). HT manifests as a natural progression of AIS due to the breakdown of the blood-brain barrier (BBB) – an anatomical structure that will be discussed in greater detail later in this chapter (see **1.3.3**) - and also as a complication of reperfusion

treatment, with increasing risk with later initiation of therapy after stroke onset (Kaur, Zhao et al., 2004, van Kranendonk, Treurniet et al., 2019, Wang, Tsuji et al., 2004, Yaghi, Willey et al., 2017). Due to advances in the subsequent European Cooperative Acute Stroke Study (ECASS) II trial, the time window of rtPA treatment was expanded from 3 to 4.5 hours (Hacke, Kaste et al., 1998). Ten years later, the time window was further extended to 6 hours with the bridging of IVT and EVT (Goyal, Menon et al., 2016, Warner, Harrington et al., 2019). Despite the great success of IVT, many patients are prevented from receiving the treatment due to delayed patient presentation or other contraindications, such as wake-up strokes, anticoagulant use, recent surgery, or bleeding (Hacke, Kaste et al., 2008). In the US in 2018, only 15.2% of patients presenting with AIS were treated with IVT (Asaithambi, Tong et al., 2020).

EVT is indicated for patients with AIS caused by the occlusion of a large artery in the anterior circulation. As an additional or alternative treatment option to IVT, EVT was first introduced in clinical stroke management in 2014 (Fransen, Beumer et al., 2014). Over time, its safety and effectiveness in treating AIS patients was confirmed to be up to 6 hours since symptom onset (Goyal, Menon et al., 2016) and for some selected patients up to a 16 (Albers, Marks et al., 2018) and, eventually, a 24-hour time window (Nogueira, Jadhav et al., 2018). EVT has been shown to significantly improve functional independence in AIS patients at 90 days, with 49% in the thrombectomy group versus 13% in the control group receiving rtPA medical treatment (Nogueira, Jadhav et al., 2018). Despite its potential, the procedure necessitates an experienced interventionalist, most often in a specialist stroke center. Complications such as vessel perforation, emboli to new territories, and hemorrhage happen rarely but, if they occur, are often fatal (Albers, Marks et al., 2018, Balami, White et al., 2018, Evans, White et al., 2017). Besides recanalization of the occluded vessel, patient management should include stroke unit care, support of respiratory

function and cardiac monitoring, glycemic and temperature control, blood pressure monitoring and control, and additional treatment with antiplatelet medication if indicated (Xian, Holloway et al., 2011).

1.2 Cerebral blood flow and the anatomy of stroke

Stroke can broadly be classified into ischemic and hemorrhagic stroke, whereby the prior constitutes about 87% of all stroke cases (Virani, Alonso et al., 2021). Hemorrhagic stroke can be subdivided into four different types: Subarachnoid, intracerebral, subdural, and epidural. Each of those has a distinct cause and requires a specialized treatment that focuses on resolving the root cause of the problem, such as coiling the aneurysm in cases of subarachnoid hemorrhage or decompression of the skull and careful medical management, including blood pressure control (Caplan, 2016). Subarachnoid hemorrhage is blood leakage from the vasculature into the subarachnoid space and is caused by arterial aneurysms, arteriovenous malformations, bleeding diathesis, or trauma of which the latter two are less common (Caplan, 2016). In a primary intracerebral hemorrhage, there is blood leakage from the small arterioles most often damaged by long-standing hypertension. Conversely, subdural and epidural hemorrhages most often occur due to trauma, whereby subdural hemorrhages arise from injured veins located between the dura and arachnoid mater, and epidural hemorrhages are caused by tears in the middle meningeal artery (Caplan, 2016).

The etiology of ischemic stroke, on the other hand, can be narrowed down to arterial, cardiac, thrombotic, and thrombophilic causes. The arterial cause of stroke is most often due to arteriosclerosis (Greek for “hardened artery”), of which the most common form is the buildup of an atherosclerotic plaque, consisting of lipid, fibrous, and collagen tissue, smooth muscle, macrophages, and other inflammatory cells (Campbell, De Silva et al., 2019), whereby the modifiable risk factors associated with the incidence are hypertension, elevated cholesterol and triglycerides, smoking, diabetes mellitus, obesity and long-standing inflammatory diseases (Boehme, Toell et al., 2019, Kuriakose and Xiao, 2020).

When the plaque has reached a critical size, it alters the mechanical properties of blood flow, creating turbulences and stasis. Platelets adhere to the irregular plaque surface and secrete chemical mediators from the platelets and the endothelium, which further increase the size of the plaque to which more platelets adhere – forming a "white thrombus" (Campbell, De Silva et al., 2019). Damaging of the endothelium by the plaque leads to its exposure to the blood, thereby activating the coagulation cascade and forming a "red thrombus". Thrombi occluding the atherosclerotic vessel may break off and embolize distally. Bifurcation sites at the ICA are the most common location in the Western population for embolic occlusion. Lower shear stresses at those sites favor intimal thickening and reduced nitric oxide release that are thought to promote the formation of cholesterol plaque formation (Campbell, De Silva et al., 2019). Besides atherosclerosis, other arterial causes of ischemic stroke are vasoconstriction, cerebral vasculitis, and small vessel diseases (SVD).

The most common cause of ischemic stroke that is of cardiac origin is atrial fibrillation, whereby the arrhythmic movement of the left atrium can lead to parts of the blood stagnating, increasing the risk of cardioembolic ischemic stroke (Campbell, De Silva et al., 2019). The most common risk factors include advanced age, obesity, hypertension, diabetes mellitus, excessive alcohol consumption, and obstructive sleep apnea (Campbell, De Silva et al., 2019). Another cardiac cause of cerebral ischemia is a hypokinetic segment of the heart following a cardiac arrest that, similar to atrial fibrillation, can lead to disordered blood flow and coagulation. When the foramen ovale, which in utero allows the flow of oxygenated placental blood from the right to the left atrium, fails to close after birth (patent foramen ovale), a paradoxical embolus can cause an ischemic stroke. Another cause of ischemic stroke can be bacterial endocarditis, which complicates stroke treatment because it is associated with an increased risk of hemorrhagic transformation after

thrombolysis. Hematological disorders, including essential thrombocytosis, polycythemia vera, and antiphospholipid syndrome, are also significant contributors to the ischemic stroke population. These disorders can also cause venous rather than arterial cerebral obstruction (Campbell, De Silva et al., 2019).

One of the main determinants affecting tissue survival is the extent to which collateral blood flow in the leptomeningeal and pial anastomoses and the Circle of Willis can accommodate and supply the penumbral region around the core area of the infarct (Campbell, De Silva et al., 2019) (**Figure 1.1**). The factors influencing the collateral flow and capacity can vary substantially between and even within one individual over time and are thought to be influenced by genetic and environmental factors (Bang, Goyal et al., 2015). Tissue that receives blood supply from most distal branches of two arteries with minimal collateral vascularity (Momjian-Mayor and Baron, 2005) are called "watershed areas". These areas are especially susceptible to ischemia from hypoperfusion, which can cause ischemic stroke that is not due to a complete vessel obstruction but rather hypoperfusion or hypoxemia because of cardiovascular surgery, for example (Momjian-Mayor and Baron, 2005). Two watershed areas within the brain are differentiated: Cortical, which occur at the junction between territories of the ACA, MCA, and PCA, respectively; and internal, which appear in the white matter between the deep and superficial perfusion systems of the MCA (Juergenson, Mazzucco et al., 2011). Augmenting the function of collateral vessels as an adjunct treatment for stroke is an attractive target of research, and inhaled nitric oxide and high-dose albumin are two agents that may hold promise as promotors of the collateral supply (Bang, Goyal et al., 2015, Ginsberg, 2018).

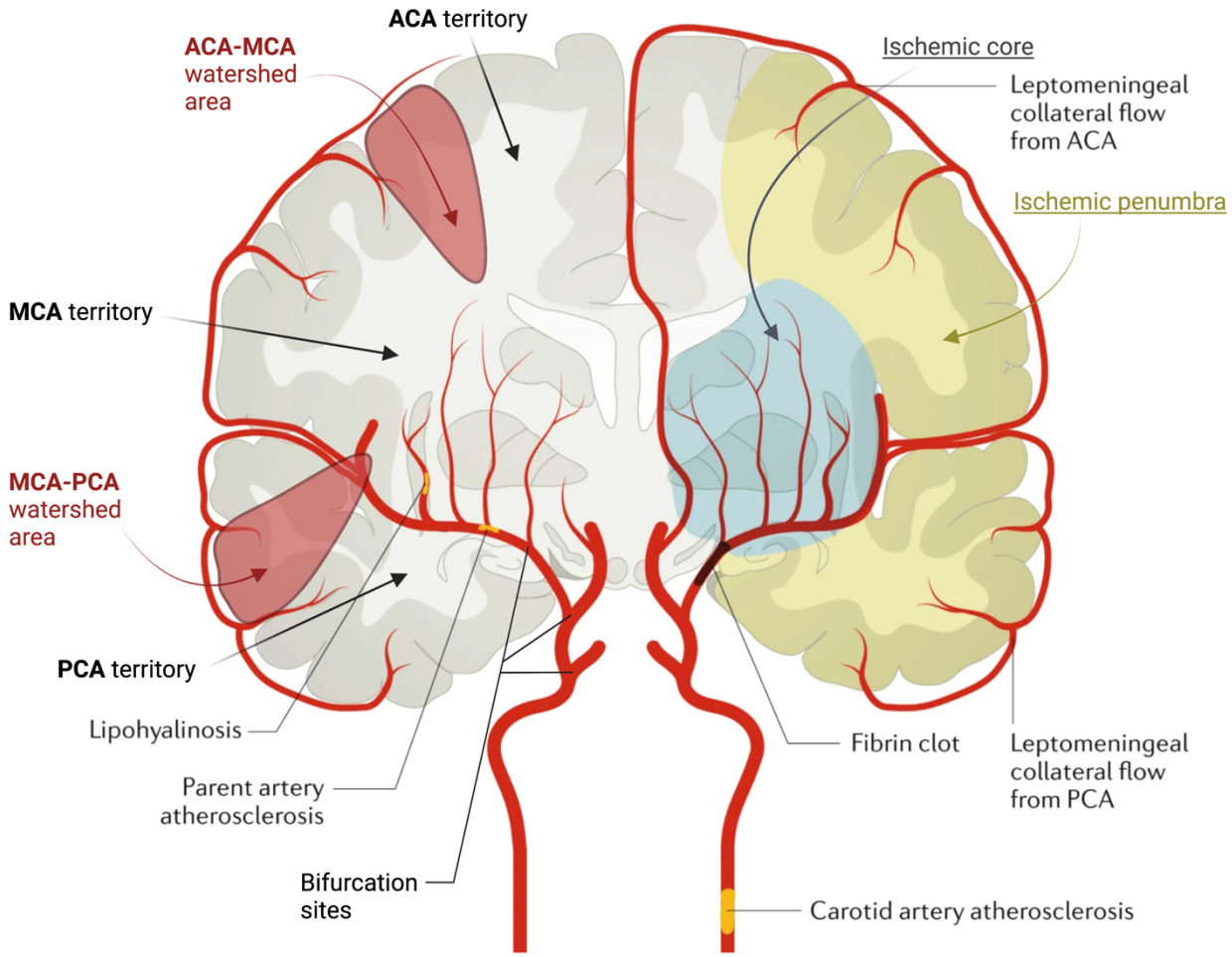

Figure 1.1 Coronal view of the brain illustrating a fibrin clot occluding the middle cerebral artery. While the ischemic core is irreversibly injured, leptomeningeal anastomoses provide some retrograde blood supply to the surrounding tissue that is at risk of dying but still salvageable. ACA-MCA and MCA-PCA watershed areas are especially susceptible to reduced blood flow due to limited collateral vascularity. Adapted from Campbell et al. (Campbell, De Silva et al., 2019) using BioRender.com.

1.2.1 Preclinical models to study stroke and treatment

Most *in vivo* studies are carried out in rodents because of their relative similarity to human cerebrovascular anatomy and physiology and comparable sensorimotor deficiencies due to brain infarction (**Figure 1.2**). But also practical considerations, such as low cost, and the small size of the rodents facilitating the easy monitoring of physiological parameters, play into the decision on which model to choose to conduct reproducible studies (Durukan and Tatlisumak, 2007). Nevertheless, when studying ischemic stroke in living organisms, it is essential to acknowledge the discrepancies between the anatomy and pathophysiology between rodents and humans. Variables that should be considered when choosing the most suitable study design include the potential influence of age, sex, and comorbidities on stroke outcome, the anatomical and functional organization of the brain, including its vasculature, as well as genetic and epigenetic variations, and the immunological profile (Macrae, 2011). Global ischemia models allow insight into the selective vulnerability and resistance of different brain regions. Still, they don't resemble ischemic stroke in humans but rather a neurological injury after resuscitation following cardiac arrest (Macrae, 2011). Focal ischemia models involve the occlusion of one of the major cerebral arteries, most commonly the MCA, using mechanical means, thrombi, or vasoconstrictors and are more representative of human stroke but remain imperfect (**Table 1.2**) (Macrae, 2011, Neuhaus, Rabie et al., 2014, Sutherland, Neuhaus et al., 2016).

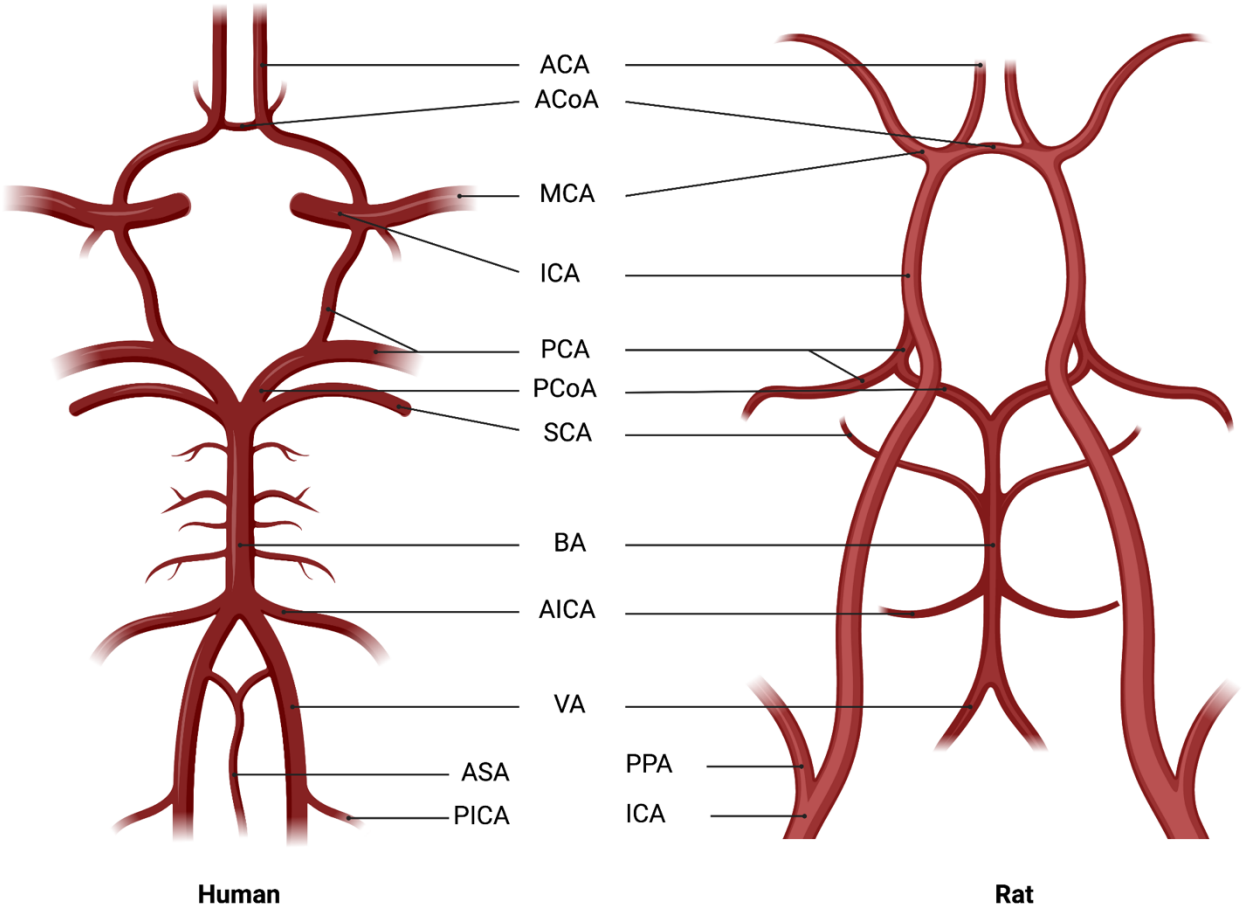

Figure 1.2 Anatomy of the circle of Willis comparing human and rat. Abbreviations: ACA: anterior cerebral artery; AcoA: anterior communicating artery; MCA: middle cerebral artery; ICA: internal carotid artery; PCA: posterior cerebral artery; PCoA: posterior communicating artery; SCA: superior cerebellar artery; BA: basilar artery; AICA: anterior inferior cerebellar artery; VA: vertebral artery; ASA: anterior spinal artery; PICA: posterior inferior cerebellar artery; PPA: pterygopalatine artery. Adapter from Farkas et al. (Farkas and Luiten, 2001) using BioRender.com.

Table 1.2 Description of the most used stroke models, their main advantages and disadvantages (adapted from Macrae) (Macrae, 2011).

Stroke model	**Description**	**Advantage**	**Disadvantage**
MCAo ligation	Electrocoagulation and permanent occlusion of a cerebral artery	Selection of exact lesion location, good reproducibility, visual confirmation of occlusion	Requires craniectomy, technically challenging, not suitable for thrombolysis studies
MCAo filament model	Coated or uncoated filament with silicone tip inserted into the MCA	Selection of location and duration of vessel occlusion, good reproducibility, retraction of the filament similar to EVT	Requires surgery, not suitable for thrombolysis studies
Pharmacological vasoconstriction (Endothelin-1)	Topical or intraparenchymal application of vasoconstricting agent that exerts its effect in a dose-dependent manner	Straightforward surgery, good reproducibility, some control over severity and duration of infarct by adjusting concentration, modifications of the intraparenchymal model allow ischemia induction in conscious rat	Topical application requires craniectomy, not suitable for thrombolysis studies
Photothrombosis	Systemic injection of a photosensitive dye (Rose Bengal or erythrosine B) and irradiation through the exposed skull with light of a specific wavelength induces thromboembolism	Good reproducibility of infarcted area and lesion size, no craniectomy needed	Photocoagulation severely damages the affected blood vessel causing early edema formation uncharacteristic in human stroke
Thromboembolism (autologous blood clot or intravascular thrombin injection)	Intraarterial injection of autologous blood clot or thrombin	Closest to clinical stroke, suitable for studies investigating thrombolysis agents	High variability over infarct size and location, secondary clot formation possible

Mechanical occlusion of the MCA produces a profound and rapid drop in CBF. The models that are producing not a permanent (electrocoagulation or permanent MCA occlusion using the filament model) but rather transient blood vessel occlusion most often include rapid reperfusion, which is usually followed by a phase of hyperperfusion where the blood flow is higher than before baseline (Sutherland, Neuhaus et al., 2016). Embolic stroke models also occlude the vessels rapidly, but the reperfusion occurs more gradually without a hyperperfusion phase (Macrae, 2011). While MCA occlusion (MCAo) models can be helpful in mimicking EVT, using thromboembolism for vessel occlusion can be beneficial in simulating reperfusion through thrombolysis therapy (Macrae, 2011). What should be of further consideration is that the rapid reperfusion and eventual hyperperfusion phase induced by recanalization of the MCA occluded with a filament leads to increased production of free radicals that damage the ischemic and surrounding tissue (Sutherland, Neuhaus et al., 2016). This secondary damage is accompanied by an increased inflammatory response, breakdown of the BBB, and an increased risk of hemorrhagic transformation and edema formation (Sutherland, Neuhaus et al., 2016). While the location of the ischemia can be relatively well controlled with the filament model, lesion size can vary quite considerably from animal to animal, mainly depending on the presence of collateral circulation (Macrae, 2011). In summary, the appropriateness of choosing one research model over another is based on considering the advantages and disadvantages of the different models and the resources available to the researcher.

1.3 The cellular and molecular effects of ischemic stroke and neuroprotective targets

1.3.1 Ischemic cascade

In ischemic stroke, the undersupply of blood leads to oxygen depletion that has substantial consequences for all cells present in the brain - neuronal, glial, and vascular (Daniele, Trummer et al., 2021). In neurons, ATP production that relies on oxygen and glucose supply decreases, which interrupts the transmembrane gradient, ultimately impairing neuronal signaling. Further, failure of the Na^+/Ca^{2+} pump increases intracellular Ca^{2+} that, in turn, releases increased levels of glutamate. Large quantities of this excitatory neurotransmitter cause excessive depolarization, and due to failed re-uptake from the synaptic cleft, its effect is sustained for even longer than normal. N-methyl-D-aspartate (NMDA) receptors are activated by excessive depolarization, leading to substantially higher conductance of Ca^{2+} ions under ischemic conditions. The subsequent increase in calcium influx and secondary release of intracellular calcium leads to the activation of calcium-dependent processes such as neuronal nitric oxide synthase (nNOS) activation and free radical production and the initiation of cell-death processes (**Figure 1.3**). As energy demands, which are measured by the AMP:ATP ratio, can no longer be sustained by aerobic glycolysis, the energy supply switches to anaerobic glycolysis, which is 15 times less efficient and produces lactic acid as a side product, that may further damage normal cellular functioning (Campbell, De Silva et al., 2019).

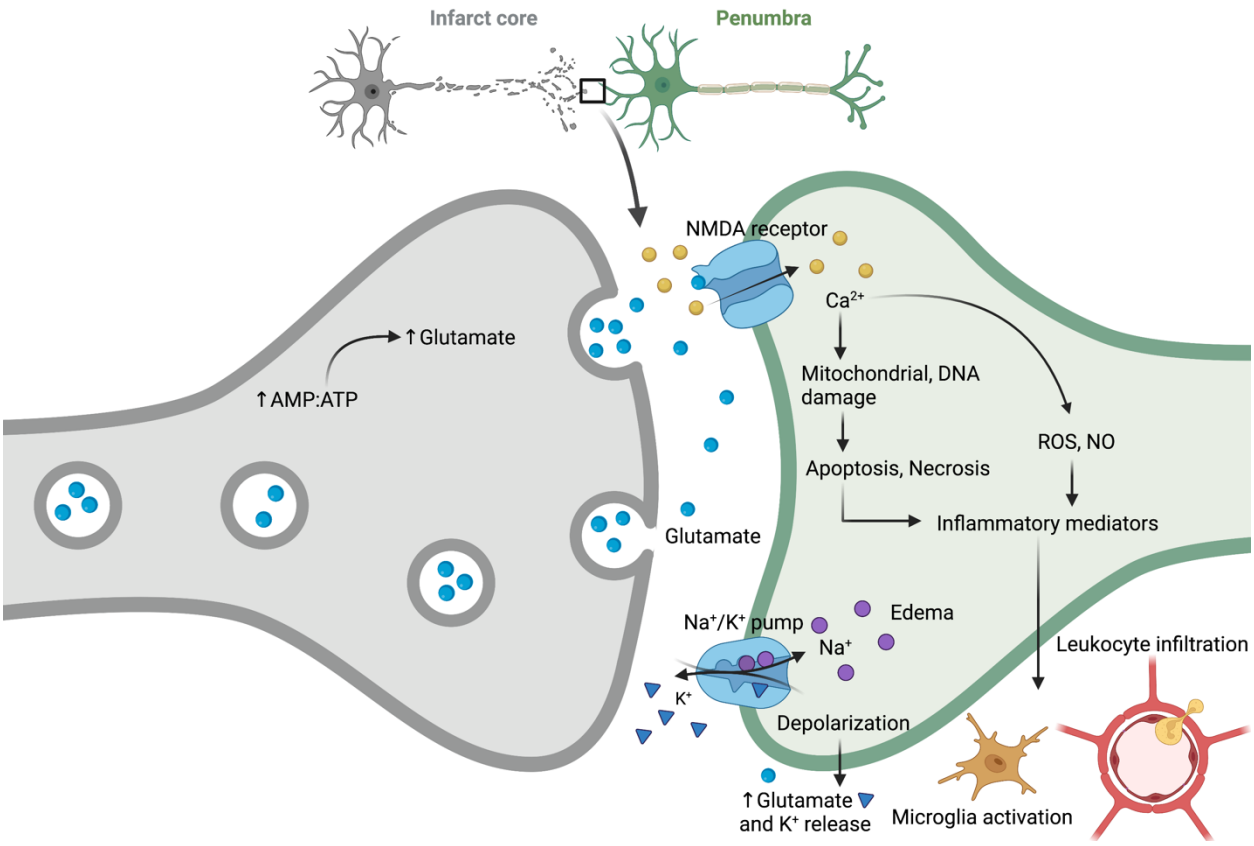

Figure 1.3 Main events of the ischemic cascade in the acute phase of stroke. Ischemic stroke is caused by the occlusion of a vessel supplying the brain. The undersupply of oxygen and nutrients reduces ATP production, which leads to loss of membrane potential and glutamate release into the synaptic cleft. This triggers the ischemic cascade in the neighboring penumbral neurons, which are not yet infarcted but at risk of dying. Increased levels of glutamate increase Ca^{2+} influx through NMDA receptors, and high intracellular levels of Na^{+} and extracellular increase of K^{+} through the impaired function of the Na^{+}/K^{+} pump. High intracellular Ca^{2+} levels induce the release of reactive oxygen species and nitric oxide. Increased Ca^{2+} levels also damage mitochondria and DNA, leading to apoptosis and necrosis. Both events signal to inflammatory mediators, which induce microglial activation and leukocyte infiltration into the brain. Increased intracellular Na^{+} levels bind water, lead to cytotoxic edema, and reinforce depolarization of the peri-infarct region through increased glutamate and K^{+} release. Created with BioRender.com.

Low oxygen levels impair the active transport of Na^+ in the extracellular space by the Na^+/K^+ ATPase pump, which results in increased water influx and subsequent cytotoxic edema. Through oxidative stress, inflammatory reactions, and the release of permeability factors such as matrix metalloproteinases (MMPs), endothelial cells lose their structural integrity and cause the BBB to become hyperpermeable, which occurs as early as 4 to 6 hours after the initial insult (Nian, Harding et al., 2020) (**Figure 1.4**).

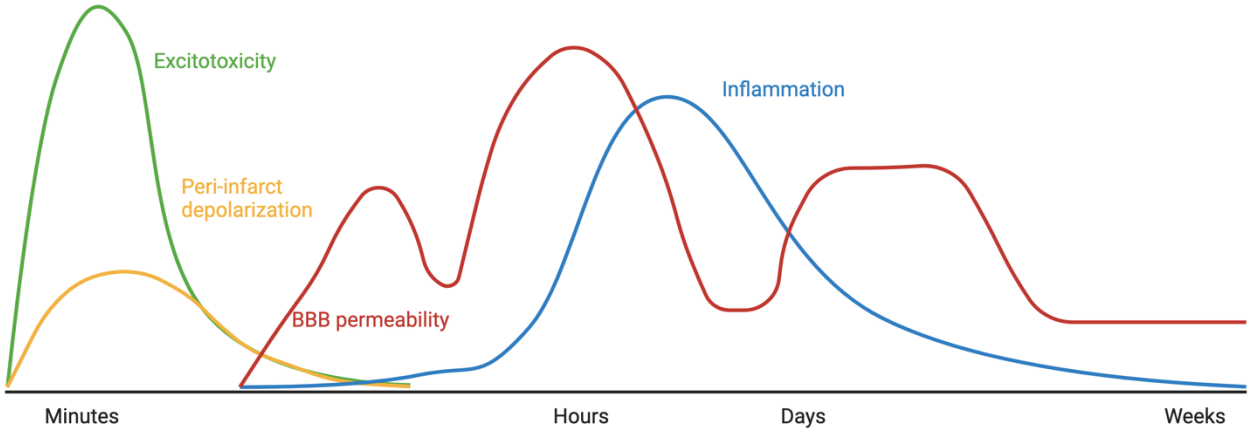

Figure 1.4 Diagram of the temporal course of the development of ischemic damage. Minutes after the onset of the perfusion deficit, excitotoxic mechanisms lead to lethal damage to brain cells. Peri-infarct depolarization contributes to the cellular damage caused in the hyperacute phase of injury. Hours after the initial event, resident immune cells called microglia become active. Soon after, systemic immune cells increase in number and infiltrate into the brain parenchyma, exacerbating the damage to the BBB. Adapted from Dirnagl et al. (Dirnagl, Iadecola et al., 1999) using BioRender.com.

The hyperpermeable BBB facilitates the escape of fluid and intravascular proteins, such as albumin, immunoglobulin-G, and synthetic compounds such as dextran, into the cerebral parenchyma, which results in vasogenic edema - an excessive accumulation of fluid that leads to increased brain volume and pressure (Michinaga and Koyama, 2015). While the previously described cytotoxic edema is an acute reaction to cellular disruptions in ionic homeostasis, vasogenic edema occurs after a slight delay, in the subacute state of disease, between days 1 and 2 in humans (Liebeskind, Jüttler et al., 2019). Edema formation as part of the ischemic cascade following the initial insult influences disease progression and therapeutic agents that target edema formation have shown promise in animal models, and some are currently under evaluation in clinical trials (Yao, Zhang et al., 2020).

Therapies aiming to improve tissue survival and overall stroke outcome, on top of reperfusion of the occluded vessel, include targeting the ischemic cascade by, for example, reducing excitotoxicity or impairing free radical production. Animal models studying treatment options to prevent calcium influx with agents such as nimodipine and agents blocking NMDA or AMPA receptors have produced only suboptimal results. And the positive results observed have been attributed to coincidental physiological rather than pharmacological protection (Hill, Goyal et al., 2020). The non-competitive NMDA-receptor antagonist MK-801, for example, was thought to be protective largely through enhancement of intra-ischemic regional blood flow rather than via a reduction of excitotoxicity. Some studies even suggest NMDA-R antagonists may have neurotoxic effects through inhibition of GABA and subsequent glutamate overactivity (Buchan and Pulsinelli, 1990, Buchan, Slivka et al., 1992). Similarly, the free radical-trapping agent NXY-059 was tested in a series of clinical studies aiming to reduce a different aspect of the ischemic cascade, but the confirmatory SAINT-2 trial was terminated early based on the futility analysis

(Lees, Zivin et al., 2006, Lyden, Shuaib et al., 2007, Shuaib, Lees et al., 2007). It has been suggested that this may be due to the inherent poor translational pipeline between pre-clinical animal work and clinical trials, with some pre-clinical work demonstrating poor uptake of NXY-059 by the BBB. These failures in translation indicate the need for improved communication between clinical and pre-clinical teams in order to facilitate new therapies (Antonic, Dottori et al., 2018, Neuhaus, Couch et al., 2017).

1.3.2 Post-ischemic inflammation

The damaged tissue within the core of the ischemic injury releases pro-inflammatory mediators such as cytokines, chemokines, damage-associated molecular patterns (DAMPs), and ROS (**Figure 1.5**). Subsequent activation of resident immune cells, mostly microglia and to a lesser extent astrocytes and endothelial cells (Jin, Yang et al., 2010, Roh and Sohn, 2018), marks the first line of the inflammatory response to ischemic injury. Inflammatory mediators increase the expression of adhesion molecules on endothelial cells (ICAM-1, E-/P-selectin) and on leukocytes (Mac-1, LFA-1, L-selectin, PSGL-1), thereby facilitating the adhesion and entry of circulating immune cells to the site of injury by alternating the tight junctions of endothelial cells and transmigration through the BBB (Frijns and Kappelle, 2002). Neutrophils, monocytes, and T-cells reaching the site of injury amplify the inflammatory response by releasing more cytokines and chemokines, in particular NADPH oxidates, myeloperoxidases (MPOs), and MMPs (most importantly MMP-9) (Jin, Yang et al., 2010). This self-perpetuating cycle of immune cell signaling and recruitment leads to an excessive inflammatory reaction that damages the surrounding tissue and aggravates cells in the ischemic penumbra. This leads to loss of endothelial tight junction integrity, breakdown of the BBB with subsequent vasogenic edema formation, eventual hemorrhagic transformation (HT), and ultimately, increased neuronal death (Jin, Yang et al., 2010).

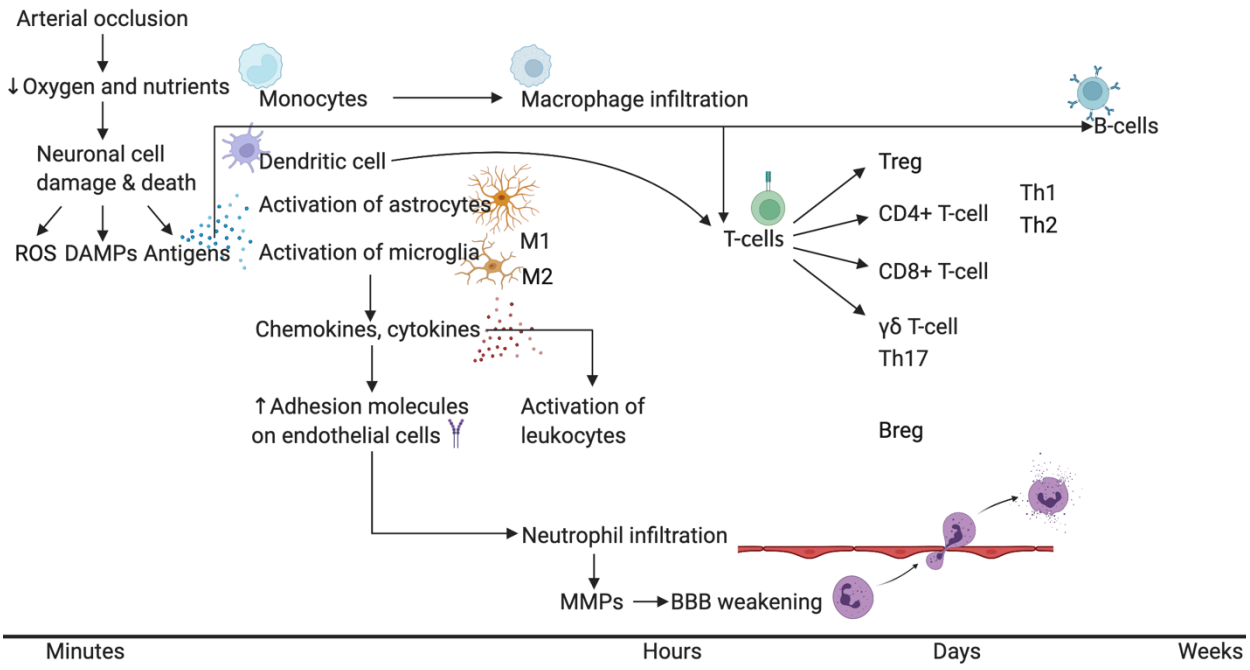

Figure 1.5 Post-ischemic immune response. Due to arterial occlusion, reduced oxygen and nutrient availability leads to neuronal cell damage and death, which secrete reactive oxygen species (ROS), damage-associated molecular patterns (DAMPs), and antigens initiating post-ischemic inflammation as outlined above. Created with Biorender.

Despite the harmful effects of the post-ischemic inflammatory response, inflammation also has several positive effects on cellular rehabilitation, depending on when it occurs after the ischemic insult. Resident microglia, in particular, have been found to have neurotrophic effects supporting brain regeneration and neurovascular remodeling in later stages of the ischemia-reperfusion (I/R) injury (Szalay, Martinecz et al., 2016). Even controlled systemic immune cell infiltration has been described to positively affect tissue regeneration if the post-ischemic immune reaction can be avoided (Iadecola, Buckwalter et al., 2020). For example, blocking adhesion molecules to decrease the infiltration of systemic immune cells successfully improved outcomes in experimental stroke models but failed to show an effect in clinical trials (Yilmaz and Granger, 2008). Recent immunomodulatory therapies for stroke patients are, therefore, not aiming to simply

reduce the inflammation altogether but rather by recognizing the time course by which the different immune cells are activated in response to ischemic injury, modulating the cellular response in such a way that the positive effects are maintained while the negative are halted (Qiu, Zhang et al., 2021).

1.3.3 Blood-brain barrier breakdown in stroke

The BBB, which is composed of endothelial cells, the basal lamina, pericytes, and astrocyte foot processes (del Zoppo, 2010), creates a uniquely dynamic boundary between blood vessels and brain parenchyma – thereby limiting and regulating the exchange of molecules, ions, and cells **(Figure 1.6)**. It can also be seen as a filter that permits the selective exchange of molecules between the different compartments and is involved in controlling CBF, angiogenesis, and neuronal development. Brain microvascular endothelial cells (BMECs) are different from endothelial cells outside the brain (Navaratna, Fan et al., 2013). They have higher numbers of mitochondria to meet the increased energy demand for maintaining BBB integrity and controlling the selective permeability across the barrier (Navaratna, Fan et al., 2013). Further, they possess receptors, ion channels, and surface proteins, alongside a negative charge and low levels of leukocyte adhesion molecules on their apical surface to strictly regulate paracellular transport through their junctional complexes. These comprise tight junctions (TJs), adherens junctions (AJs), and GAP junctions (GJs). TJs, composed of claudins, occludins, and junctional adhesion molecules, limit the permeability of polar solutes and the passage of lipids and proteins (Stamatovic, Johnson et al., 2016). AJs, made up of cadherins and catenins, and GJs, made up of connexins, are primarily responsible for structural support and intercellular communication, respectively (Stamatovic, Johnson et al., 2016).

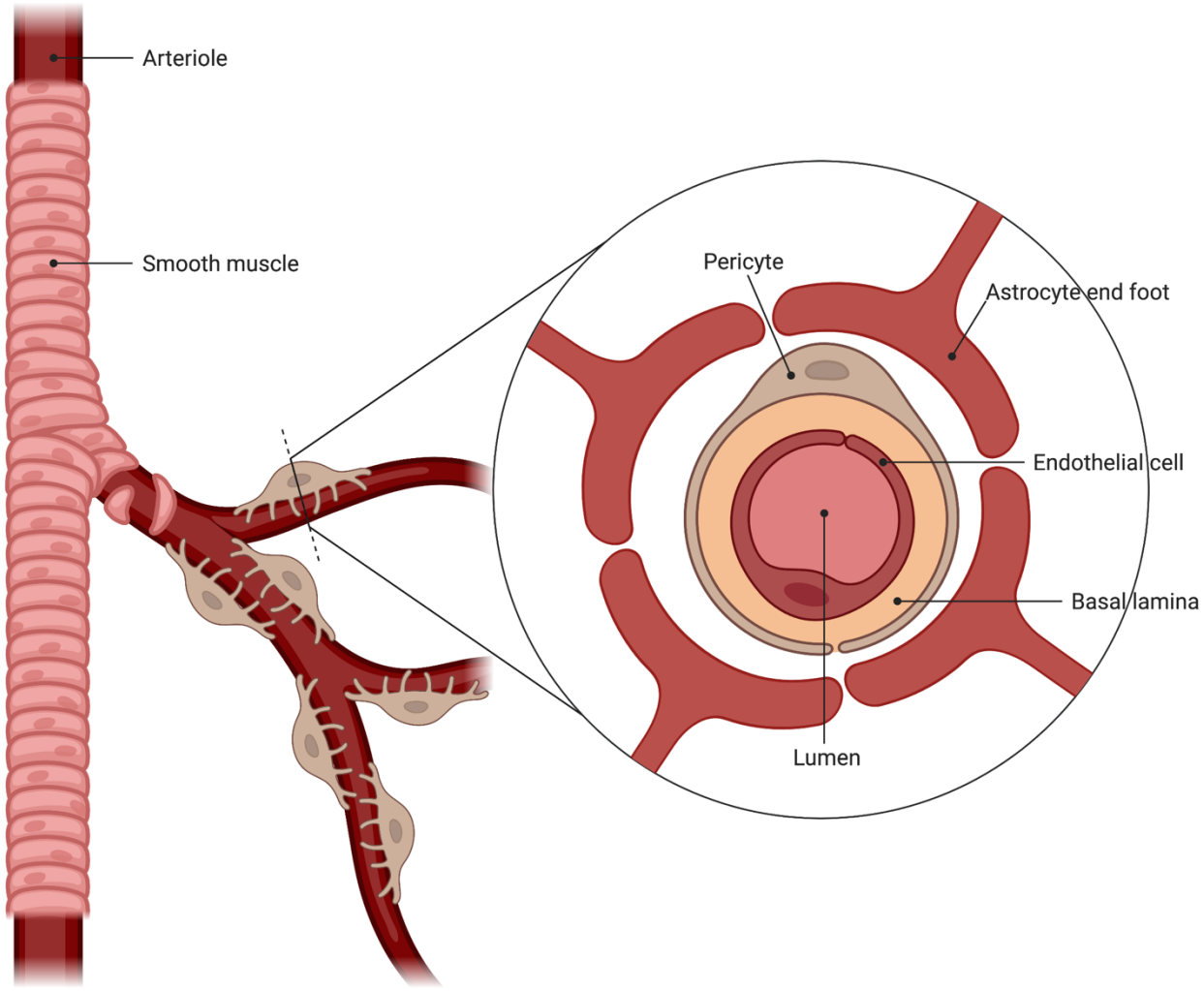

Figure 1.6 Schematic illustration of the BBB and its main components. The BBB, which is composed of endothelial cells, the basal lamina, pericytes, and astrocyte foot processes, creates a uniquely dynamic boundary between blood vessels and brain parenchyma – thereby limiting and regulating the exchange of molecules, ions, and cells. Created with BioRender.com.

Transport across the BBB can broadly be classified into paracellular and transcellular, whereby the former delineates passive diffusion of molecules through TJs, and the latter is most often an active process. Transcellular transport involves receptor-mediated transcytosis, active efflux, adsorptive mediated transcytosis, and carrier-mediated transit that can sometimes also be a passive transcellular process (Bernardo-Castro, Sousa et al., 2020, Stamatovic, Johnson et al., 2016).

The cells of the BBB each have distinct roles within the unit. Pericytes are smooth muscle cells that are wrapped around the outside of the capillaries and help regulate CBF, maintain the BBB, control angiogenesis and vascular development (Dalkara, 2019, Dalkara, Alarcon-Martinez et al., 2019). Astrocytes, making up 20-40% of all glial cells, support the cellular components of the BBB metabolically by the provision of energy substrates such as glutamate and by regulating the extracellular ionic environment (Liu and Chopp, 2016). The basement membrane (BM), which is comprised of extracellular matrix, collagen type IV, laminin, heparin sulfate, and proteoglycans, anchors the other cellular components onto itself and provides stability within the network (Xu, Nirwane et al., 2019). Disruption of the BBB due to ischemic stroke is a dynamic process mediated by the effect of pathophysiological events on different cell types of the BBB at different time points from hours to weeks after the initial insult (Arba, Rinaldi et al., 2020).

While the dynamics of the BBB were traditionally thought to be biphasic, with two "open" periods in between a closed one, recent studies have suggested that it is more a continuous opening of the BBB with the two above mentioned events, the hyperacute hypoxic damage, and the subacute inflammatory response, creating two peaks in the permeability of the barrier without completely closing in between (Bernardo-Castro, Sousa et al., 2020) (**Figure 1.4**). The permeability of the BBB initially dramatically increases within the first hours after the onset of

ischemia. After 72 to 96 hours, a secondary rise in BBB permeability delineates the effects of the inflammatory reaction which damages the protective barrier (Arba, Rinaldi et al., 2020).

One main target in stroke therapy research is to reduce the excessive primary opening of the BBB in the hyperacute stage of the disease, which can be achieved by upregulating endogenous protective mechanisms. For example, the transmembrane protein CD151 functions to maintain vascular stability and as shown by a preclinical trial, upregulation in the early phases of the stroke was able to preserve BBB integrity (Xu, Gao et al., 2021). Reducing damaging compounds that are released in the ischemic process is another way to combat BBB permeability (Lakhan, Kirchgessner et al., 2013). For example, inhibition of MMPs in the early stages of diseases has been shown to ameliorate BBB breakdown and reduce the rate of HT (Lakhan, Kirchgessner et al., 2013), and the antibiotic minocycline has been used to reduce the cytotoxic M1 phenotype of microglia, both of these processes are known to induce BBB damage. (Lees, Zivin et al., 2006, Lyden, Shuaib et al., 2007, Yang, Huang et al., 2019).

1.4 mTOR and the metabolic effects of stroke

BBB breakdown is one of the major targets of novel neuroprotective therapies. However, neuroprotection as a potential treatment for ischemic stroke carries a long and disappointing history and has many explanations that encompass both problems with the preclinical assessment of these drugs and the design and implementation of clinical trials (Chamorro, Lo et al., 2021, Lyden, 2021). Stroke is associated with a broad range of changes in cellular metabolism. The core area of dead tissue is surrounded by a potentially viable penumbra, where metabolism is reduced, and low oxygen levels within this region prohibit oxidative metabolism and ensure that any remaining glucose is metabolized via glycolysis in all cells of the NVU (Campbell, De Silva et al., 2019, Savitz, Baron et al., 2017, Tymianski, 2017). Beyond cellular energetics in the hyperacute phase, metabolic changes are also key to longer-term responses, such as post-ischemic activation of immune cells (Campbell, De Silva et al., 2019).

To date, we have an incomplete understanding of how these metabolic changes differ between cell types of the NVU and how this affects recovery and injury resolution, and it is becoming increasingly clear that targeting only neurons in ischemic stroke is insufficient considering the widespread multicellular dysfunction (del Zoppo and Hallenbeck, 2000, Lo, Dalkara et al., 2003). By investigating and targeting a ubiquitous pathway expressed in several different cell types, we may be able to abrogate the effects of ischemia more effectively on many different cell populations. One such possibility is the serine-threonine kinase mTOR, which integrates information about cellular energy levels and translates it into downstream actions of either cellular proliferation or breakdown, depending on whether energy levels are high or low, respectively (Liu and Sabatini, 2020). There is substantial evidence that the regulation of mTOR

activity is crucial to cellular health during periods of ischemia, and as such, targeting it remains a promising avenue for novel neuroprotective agents (Papadakis, Hadley et al., 2013).

1.4.1 Structure and function of mTOR

In 1964, a team of researchers found a macrolide molecule with potential antifungal activity in a soil sample they took from the Island of Rapa Nui (Easter Island) (Laplante and Sabatini, 2009). Subsequent investigations associated "rapamycin" with antiproliferative, immunosuppressive, and neuroprotective functions, but it was not until 1990 when Schreiber and colleagues found rapamycin exhibited those effects when bound to the prolyl-isomerase FKBP-12 (Laplante and Sabatini, 2009). In 1994, it was discovered that rapamycin caused its effect by binding to the 289kDa serine-threonine kinase, which was called the mammalian target of rapamycin, mTOR. mTOR's function has extensively been studied since then and has gained recognition as the node in a network of complex functions that center around cell growth and metabolism (Laplante and Sabatini, 2009). Its regulation of cellular processes during periods of cellular austerity also makes it an integral mechanism by which all cells might cope with extrinsic stressors, such as ischemia (Liu and Sabatini, 2020) (**Figure 1.7**).

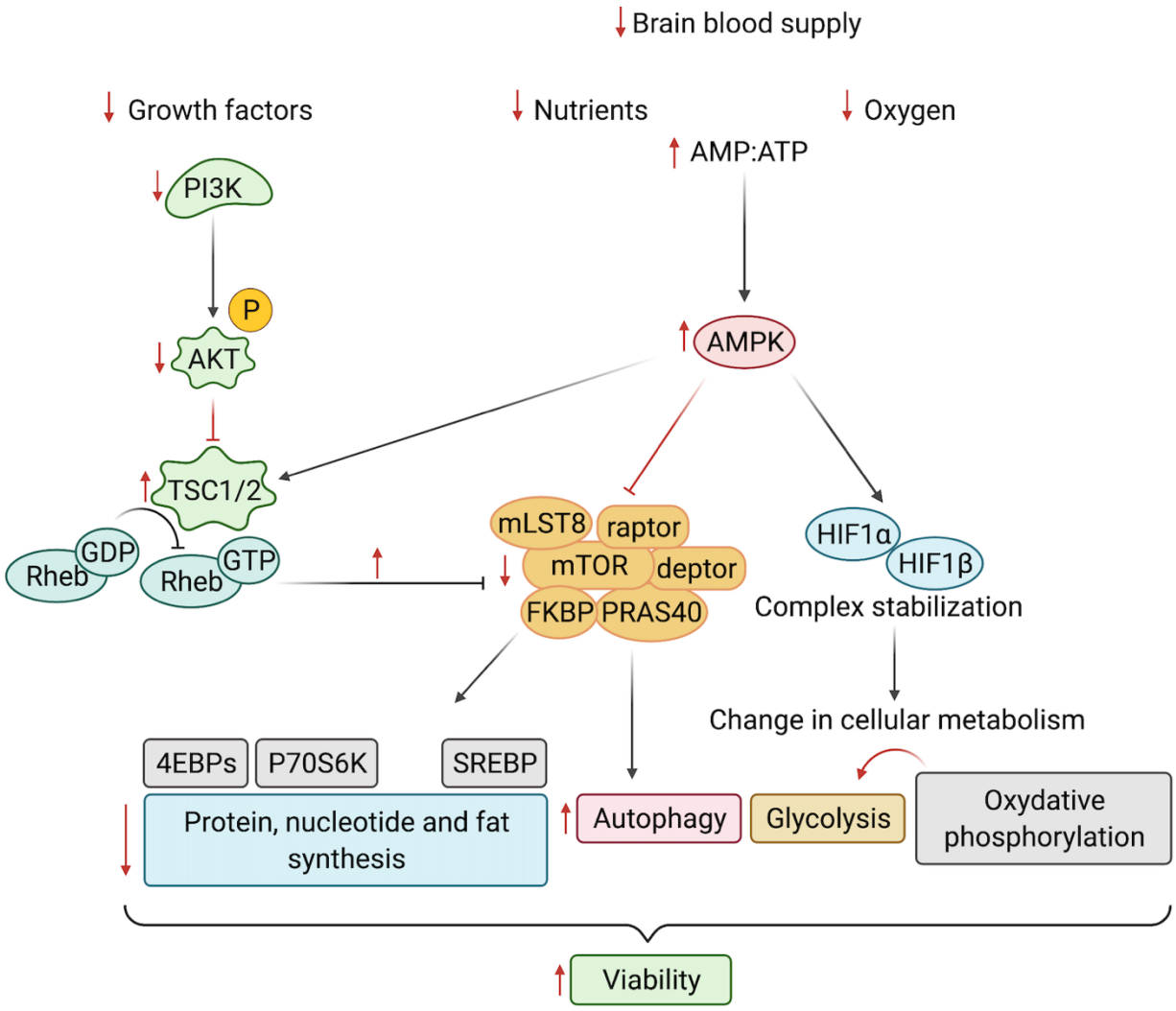

Figure 1.7 PI3K, Akt, and mTOR pathways in response to ischemic stroke. Cerebral ischemia reduces the delivery of growth factors, nutrients, and oxygen to cells. Reduced growth factor sensing induces a reduction of the P13K/AKT pathway, increasing TSC1/2 activity and its inhibitory effect on mTORC1. Lower nutrient levels, most importantly glucose and amino acids, and low oxygen levels are sensed as lower levels of energy (increased AMP: ATP). This, in turn, induces the AMPK pathway with its inhibitory effect on mTORC1. AMPK also stabilizes the hypoxia-inducible factor HIF1α/HIFβ complex, which changes cellular metabolism from oxidative phosphorylation to glycolysis. Reduced mTORC1 activity reduces anabolic processes such as protein synthesis (via 4EBPs and P70S6K), nucleotide synthesis (via P70S6K), and lipogenesis (via SREBP) and increases autophagy. The increase of catabolic and decrease of anabolic cellular processes ultimately lead to increased cellular survival. Created with BioRender.com.

In mammals, mTOR encompasses two distinct complexes, mTORC1, and mTORC2, that can be distinguished based on their accessory proteins, the signals they respond to, and their downstream effects (Liu and Sabatini, 2020). The core components of mTORC1 are mTOR, mammalian lethal with sec-13 protein 8 (mLST8), regulatory associated protein of TOR (raptor); and for mTORC2 mTOR, rapamycin-insensitive companion of mTOR (rictor), stress-activated protein kinase-interacting protein (mSIN1) and mLST8 (Laplante and Sabatini, 2009). As mentioned above, the central function of mTORC1 is to integrate information about the nutritional abundance and environmental status and translate it into a balanced interplay between anabolism and catabolism in the cell. mTORC2, on the other hand, is the activator of several pathways that favor cellular survival and govern cytoskeletal behavior. mTORC1 is acutely inhibited by rapamycin, while mTORC2 responds only to chronic rapamycin treatment (Liu and Sabatini, 2020). mTORC1 needs to receive information that all of the following substrates are available in large enough amounts: amino acids, insulin/growth factors, ATP, and oxygen (Sabatini, 2017). All of these have their biochemical pathways that ultimately either promote the activity of mTORC1 and downstream anabolic processes or favor its inactive state to ensure an energy-preserving cellular state where predominantly catabolic processes are activated.

Growth factors, for example, inactivate the tuberous sclerosis complex (TSC), which consists of TSC1, TSC2, and TBC1D7, and has an inhibitory function on mTORC1 by converting the Rheb-GTP (active) to the Rheb-GDP state (inactive). Therefore, energy abundance in the form of growth hormones can readily inhibit TSC activity and activate mTORC1. Conversely, low levels of ATP activate the AMP-activated protein kinase (AMPK), which inhibits mTORC1 activity to preserve as much ATP as possible (Sabatini, 2017). Of the 21 available amino acids, arginine and leucine, in particular, are essential for mTORC1 activity by anchoring the mTORC1,

once translocated to the lysosome, to Rag GTPases. Once bound to the lysosomal surface, mTORC1 can only be activated by the small GTPase Rheb in its GTP-bound, so energy-rich-state, which is promoted by growth factors, low levels of cellular stress, sufficient oxygen levels (Sabatini, 2017).

Less anabolic capacity is reflected by decreased *de-novo* protein and lipid synthesis, accompanied by the accumulation of potentially harmful metabolic by-products and excessive oxidative stress. The cell's autophagic function is upregulated, which induces a restorative effect on cellular function whereby misfolded, old, and redundant proteins and other cellular components are recycled and reused for energy supply. mTORC1 is the nexus of metabolism that ensures cellular survival by sensing upstream energy levels through amino acid and growth factor availability, AMP: ATP ratio, and oxygen levels (Liu and Sabatini, 2020).

1.4.2 Stroke and mTOR

The adult human brain exhibits a high expression of mTOR, especially in neurons and, to some extent, glial cells, and its activity is modulated by neuron-specific factors, of which the most important are neurotransmitters (glutamate, GABA, dopamine, serotonin) and neurotrophic factors (brain-derived neurotrophic factor BDNF and insulin-like growth factor 1 IGF-1) (Perez-Alvarez, Villa Gonzalez et al., 2018). A well-regulated mTOR pathway is essential for normal CNS development and maturation, and disruption is detrimental to normal brain structure and function and is associated with many diseases, including epilepsy, tumor growth, autism, and cognitive disability (Jaworski and Sheng, 2006, Perez-Alvarez, Villa Gonzalez et al., 2018). Further, disrupted mTOR functioning also leads to an imbalance of protein synthesis and breakdown, which is associated with the neurodegenerative diseases that are defined by increased accumulation of

protein aggregates, such as Alzheimer's, Parkinson's, and Huntington's (Perez-Alvarez, Villa Gonzalez et al., 2018).

Cerebral ischemia has also been shown to profoundly affect mTOR activity. mTOR regulation aims to limit the damage caused by ischemia by modulating neuronal autophagy and apoptosis, as well as promoting neurogenesis and angiogenesis (**Figure 1.7**) (Dutta, Rutkai et al., 2015, Mateos, Perez-Alvarez et al., 2016). In stroke, the undersupply of blood glucose in the brain, sensed as an increased AMP:ATP ratio by AMPK, enhances the activity of TSC1 with subsequent downstream inhibition of mTORC1 (Perez-Alvarez, Villa Gonzalez et al., 2018). Previous work from our lab has shown that resistant cells within the hippocampus (CA3) can up-regulate hamartin (TSC1) during global ischemia, leading to mTORC1 inhibition, thereby increasing productive autophagy to promote cell survival (Papadakis, Hadley et al., 2013). Low oxygen levels in the brain are also sensed via AMPK and REDD1, which induce TSC and block mTOR phosphorylation, thereby favoring catabolic processes such as autophagy while halting anabolic cell functions, including protein and lipid synthesis (Perez-Alvarez, Villa Gonzalez et al., 2018). In addition, ischemia induces the nuclear translocation and transcription of the heterodimer complex HIF1α and HIF1β that, when bound together, reprogram gene expression that facilitates cellular survival during hypoxia by switching the energy supply from oxidative phosphorylation to glycolysis and inducing angiogenesis via AMPK (Chen and Sang, 2016).

The role of mTORC1 as a target for neuroprotection following cerebral ischemia is still being investigated with some controversial findings. While most research groups report beneficial effects on stroke outcomes by inhibiting mTORC1 activity (Buckley, Hess et al., 2014, Chauhan, Sharma et al., 2015), some research groups suggest a positive effect on stroke outcomes by enhancing mTORC1 activity (Guo, Cao et al., 2014, Wang, Han et al., 2016). Research has been

trying to mimic the endogenous neuroprotective regulation of mTORC1 inhibition in response to cerebral ischemia by using exogenous pharmacological agents like rapamycin. Enhancing autophagy, in particular, seems to be a beneficial endogenous response to energy scarcity that improves neuronal survival following stroke. Still, the sustained increment of autophagy over more extended periods or doses can be detrimental to neuronal health (Perez-Alvarez, Villa Gonzalez et al., 2018). Therefore, to maintain neuronal viability, there is a need to fine-tune our knowledge of mTORC1 signalling and downstream autophagy activity in response to cerebral ischemia.

1.4.3 Diet

One potential non-pharmacological way of modulating the mTOR pathway is by interfering upstream of metabolism. Dietary interventions such as calorie restriction (CR), time-restricted eating, and fasting extend the lifespan of yeast, nematodes, fruit flies, rodents, and non-human primates (Fontana, Partridge et al., 2010, Yu and Mattson, 1999, Zhou, Kreuzer et al., 2019). In humans, CR has been shown to improve several pathologies, including metabolic syndromes and glucose control in diabetic patients, cancer, arthritis, asthma, and surgical tissue injury (de Cabo and Mattson, 2019).

Evidence studying the effects of CR, time-restricted eating, or fasting on cardiovascular disease and ischemic stroke is scarce. So far, experimental stroke studies in rodents showed that dietary restriction before the ischemic injury reduced stroke volume and improved neurological function by acting on a variety of cellular and metabolic mechanisms, including post-ischemic excitotoxicity, oxidative damage, apoptosis, inflammation, and autophagy (Bruce-Keller, Umberger et al., 1999, Greene, Todorova et al., 2001, Jamrozik, Broadhurst et al., 1994, McCay, Maynard et al., 1975, McDonald and Ramsey, 2010, Sohal and Weindruch, 1996, Zheng, Lee et

al., 2003). For example, fasting has been shown to upregulate mechanisms that protect against glutamate toxicity by increasing the efficiency of glutamate reuptake in astrocytes (Ribeiro, Quincozes-Santos et al., 2009). In a mouse model of focal ischemia, where the intervention group was subjected to intermittent fasting (IF), the fasted mice had lower infarct volumes and higher levels of BDNF compared to the control stroke group (Lindvall, Ernfors et al., 1992, Sommer, Kollmar et al., 2003, Yu and Mattson, 1999). CR has also been shown to induce protective mechanisms that block ROS generation and minimize oxidative stress from acute ischemic insult (Manzanero, Gelderblom et al., 2011). A central mediator of ROS production that exerts antioxidant effects in the ischemic brain is HO-1, and studies have shown its upregulation with IF (Arumugam, Phillips et al., 2010, Panahian, Yoshiura et al., 1999). Additionally, SIRT1 induces deacetylase activity which directly inhibits p53 and FOX53, which are potent inducers of apoptosis, thereby improving neuronal survival (Brunet, Sweeney et al., 2004, Halterman and Federoff, 1999).

So far, only one study examined the effects of a long-term hypocaloric diet following a focal stroke in mice and found that after 56 days, mice that were kept on a CR diet had smaller stroke volumes, improved neuronal function, and survival (de Carvalho, Sanchez-Mendoza et al., 2021). Further, the treatment group exhibited increased brain capillary density in the striatal peri-infarct region, together with increased levels of BDNF and SIRT1, suggesting improved neuroprotection and promotion of peri-infarct remodeling.

While clinical data on the effects of dietary restriction in the acute phase of stroke are still missing, there is a large body of literature describing the devastating impact of high levels of glucose in stroke patients, undermining the importance of strict glucose control for improved patient outcome (Bruno, Levine et al., 2002). By promoting lactic acidosis and free radical

production, hyperglycemia may directly challenge tissue by inducing lipid peroxidation and cell lysis in metabolically challenged tissue, as is the case with ischemia (Kawai, Keep et al., 1997, Lindsberg and Roine, 2004). Studies have found that lowering glucose in the acute phase diminishes infarct progression from the challenged penumbra. One reason might be that high glucose levels challenge tissue by increasing lactic acid levels, free radical production, and vascular reactivity.

In vitro studies have shown that high-glucose conditions induce numerous changes in the cell's aerobic metabolism and a shift toward the oxidation of lipids and amino acids, leading to neuronal injury (Koziel, Woyda-Ploszczyca et al., 2012). Animal models of stroke have investigated the effects of hyperglycemia on vascular reactivity and found an indirect relationship with blood glucose concentrations and CBF measured by Doppler flowmetry during the occlusion and after recanalization. These findings suggest that high glucose concentrations induce progressive cerebrovascular changes during ischemia and affect hemodynamic recovery on reperfusion. These changes are not yet well understood but may involve endothelial cell injury. Paljärvi and colleagues found that reperfusion after global ischemia caused excessive endothelial cell swelling and decreased luminal diameter in hyperglycemic rats compared to normoglycemic controls (Paljärvi, Rehncrona et al., 1983). The BBB, in particular, is well known to be vulnerable to extreme changes in blood sugar. A study using a hemorrhagic stroke model in rats has shown that hyperglycemia aggravated edema formation in the area around the insult (Song, Chu et al., 2003).

Bringing non-pharmacological interventions to the forefront of stroke research may be essential to rapid and effective translation. Dietary changes are easy to implement and control in the environment of a stroke unit and do not require FDA approval, unlike new pharmacological

therapies. However, our understanding of how these changes may affect different cell types within the body and the brain after a stroke is limited and remains crucial for developing this strategy as a novel therapy.

1.5 Aims of this thesis

In this thesis, I will investigate how interfering with mTOR signaling using pharmacological and non-pharmacological means affects the outcomes of ischemia. The specific aims of my thesis are:

1. To provide a detailed overview of rapamycin's effects on the microvasculature and BBB integrity in an *in vivo* model of ischemic stroke.
2. To investigate the molecular and functional effects of rapamycin treatment *in vitro* on pericytes and endothelial cells during and after oxygen-glucose deprivation.
3. To study how fasting post-stroke impacts inflammation and lesion volume in an *in vivo* study and benchmark the findings to the neuroprotective drug rapamycin.

Chapter 2: Characterization of the effects of mTOR inhibition in stroke

2.1 Introduction

Ischemic stroke exerts a myriad of downstream effects that go beyond isolated neuronal death, such as the breakdown of the BBB (Campbell, De Silva et al., 2019). The BBB, which is composed of endothelial cells, the basal lamina, pericytes, and astrocyte foot processes (del Zoppo, 2010), creates a uniquely dynamic boundary between the circulation and the brain parenchyma – thereby limiting and regulating the exchange of molecules, ions, and cells (Abbott, Patabendige et al., 2010). Current treatment options for ischemic stroke are limited to recanalization of the occluded vessel, and no treatment option that targets the microvascular structures has translated into practice (Campbell, De Silva et al., 2019). Pharmacological inhibition of mTORC1 with the FDA-approved anti-rejection medication rapamycin has been shown to protect brain tissue from dying in experimental models of stroke (Beard, Hadley et al., 2019, Hadley, Beard et al., 2019). However, the mechanism by which rapamycin exerts its cytoprotective effects and which cerebral cells and anatomical structures it is targeting are still being explored. In addition to incompletely understood mechanisms, rapamycin and other experimental therapies are subject to poor translation in stroke research, which can be in part attributed to inadequate end-point analysis. Studying the acute and sub-acute phases of stroke is key to determining their viability for therapeutic intervention, highlighting the importance of study designs that take the translational aspect under careful consideration.

Traditionally, histopathological and immunohistochemical analyses have been the primary way to characterize the effects of stroke in rodent models. While providing excellent structural detail and specificity, these approaches have two significant limitations; first, they prohibit the longitudinal assessment of lesion progression and evaluation of potential effects of therapeutic

interventions and second, they do not provide insight into the active and dynamic processes of the ischemic lesion. This has thus driven a shift from solely neuropathological analysis to non-invasive *in vivo* imaging (Canazza, Minati et al., 2014). Some of the imaging techniques used in stroke patient diagnostics, including MRI, CT, PET, and SPECT, are emerging in preclinical rodent work, and MRI has proven to be an optimal tool for translational studies. The clinical and preclinical scanners are identical in their concept, and animal-dedicated machines are increasingly equipped with sequences compatible with those in the clinical setting (Abraham and M., 2016). MRI in rodent models has been imperative for pathophysiological studies and the development of novel treatment options (Denic, Macura et al., 2011).

Sequences used in MRI can detect different aspects of the ischemic lesion (Canazza, Minati et al., 2014). For example, T2w-MRI provides anatomical information, whereas more dynamic sequences such as diffusion- and perfusion-weighted imaging (DWI and PWI, respectively) can detect tissue microstructure, metabolism, and hemodynamics, and in stroke, inform about potentially salvageable brain tissue using the PWI/DWI mismatch coefficient (Canazza, Minati et al., 2014). Because brain damage following cerebral ischemia is a dynamic process that changes over time, assessment with MRI requires these varied imaging modalities to suit the particular pathophysiological state of the lesion.

Generally, DWI has emerged as the gold standard for the acute phase. While conventional MRI sequences (T1w, T2w) may not demonstrate an infarct for 6 hours, an increased DWI signal in the affected brain tissue can be observed within minutes after the vessel occlusion, and animal and human studies suggest that some DWI lesions might be reversible with early recanalization (Nagaraja, Forder et al., 2020, Tan, King et al., 2006). The increased signal intensity (hyperintensity) progresses through a stereotypic sequence of apparent diffusion coefficient

(ADC) reduction, followed by a subsequent increase, pseudo-normalization, and, finally, permanent elevation, with reported sensitivity and specificity ranging from 88-100% and 86-100%, respectively (Tan, King et al., 2006). Assessing the diffusion movement of water molecules, the increased signal intensity (hyperintensity) seen in ischemic stroke tissue is thought to come from the interrupted blood supply that causes arrest of the fluid movement across the intracellular space.

The pathophysiological effects dominating lesion progression after stroke onset change over time. PWI, in combination with DWI, assesses the mismatch between diffusion and perfusion of blood (diffusion-perfusion mismatch, DPM) that can give valuable information on the disease state in the acute phase (up to 24 hours). The brain area identified as having a DPM is an area of critical hypoperfusion but not yet infarcted tissue, that is, the ischemic penumbra or "tissue at risk", which will transition to ischemic core tissue over time without successful therapy. Since patients with larger penumbral zones and smaller DWI lesions are generally thought to benefit more from reperfusion therapy than patients presenting with a minor DPM lesion at higher risk for hemorrhagic transformation, DPM can be a valuable imaging modality that aids in treatment decision making (Cao and Dong, 2021). One primary goal of neuroprotection research is to "freeze" the penumbra until reperfusion is complete, thereby limiting transformation from potentially salvageable to ischemic brain tissue that is irreversibly lost. For neuroprotective therapy research, DPM can, therefore, also be a powerful tool to assess the effects of neuroprotective therapies in stroke research by investigating their impact on the cerebrovascular and penumbral zone.

With the evolution of tissue necrosis over time concomitant with the breakdown of the BBB, the subacute phase (24 hours to 5 days post-stroke) is marked by serum proteins passing

from the vasculature to the brain, causing vasogenic edema, which is the leading cause of early deterioration and death in patients with large supratentorial strokes (Dostovic, Dostovic et al., 2016). T2w MRI imaging is the most sensitive imaging modality during this phase. It can give valuable information about edema formation and disease progression and aid in decision-making about further treatment and patient management. For neuroprotection research, T2w imaging can provide valuable information about potential treatment efficacy (Dijkhuizen and Nicolay, 2003).

During the subacute and chronic phase, dynamic and plasticity events, including the progression of BBB breakdown and axonal sprouting, define disease progression and require dynamic MRI modalities such as diffusion tensor imaging (DTI) and functional MRI (fMRI) for detection (Percie du Sert, Alfieri et al., 2017). MRI with contrast enhancement has been the imaging technique of choice for quantitative measurement of BBB breakdown. The accumulation of a gadolinium-based contrast agent in the extracellular extravascular space is detected via T1w imaging (Kilkenny, Browne et al., 2010). Using gadolinium-enhanced T1w imaging in a disease state where tissue fate is still malleable is a valuable option for evaluating the effectiveness of neuroprotective therapies aiming to maintain the BBB integrity.

While a large body of literature reports reduced stroke volume and improved neurological function using the mTOR inhibitor rapamycin in stroke (Bochelen, Rudin et al., 1999, Buckley, Hess et al., 2014, Chauhan, Sharma et al., 2011, Chi, Barsoum et al., 2016, Chi, Mellender et al., 2016, Guo, Feng et al., 2014, Li, Wang et al., 2016, Qi, Su et al., 2014, Sharkey and Butcher, 1994, Sheng, Zhang et al., 2010, Su, Zhang et al., 2014, Xie, Sun et al., 2014, Xie, Wang et al., 2014, Yan, Zhang et al., 2011, Yang, Zhong et al., 2015, Yin, Ye et al., 2012), only a few papers have investigated the effects of rapamycin treatment on structural changes of the BBB after transient middle cerebral artery occlusion (tMCAo) (Beard, Hadley et al., 2019, Chi, Mellender et al., 2016,

Guo, Feng et al., 2014, Sheng, Zhang et al., 2010, Su, Zhang et al., 2014, Yang, Zhong et al., 2015, Yin, Ye et al., 2012), of which five reported decreased BBB breakdown due to rapamycin treatment (Guo, Feng et al., 2014, Sheng, Zhang et al., 2010, Su, Zhang et al., 2014, Yang, Zhong et al., 2015, Yin, Ye et al., 2012). However, many of these studies used treatment before the stroke, which is translationally irrelevant. To effectively repurpose a drug as rapamycin for stroke, studies need to use it at an appropriate time point – either as an adjunct to reperfusion or during the post-stroke period – and study clinically relevant outcomes, including structural changes of the microvasculature.

2.1.1 Aims

The aims of this chapter are, therefore:

1. To understand how mTORC1 inhibition affects lesion volume and functional outcome as assessed by T2w MRI imaging and behavioral analysis, respectively.

2. To examine the effects of rapamycin on diffusion and perfusion changes in the subacute phase.

3. To study the effect of mTORC1 inhibition on the integrity of the BBB using contrast agent MRI.

2.2 Materials and methods

2.2.1 Ethics and animal care

All experimental procedures were approved by the UK Home Office (1986 Animal Act, Scientific Procedures), conducted in accordance with local ethical guidelines at the University of Oxford, and where possible conformed to the ARRIVE and IMPROVE guidelines for animal and pre-clinical stroke work (Kilkenny, Browne et al., 2010, Percie du Sert, Alfieri et al., 2017). Male Wistar Han rats (250g - 320g, Envigo Research Model Services in Blackthorn, England) were housed in individually ventilated cages under a 12-hour light/12-hour dark cycle with *ad libitum* access to food (standard food pellets) and water. The principal investigator began daily animal handling, weighting, and training the rats for the adhesive removal test (see below) 3 days before the surgery.

2.2.2 Sufficient statistical power

To avoid the occurrence of false-negative or false-positive findings resulting from low statistical power, preliminary data from our research group was considered (Beard, Li et al., 2020). Power analyses were performed to determine the necessary sample size. A sample size of 9 rats per group was used, which was found to be sufficient to detect biologically significant effects while minimizing the number of animals required to achieve the research objectives of this study. For example: for the *in vivo* studies assessing the impact of rapamycin treatment on rats that have undergone MCAo, previous work has shown a significant reduction in lesion volume after injection upon reperfusion compared to control (Beard, Li et al., 2020). Analysis of these results gives an effect size of 35%, with an alpha of 0.05 and a power of 0.8. Using these for *a priori*

power analysis shows that a group size of 9 is sufficient to see a significant result for rapamycin treatment in MCAo.

2.2.3 Controls

Appropriate control groups were included in all experiments. For the comparison with rapamycin, vehicle groups were used. Since naïve groups were included in similar animal studies undergoing the same intervention, and the investigators tried to minimize the number of animals used, none were included in this study. Where possible, within-subject controls were used, for example, when comparing the extent of stroke expansion on the ipsilateral versus contralateral hemisphere.

2.2.4 Excluded animals

A total of 4 animals were excluded from the study, 3 of which had an insufficient Laser Doppler Flow (LDF) drop during filament insertion, and 1 due to filament-induced subarachnoid hemorrhage (SAH). This is a rare but known surgical complication, which in this case, occurred before either the treatment or the vehicle was administered.

2.2.5 Randomization and blinding

To prevent accidental bias in the *in vivo* experiments, animals were allocated to a specific experimental group to receive either rapamycin (Sigma Aldrich, 250 μg/kg, n=9) or vehicle (<5% ethanol in saline, n=9), administered by a surgeon blind to treatment allocation (AMS). Blinding was continued throughout the whole experiment and until data acquisition was complete.

2.2.6 Cerebral blood flow measurements

Rats were initially anesthetized by inhaling 5% isoflurane in 70% N_2O and 30% O_2 and maintained at 1-2% isoflurane in 70% N_2O and 30% O_2. The rat's head was shaved and disinfected using a 70% ethanol and 30% chlorhexidine solution before an aseptic incision of 2 mm right from the midline and 25 mm in length was made. Skin, fat, and connective tissue were separated from the skull bone, and the Bregma was exposed. A fibreoptic probe was firmly positioned on the intact skull surface using superglue and cyanoacrylate glue. The coordinates for probe positioning were 1 mm posterior to the Bregma and 5 mm lateral to the midline, based on the Allen brain atlas (Cuccione, Versace et al., 2017, Spratt, Fernandez et al., 2006). An LDF apparatus (Oxyflo 2000 Optronix, Oxford, UK) was used to continuously monitor cerebral perfusion of the lateral MCA territory, corresponding to the core territory after MCA occlusion. LDF traces were recorded onto a Windows XP workstation running with WinDaq Data Acquisition Software (Dataq Instruments, Akron, Ohio, USA).

2.2.7 Focal cerebral ischemia

This study used 22 rats in total, and all surgical procedures were conducted under sterile conditions. During the surgery, the core body temperature of all animals was maintained at 37.0 ± 0.5°C using a rectal thermometer connected to a feedback-controlled heating pad (Harvard Apparatus, Cambourne, UK). Physical parameters, including body temperature and respiratory rate, were checked and recorded every 15 minutes throughout the surgical intervention. Respiration was kept between 50 and 60 breaths per minute by adjusting the isoflurane concentration. Focal brain ischemia was induced by transient occlusion of the MCA for 90 minutes, according to a previously described method (McLeod, Beard et al., 2013, Spratt,

Fernandez et al., 2006, Sutherland, Neuhaus et al., 2016). Briefly, the neck was shaved and disinfected using a 70% ethanol and 30% chlorhexidine solution. A thoracic midline incision at the level of the manubrium extending 3 mm rostrally was made. The mylohyoid and masseter muscles were separated, fat and connective tissue removed, and the common carotid artery (CCA) exposed. The supra-thyroid and occipital arteries were carefully cauterized using an electrical cauterizer connected to an electrical coagulation system (Aesculap GN60, Tuttlingen, Germany). Two ties with approximately 5 mm distance in between were made on the furthest point of the external carotid artery (ECA) that was still visible to the surgeon. A loose tie, serving as a safety tie, was positioned at the lower portion of the CCA. Another loose tie was attached to the ECA close to the ECA and internal carotid artery (ICA) junction. Next, a clamp (Acland Single Clamp B-2V, Mercian, Bromsgrove, UK) was firmly attached to the CCA, and the time of CCA occlusion was noted. The ECA's portion visible between the two firm ties was cauterized. A clamp (Acland Single Clamp B-2V, Mercian, Bromsgrove, UK) was attached to the ICA, and the time of ICA occlusion was noted. The ECA stump was incised, and a silicon-coated filament (Doccol Monofilament 4-0, Doccol Corporation, Sharon, USA) was inserted through the incision. It was then maneuvered across the ECA/ICA junction and into the ICA until the filament reached the height of the ICA clip. The ICA clip was removed, and the filament advanced forward and past the junction of the pterygopalatine artery and up the ICA. The filament was very slowly and carefully pushed forward under observance of the CBF monitoring until a sudden drop in the blood flow was noted. MCAo was confirmed by a >70% decrease in LDF signal from baseline. Selection of a 70% decrease as the threshold was chosen based on previous studies reporting an infarct threshold of 20-30% of baseline (Bardutzky, Shen et al., 2005, Jacewicz, Tanabe et al., 1992). The filament was secured, the CCA clip removed, and the time of MCA occlusion (MCAo) was noted.

MCAo was sustained for 90 minutes, and physical parameters were checked every 15 minutes. After, the microfilament was gradually withdrawn by holding the ties on the ECA tightly and pulling the thread gently against the tension. Reperfusion was confirmed by visual reperfusion of the proximal ICA and a sudden increase in the recorded CBF. The filament was then secured in place. Immediately after, rapamycin or vehicle was administered through intravenous tail vein injection. From the time of reperfusion, the rat was kept under constant monitoring for another 90 minutes before the experiment was ended. The CBF probe was removed, and the head and neck wounds were cleaned and closed (4-0 Vicryl Rapide Undyed 1x18" P-3, Somerville, US). Animals received 0.05 mg/kg marcaine into the wound to alleviate pain and 2 ml of saline solution subcutaneously. The rectal thermometer was removed, isoflurane turned off, and the gases changed to 0% N_2O and 100% O_2. Upon awakening, the animal was put in a pre-warmed cage, using a heating mat underneath the cage, with recovery food (peanut butter and jelly) and water on the cage floor for easy access. The animal was closely monitored for an additional 3 hours after awakening with post-surgical check-ups every 15 minutes.

2.2.8 Behavioral measurements

The well-being and behavior of the animals were assessed using a standard welfare scoring system (**Table 2.1**) and somatosensory and motor function testing tools, including the Bederson scale (**Table 2.2**), the Garcia scale (**Table 2.3**), and the adhesive removal test.

2.2.8.1 Welfare assessment

During the 3 days following surgery, the rats underwent daily welfare scoring. Scores of less than 4 were considered mild, whereas 7 and above were considered a severe impairment, respectively.

Table 2.1 Welfare scoring system, comprised of 5 categories.

	Scoring
Appearance	
Normal	0
Lack of grooming	1
Coat staring/ocular discharge/nasal discharge	2
Piloerection/hunched posture	4
Food and water intake	
Maintaining body weight within 5% of baseline weight	0
Weight loss 5-10%	1
Weight loss 10-15%	2
Weight loss > 10-15%	4
Weight loss > 10-15%, sustained for ≥ 48 hours	12
Natural behavior	
Normal	0
Minor change in spontaneous activity	1
Substantial change in spontaneous activity	2
Restless or very still	4
Chewing limb, lameness, loss of body supply to leg	12
Cerebral function	
Normal	0
Minor/moderate circling and/or hemiparesis	2
Severe circling and/or hemiparesis/hemiplegia	6
Fitting or ataxia	12
Postoperative complications	
Difficulty in breathing	4
Excessive bleeding	4
Infection	4
Wound breakdown	4

2.2.8.2 Neurological assessment

Further, neurological assessments to measure neurological impairments post-stroke were performed on all three days following surgery. Tests involved Bederson (Bederson, Pitts et al., 1986), Garcia (Garcia, Wagner et al., 1995), and the adhesive removal test (Schaar, Brenneman et al., 2010).

Bederson: The Bederson scale is a global assessment for measuring neurological impairments associated with stroke. Tests include forelimb flexion, resistance to lateral push, and circling behavior. A grading scale of 0 to 3, with 0 being not affected and 3 being severely affected, is used to assess behavioral deficits following stroke objectively. (**Table 2.2**).

Garcia scale: Neurological impairment scoring system (Neuroscore), comprised of 6 tests, was modified from Garcia et al. (1995) (Garcia, Wagner et al., 1995). The Garcia scale involves a battery of 6 tests to evaluate various sensorimotor deficits, including spontaneous activity, symmetry in four limb movement, forepaw outstretching, climbing, body proprioception, and response to vibrissae touch. Each of the 6 tests is assessed on a grading scale of 0 to 3, with 0 being not affected and 3 being severely affected, representing a minimum score of 0 and a maximum score of 18 points (**Table 2.3**).

Adhesive removal test: A 7 x 7 mm adhesive wash-proof plaster was placed on the forepaw, and the "time-to-contact" and "time-to-remove" were measured from both forepaws. The test was replicated twice in each trial. This test describes paw and mouth sensitivity (time-to-contact) and dexterity (time-to-remove). Two daily training sessions 3 days before the surgical procedure were performed to decrease inter-individual differences in this test.

Table 2.2 Bederson scale

	Scoring
Spontaneous activity, evaluated for 5 minutes in the home cage	
Moves around, reaches at least 3 sides of the cage	0
Moves around, reaches less than 3 sides of the cage	1
Barely moves in cage, does not rise to any side of the cage	2
Does not move at all	3
Symmetry in the movement, when suspended by the tail	
Both sides extend symmetrically	0
Contralateral forepaw shows slightly diminished movement	1
Contralateral forepaw shows severely diminished movement	2
Contralateral forepaw does not move at all	3
Climbing a wire grid	
Normal climbing	0
Able to climb but contralateral side is weaker	1
Failure to climb	2
Reaction to touch on either side of trunk	
Symmetrical response	0
Slower or less sensitive response on the contralateral side	1
No response on the contralateral side	2
Response to vibrissae touch on either side	
Symmetrical response	0
Slower or less sensitive response on the contralateral side	1
No response on the contralateral side	2

Table 2.3 Garcia scale

		Scoring
Flexion		
Normal	Both forelimbs extend towards the floor	0
Deficit	Any degree of forelimb flexion	1
Lateral push		
Normal	No reduction in resistance to lateral push towards paretic side	0
Deficit	Consistent reduction in resistance to lateral push towards paretic side	1
Circling		
Normal	No circling	0
Deficit	Consistent circling	1

2.2.9 Magnet resonance imaging

All MRI acquisitions were carried out on a 9.4T horizontal-bore scanner (Agilent Technologies Inc., Santa Clara, USA) with a 72 mm volume transmit coil and a 4-channel surface receive array (Rapid Biomedical, Rimpar, Germany). The animal's anesthesia was induced with 5% isoflurane in 70% N_2 and 30% O_2 and maintained at 1-2% isoflurane in 70% N_2 and 30% O_2. The rats were placed in a cradle equipped with a stereotaxic holder, a rectal thermometer, and a pressure probe to monitor respiration. The rectal thermometer was connected to a feedback-controlled heating pad (Harvard Apparatus, Holliston, United States) to maintain core body temperature at 37.0 ± 0.5°C, and respiration was kept between 50 and 60 breaths per minute by adjusting isoflurane concentration. Physical parameters were recorded and checked regularly throughout the imaging session.

Acquisition of baseline maps for T1 and T2 relaxation times (seconds), arterial spin labeling (ASL) for measuring CBF (mL/100g/min), and apparent diffusion coefficient (ADC) for delineating diffusion (μm²/ms) were performed. T1 and T2 data were acquired using a spin-echo echo-planar imaging (EPI) readout with FOV = 32 x 32 mm², matrix = 256 x 256 mm², thickness = 1 mm, 10 slices. T1w images were taken with a scan repetition time (TR) and echo time (TE) of

500 ms and 20 ms, respectively. The parameters were identical for imaging acquisition, both before and after administration of 150 µL gadodiamide (Omniscan, Germany) via an indwelling tail vein cannula. T1-map scans (repetition time/echo time [TR/TE] = 1000 ms/27.16 ms) were obtained using an inversion recovery sequence (TI=13.14, 29.3, 65.3, 145, 324, 723, 1610, 8000 ms). T2w anatomical imaging scans (TR = 3000 ms, TE_{eff} = 51.26 ms) were obtained with an echo spacing (ESP) of 8.54. ASL and ADC data were acquired using a spin-echo echo-planar imaging (EPI) readout with a field of view (FOV) = 32 x 32 mm², matrix = 64 x 64 mm², thickness = 1 mm, 10 slices. Fast spin-echo multi-slice (FSEMS) scan sequences (TR = 1000 ms, TE_{eff} = 40, ESP = 10 ms) were acquired using a midline and axial orientation with FOV = 50 x 50 mm², matrix = 256 x 256 mm², thickness = 2 mm, single slice. Based on the acquired FSMES-images, the labeling plane for ASL imaging (6.2 mm thickness) was placed in the rat's neck at a 45° angle to the animal's rostrocaudal axis. CBF maps were generated by multiphase pseudo-continuous arterial spin labeling (Larkin, Simard et al., 2019). ADC maps were generated from diffusion-weighted images acquired in 3 orthogonal directions for b=0/mm² and b=1000 s/mm². DW imaging scans were obtained using a two-dimensional spin-echo echo-planar imaging (SE-EPI) sequence. For contrast-enhanced T1w spin echo, multi-slice images were taken before and immediately after 0.15 ml injection of gadolinium-based contrast agent (GBCA).

2.2.9.1 MRI analysis

Imaging segmentation and image analysis were performed using itk SNAP (Version 3.8.0, 2019) (Yushkevich, Pashchinskiy et al., 2019). On T2w maps, areas of ischemia were identified as hyperintense regions (Milidonis, Marshall et al., 2015). On T1w maps, the image before Gd injection was subtracted from the image taken after, and areas of BBB breakdown were identified

as hyperintense regions (Huang, Wu et al., 2019). On ADC maps, areas of ischemia were identified as regions of reduced diffusion relative to the same area on the contralateral hemisphere. Similarly, on ASL maps, ROI was identified by areas with marked blood flow disturbances relative to the same area on the contralateral hemisphere. In all imaging modalities, ROIs were selected manually by the main investigator blinded to treatment or control (AMS).

2.2.10 Tissue processing

After imaging, rats were killed by intraperitoneal pentobarbital injection (800 mg/kg) (Zatroch, Knight et al., 2017). For further tissue processing, rats were randomly assigned to either one of two groups: Immunohistochemistry (IHC) or Western Blotting (WB). Rats of the IHC group were transcardially perfused using heparinized saline and PFA (4% dilution in heparinized saline). Brains were collected, post-fixed in PFA (same dilution) overnight, and moved into sucrose (30% solution in PBS). In the WB group, rat brains were collected without perfusion and sliced into 2 mm thick coronal sections with an ice-cold stainless-steel matrix (Kent Scientific). Areas of the striatum and cortex of 1 mm^2 from both hemispheres were taken from one section and snap-frozen on dry ice. The spleens of both groups were collected *in toto* and snap-frozen on dry ice.

2.2.11 Western blotting of mTOR proteins and autophagy markers

2.2.11.1 Whole-cell homogenization

All steps were performed on ice. Tissue from the cortical ipsilateral lesion side, each weighing approximately 4 mg, was homogenized in a mixture of 240 µl lysis buffer and protease inhibitor cocktail, using a syringe with needles of decreasing diameter for fine homogenization. The homogenate was then centrifuged at 13000 rpm at 4°C for 30 minutes, after which the supernatant was pipette in a fresh new Eppendorf tube, and the pellet re-suspended in 160 µl lysis buffer for repeated centrifugation at 13000 rpm at 4°C. The supernatants were combined, and the pellet was discarded.

2.2.11.2 Protein quantification

Protein quantification was performed using the BCA assay (Pierce BCA Protein Assay Kit, 23225, Thermo Fisher Scientific), which works by measuring the amount of reduced cuprous ion (CU1+) that is generated by chelating copper (CU2+) to proteins in the sample. The reduced cuprous ion then reacts with BCA, producing a purple water-soluble complex (BCA-copper reaction). The assay was performed according to the manufacturer's instructions. Briefly, replicates of 25 µl protein standards with known protein concentrations and the unknown reagents were mixed with 200 µl working reagent, respectively. After 30 minutes in the incubator (37°C, 5% CO_2 in humidified air), the light absorbance at 562 nm was measured. The replicate values of light absorbance were averaged, and the protein concentration (µg/ml) of the standards and their light absorbance at 562 nm was facilitated to draw a standard curve and interpolate the missing protein concentration values of the unknown.

2.2.11.3 Gel electrophoresis

Equal amounts of the original sample to obtain 50 µg of protein were calculated and mixed with appropriate quantities of lysis buffer and 22.5 µl of Laemmli sample buffer (161-0737, Bio-Rad, with DTT) to obtain a loading volume of 45 µl. After heating the protein solutions to 95°C for 5 minutes, the bands and two ladders (161-0376, Bio-Rad) were loaded onto a gradient gel (insert product specifications here) in a chamber filled with running buffer (x 10 stock of 0.025 M Tris Base, 0.2 M Glycine, 0.1% (w/v) SDS in distilled water). The gel was run at a constant 200 V for 42 minutes or until visual confirmation that the ladder had run entirely. The Polyvinylidene difluoride (PVDF) membrane onto which the gel was transferred was previously rehydrated and prepared according to the manufacturer's instructions. Protein transfer from the gel to the membrane was kept under cooling conditions and over 45 minutes at a constant charge of 120 V, using transfer buffer (0.025 M Tris Base, 0.2 M Glycine, and 10% methanol in distilled water).

2.2.11.4 Protein detection

All steps were performed under gentle agitation. To detect 3 proteins with distinct molecular weights, the membrane onto which proteins were transferred from a gradient gel was cut between the molecular weight ladders 37 and 50 kDa, as well as 75 and 100 kDa. Membrane pieces were then blocked in PBS containing 5% BSA and 0.1% Tween-20 for 1 hour at room temperature before being incubated in primary antibody (**Table 2.4**) in 5% PBS-T solution overnight. After 3 x 5-minute-washes in PBS-T, the membrane was incubated in secondary antibody goat anti-rabbit (IgG H&L (HRP), ab6721, Abcam, dilution 1:2000) in 5% BSA PBS-T for 1 hour at RT. After 3 x 5-minute-washes in PBS-T, the membrane was developed using enhanced chemiluminescence (ECL; 12644055, Fisher Scientific) for 5 minutes and immediately imaged after that. Western Blot

analysis and quantification were performed using densitometry and corrected for loading using β-tubulin that was used as the housekeeping protein (**Table 2.4**). The membrane was probed for antibodies twice, using the following mild antibody-stripping protocol: The membrane strips were incubated in mild stripping solution (7.5 g glycine, 0.5 g SDS, 5 ml Tween-20, pH to 2.2, and dilute up to 500 ml distilled water) for 2 x 7 minutes, following by 2 x 10-minute-washes in PBS, and 2 x 5-minute washes in PBS-T, before blocking again in 5% BSA and 0.1% Tween-20.

Table 2.4 Primary antibodies used for Western Blotting

Antigen	**Molecular weight (kDa)**	**Source**	**Manufacturer**	**Dilution**
mTOR	289	Rabbit	Cell Signaling (#2972)	1:1000
Phospho – mTOR (Ser2448)	289	Rabbit	Cell Signaling (#2971)	1:1000
β-Tubulin	55	Rabbit	Cell Signaling (#2146S)	1:1000

2.2.12 Statistical analysis

The experimental design and number of animals have been determined and optimized to test the specific hypotheses of the project and follow the standards for scientific reporting and reproducibility (Munafò, Nosek et al., 2017). Statistical analyses were performed at the end of the experiment, and no further animals were included at that point. Power calculations were performed to avoid the occurrence of false-negative or false-positive findings. Statistical tests were performed using Graphpad Prism 8.42 (La Jolla, USA). The D'Agostino and Pearson normality tests were performed on all data. Appropriate statistical tests were chosen based on the normality of the data. To compare differences between the two treatment groups, an unpaired Student's t-test was used. Differences in CBF from LDF tracing were assessed using repeated-measures (RM) two-way ANOVA. Multiple comparisons were performed using the Bonferroni test. The correlation of imaging parameters with functional outcomes was analyzed by simple linear regression of correlation. Data are presented as mean ± standard error of the mean (SEM).

2.3 Results

2.3.1 Rapamycin improves post-recanalization blood flow in the acute phase

CBF of the MCA territory from the ipsilateral cortex was recorded. The microfilament was gradually withdrawn 90 minutes after the MCA occlusion. Reperfusion was confirmed by visual reperfusion of the proximal ICA and a sudden increase of the recorded CBF in the MCA territory. Immediately after filament removal, rapamycin or vehicle was administered via the tail vein. Changes in CBF are expressed as a % of pre-rapamycin administration at 90 minutes post-MCAo, the time point immediately before re-canalization. The CBF was recorded for another 90 minutes from the time of reperfusion. Analysis showed an overall change in blood flow over time and a difference between vehicle and rapamycin at different times during recording ((**Figure 2.1 (A)**; RM two-way ANOVA: $F(1,9)=2.353$, $p=0.1594$ for treatment, $F(19,160)=2.757$, $p=0.0003$ for time, $F(19,160)=1.981$, $p=0.0120$ for interaction). No difference in blood flow was measured at the time points immediately before re-canalization before treatment administration (-66.16 ± 6.173 vs. -56.58 ± 2.888) in vehicle and rapamycin groups, respectively. After treatment administration, the blood flow of the MCA territory was significantly increased in the rapamycin group compared to the control (**Figure 2.1 (B)**; t-test; $p<0.0001$).

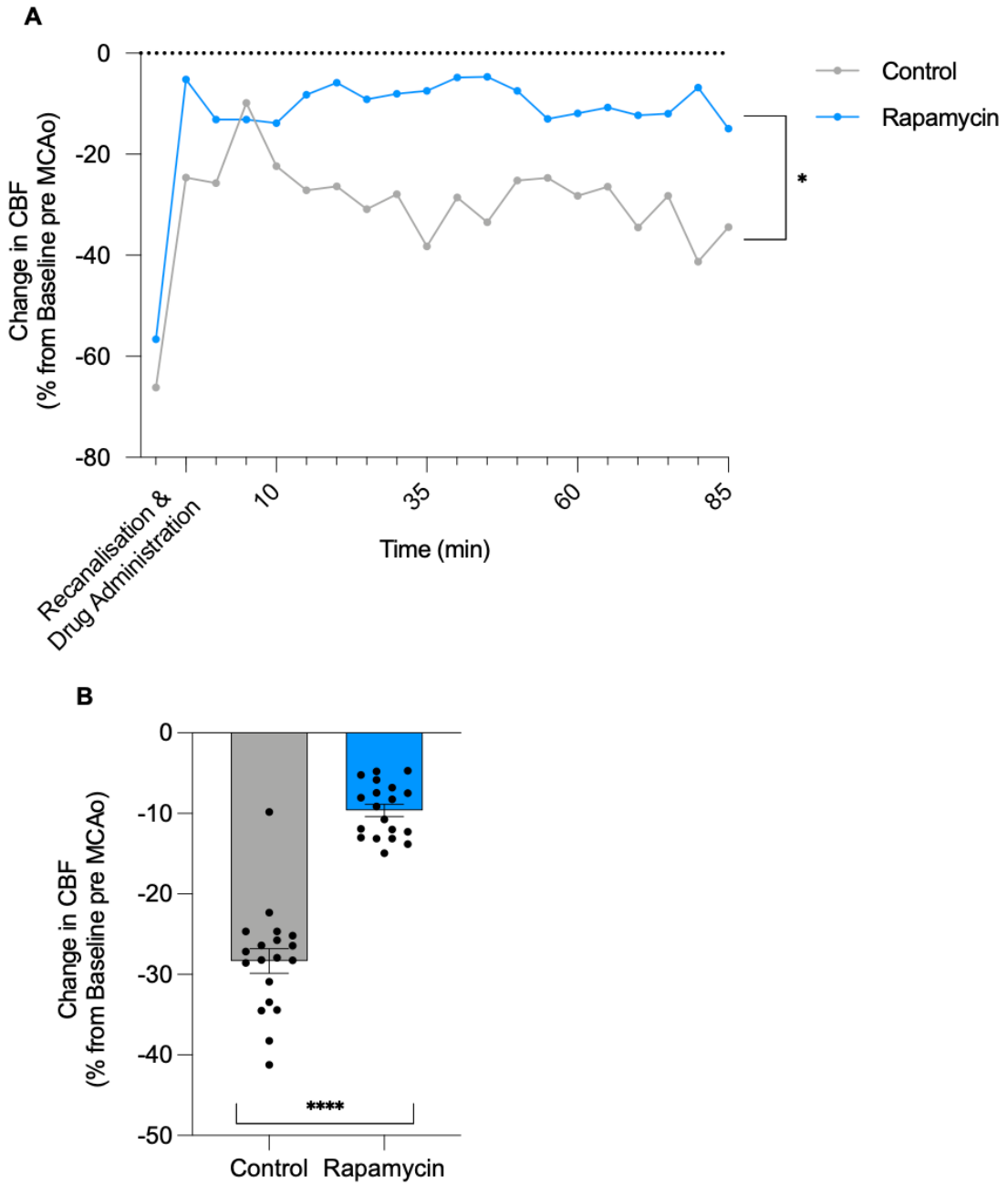

Figure 2.1 Rapamycin improves post-recanalization blood flow acutely. **(A)** Cerebral blood flow (CBF) of the middle cerebral artery (MCA) territory after recanalization and rapamycin treatment. **(B)** Change in CBF calculated as % change from before middle cerebral artery occlusion (MCAo). Data for **(B)** are mean ± SEM; ****p<0.0001 when compared to vehicle-treated cells. n=19 for all groups.

2.3.2 Rapamycin does not alter diffusion or perfusion at 3 days

After evaluating rapamycin's effect on blood flow in the hyperacute phase, the next aim was to investigate rapamycin's effects on dynamic changes in the subacute phase of disease progression at 72 hours. The changes in the apparent diffusion of water in the stroke region were assessed using diffusion-weighted MRI and subsequently produced ADC maps. Relative diffusion within the stroke area was calculated as follows: diffusion of the stroke region/diffusion of the mirrored region in the contralateral hemisphere. No significant difference in diffusion was observed between the vehicle and rapamycin-treated group (**Figure 2.2 (A)**; t-test; p=0.4478; vehicle: 0.8415 ± 0.02009; rapamycin 0.8161 ± 0.02493). The mean diffusion (in 10^4 mm^2/sec) of vehicle- and rapamycin-treated animals was 6.440 ± 0.1757 and 6.625 ± 0.1830 in the ipsilateral, and 7.667 ± 0.2357 and 7.875 ± 0.1250 in the contralateral hemisphere, respectively.

Using ASL imaging, perfusion was assessed and compared to the non-ischemic hemisphere (relative perfusion of the stroke region = perfusion of the stroke region/perfusion of the same region in the contralateral hemisphere). No difference in perfusion was observed between the vehicle- and rapamycin-treated animals (**Figure 2.2 (B)**; t-test; p=0.5805; vehicle: 0.9443 ± 0.1890; rapamycin 0.8277 ± 0.09931). The mean perfusion and absolute deviation (in ml/100g/min) on the ipsilateral hemisphere were 90.3269 ± 34.8987 and 79.0598 ± 26.0134 in the vehicle- and rapamycin-treated group, respectively. On the contralateral hemisphere, mean perfusion and absolute deviation were 101.1121 ± 12.1069 and 98.1982 ± 17.6314 in the vehicle- and rapamycin-treated groups, respectively. Given the perfusion of individual pixels within the stroke area, the perfusion abnormality was differentiated into hypoperfused and hyperperfused areas. The perfusion abnormality of rapamycin-treated animals consisted of 65% hypoperfusion

and 35% hyperperfusion, whereas in the control group, 56% was hypoperfusion and 44% hyperperfusion, respectively.

Perfusion (ASL) and diffusion (ADC) MRI images were projected on top of each other. Area of mismatch, where perfusion abnormality but no diffusion deficit was recorded, was calculated. At 3 days post-stroke, there was no statistically significant difference in the volume of DPM between vehicle- and rapamycin-treated animals (**Figure 2.2 (C)**; t-test; p=0.2128; vehicle: 137.7 ± 12.53; rapamycin: 163.2 ± 14.71).

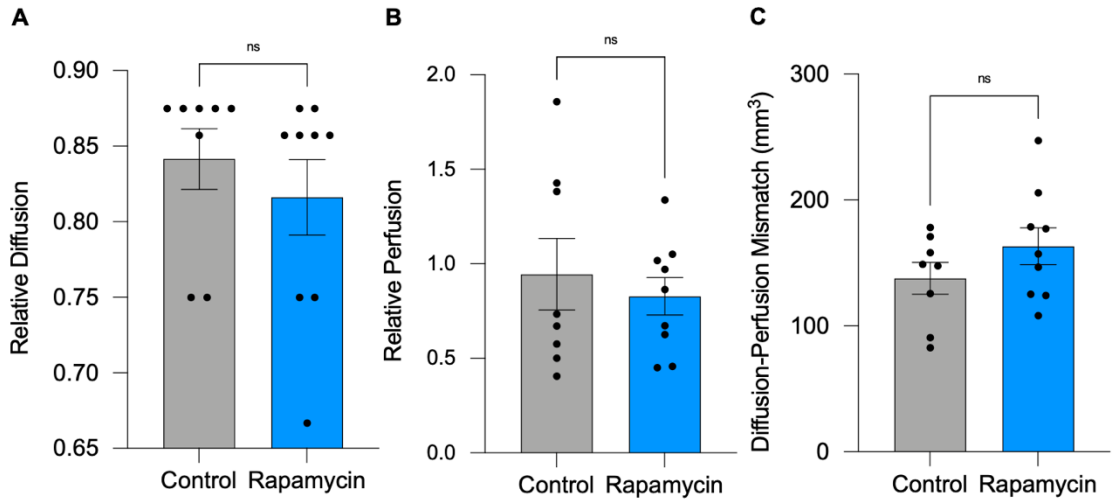

Figure 2.2 Rapamycin does not alter diffusion, perfusion, or diffusion-perfusion mismatch. **(A)** Ipsilateral diffusion of the stroke area relative to the same area on the contralateral hemisphere was assessed with MRI (ADC sequence) 3 days post-stroke. **(B)** Ipsilateral perfusion of the stroke area relative to the same area on the contralateral hemisphere assessed with MRI (ASL sequence) 3 days post-stroke **(C)** Diffusion-perfusion mismatch as an estimation of penumbral volume assessed with MRI (ASL and DWI sequences) 3 days post-stroke. Data are mean ± SEM, n=9 for all groups.

2.3.3 Rapamycin significantly reduces stroke volume

To evaluate stroke volume in the subacute phase, structural T2w MRI imaging was performed 3 days post-stroke. Stroke volume was corrected for edema formation using the formula by Kaplan et al. (Kaplan, Brint et al., 1991): Corrected infarct size = infarct volume x (volume of contralateral hemisphere/volume of the ipsilateral hemisphere). Analysis of lesion volume showed a significant reduction in the rapamycin-treated group compared to control, with a mean reduction of more than half when treated with rapamycin (**Figure 2.3 (A)**; t-test; p=0.0114; vehicle: 113.3.44 ± 22.75; rapamycin 44.77 ± 10.31).

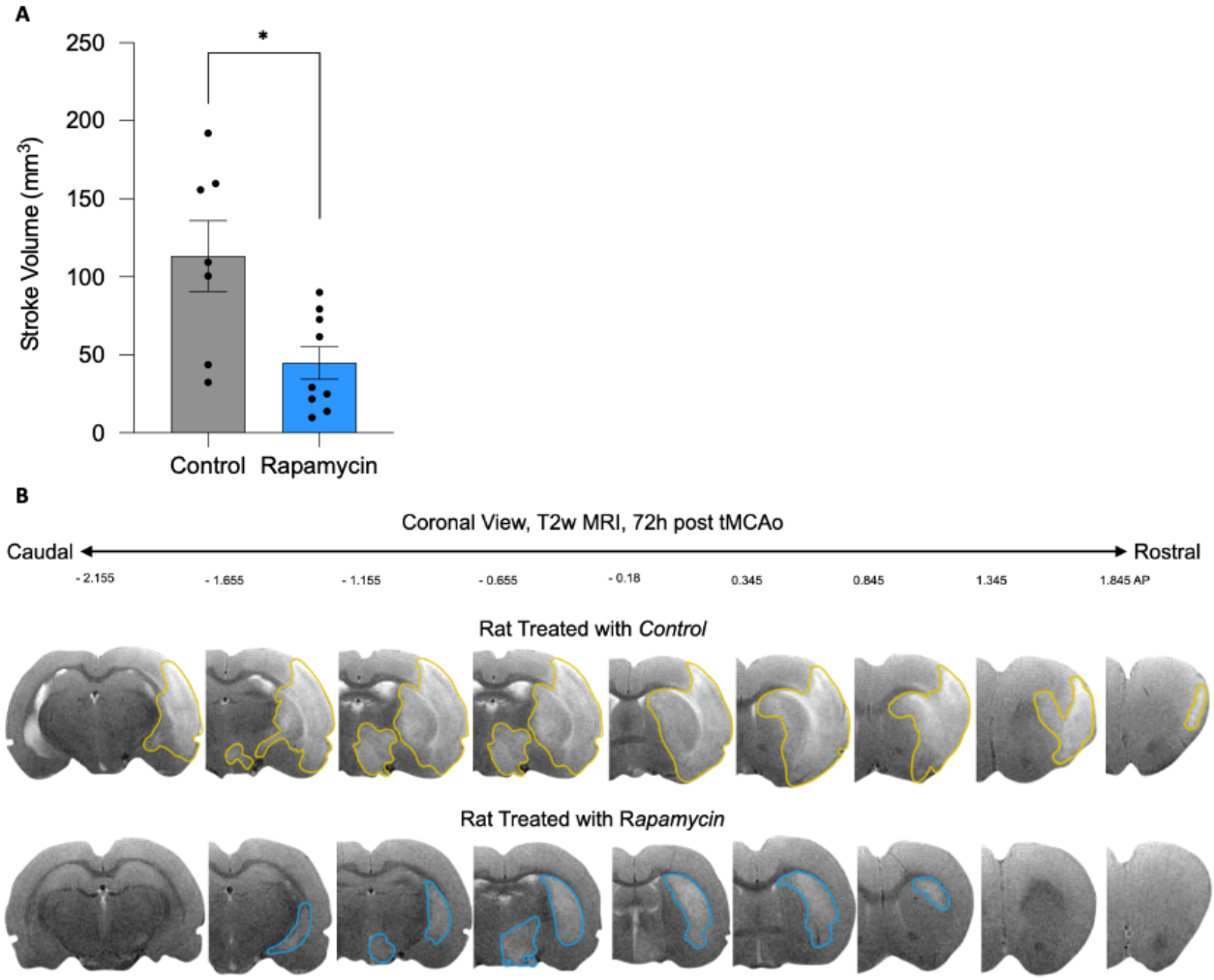

Figure 2.3 Rapamycin significantly reduces stroke volume. **(A)** Stroke volume assessment with MRI (T2w sequence) 3 days post-stroke, with correction for edema. **(B)** Coronal view, T2w MRI of representative stroke brains. Data are mean ± SEM, *p<0.05, when compared to vehicle-treated cells. n=7 for vehicle- and n=9 for rapamycin.

2.3.4 The effect of rapamycin on edema formation and BBB integrity

Edema formation of the T2w images was assessed using the edema calculation after Kaplan (Kaplan, Brint et al., 1991): Extent of edema = (volume of the ipsilateral hemisphere – the volume of the contralateral hemisphere)/volume of the contralateral hemisphere. Edema formation was not significantly reduced in rapamycin-treated animals compared to the control group. (**Figure 2.4 (A)**; t-test; p=0.1129; vehicle: 14.25 ± 2.541; rapamycin 9 ± 1.886). Further, T1w imaging with gadolinium injection was performed to assess BBB integrity. 4 additional animals had to be excluded because the amount of Gd reaching the area of interest was insufficient. There was a trend towards reduced BBB breakdown in the rapamycin-treated group, but significance could not be reached (**Figure 2.4 (B)**; t-test; p=0.0606; vehicle: 7.647 ± 1.837; rapamycin 3.270 ± 0.9535).

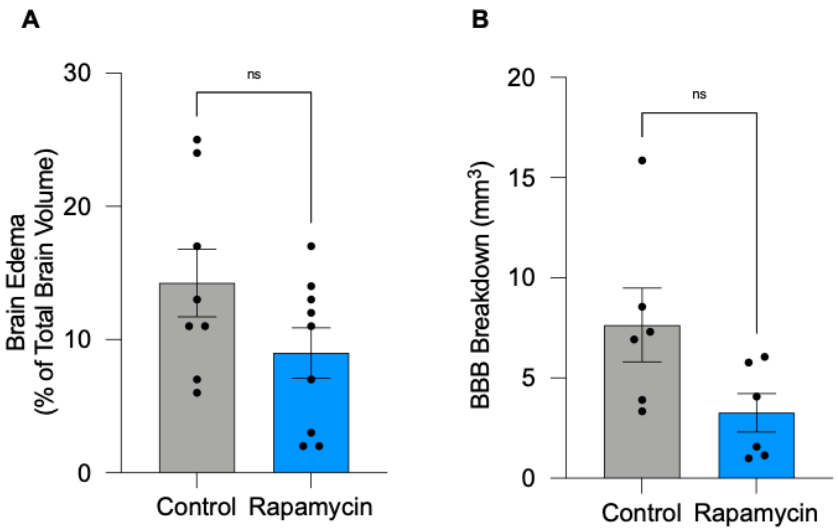

Figure 2.4 The effect of rapamycin on edema formation and BBB integrity**. (A)** Rapamycin did not reduce edema formation (p=0.0606). Brain edema expressed as a percentage of whole-brain volume, assessed with MRI (T2w sequence) 3 days post-stroke. Data are mean ± SEM, n=8 for vehicle, and n=9 for the rapamycin-treated group. **(B)** BBB breakdown assessment with contrast-enhanced T1w spin echo, multi-slice images were taken before and immediately after 0.15 ml injection of gadolinium-based contrast agent (GBCA) and corrected for edema formation. Data are mean ± SEM, n=6/group in all groups.

2.3.5 Rapamycin significantly improves functional outcome

Neurological outcomes of all animals 3 days following tMCAO were assessed. The Garcia scale was used for evaluating sensorimotor deficits due to stroke. This testing battery consists of 6 different tasks, where performance is graded on a scale of 0-3, with 0 being not affected and 3 being severely affected by the stroke, representing a minimum score of 0 and a maximum score of 18 points. Blinded testing and analysis revealed that rats treated with rapamycin compared to control performed significantly better (**Figure 2.5 (A)**; t-test; p=0.0295; vehicle: 11.67 ± 0.2887; rapamycin: 12.78 ± 0.3643). Similarly, the Bederson scale measures neurological impairments following stroke. The grading scale of 0-3 differentiates the animals from being not affected (0) to being severely affected (3) by the stroke. Rats treated with rapamycin compared to control showed a trend towards a lower Bederson score, though statistical significance could not be reached (**Figure 2.5 (B)**; t-test; p=0.0962; vehicle: 2.111 ± 0.2003; rapamycin: 1.556 ± 0.2422). The adhesive removal test was used to test sensory deficits. To decrease inter-individual differences within this test, training sessions from 3 days before the surgical procedure (2 trials per day) were performed. The time used for noticing the sticky tape on the contralateral forepaw was analyzed and compared amongst the rapamycin and vehicle groups. Rapamycin-treated animals required significantly less time to notice the adhesive tape on their forepaw, indicating improved sensory functioning (**Figure 2.5 (C-D)**; t-test; p=0.0002; vehicle: 78.11 ± 3.917; rapamycin: 50.89 ± 4.029). There was a modest correlation between stroke volume and neurological test results, with larger lesions leading to worse functional outcomes (**Figure 2.6**; simple linear regression correlation; stroke volume vs. Garcia r=-0.5502, p=0.0272; stroke volume vs. Bederson r=0.6138, p=0.0114; stroke volume vs. time to notice of contralateral forepaw in adhesive removal test r=0.5486, p=0.0278; n=16).

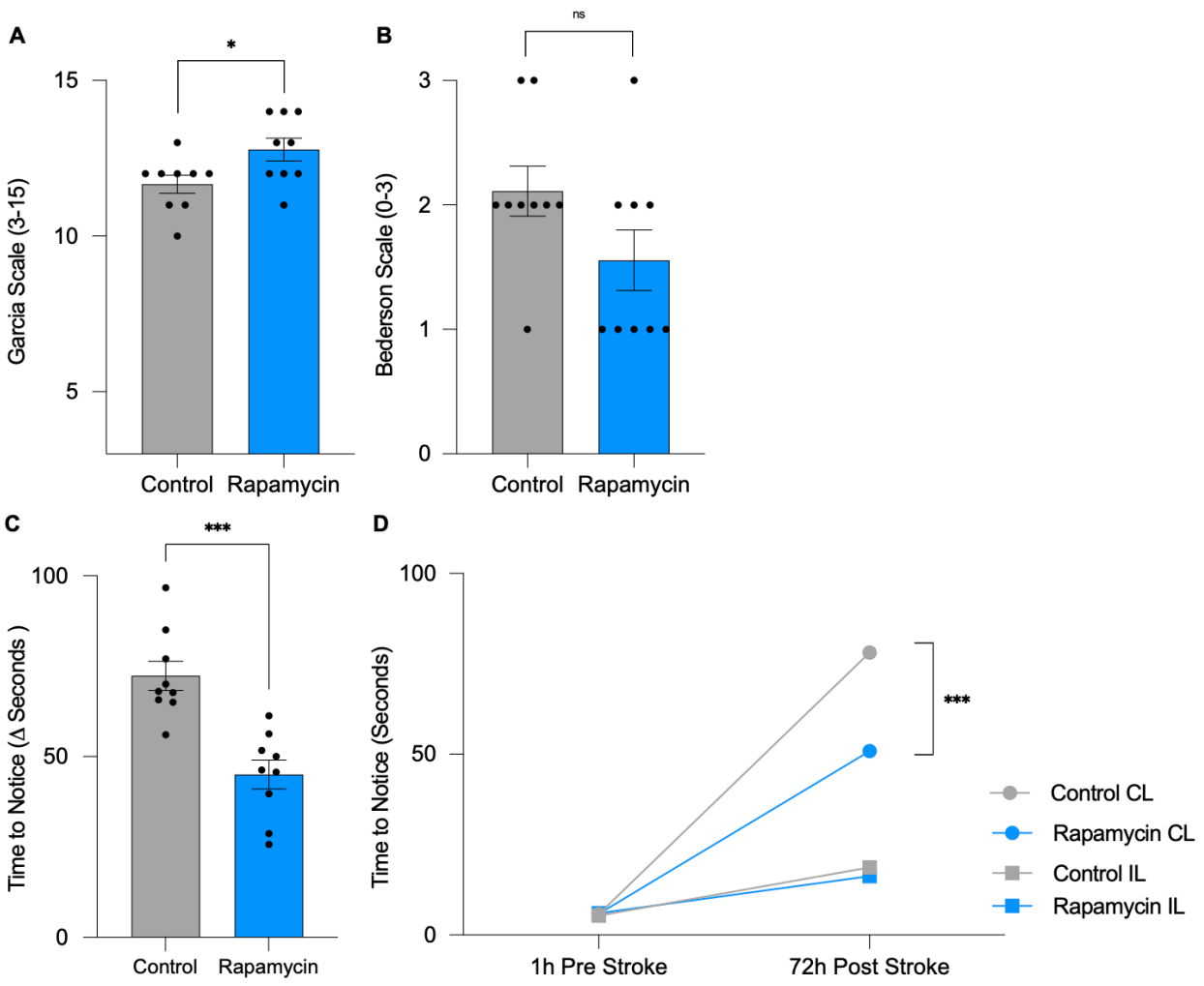

Figure 2.5 Rapamycin significantly improves functional outcomes. **(A)** Neurological assessment with Garcia scale 72 h post-stroke (3-15 points). **(B)** Neurological assessment with Bederson scale 72 h post-stroke (0-3 points). Data are mean ± SEM, *p<0.05 when compared to vehicle-treated cells. n=9 for all groups. **(C)** Rapamycin significantly reduces sensorimotor deficits assessed by the adhesive removal test. Time to notice the left paw (contralateral to stroke side), calculated as the difference between baseline and 72 h post-stroke (seconds). **(D)** Graphical illustration of time-to-notice over time and of different treatment groups. Data are mean ± SEM, ***p<0.001, when compared to vehicle-treated cells. n=9 for all groups. Abbreviations: CL: Contralateral; IL: Ipsilateral.

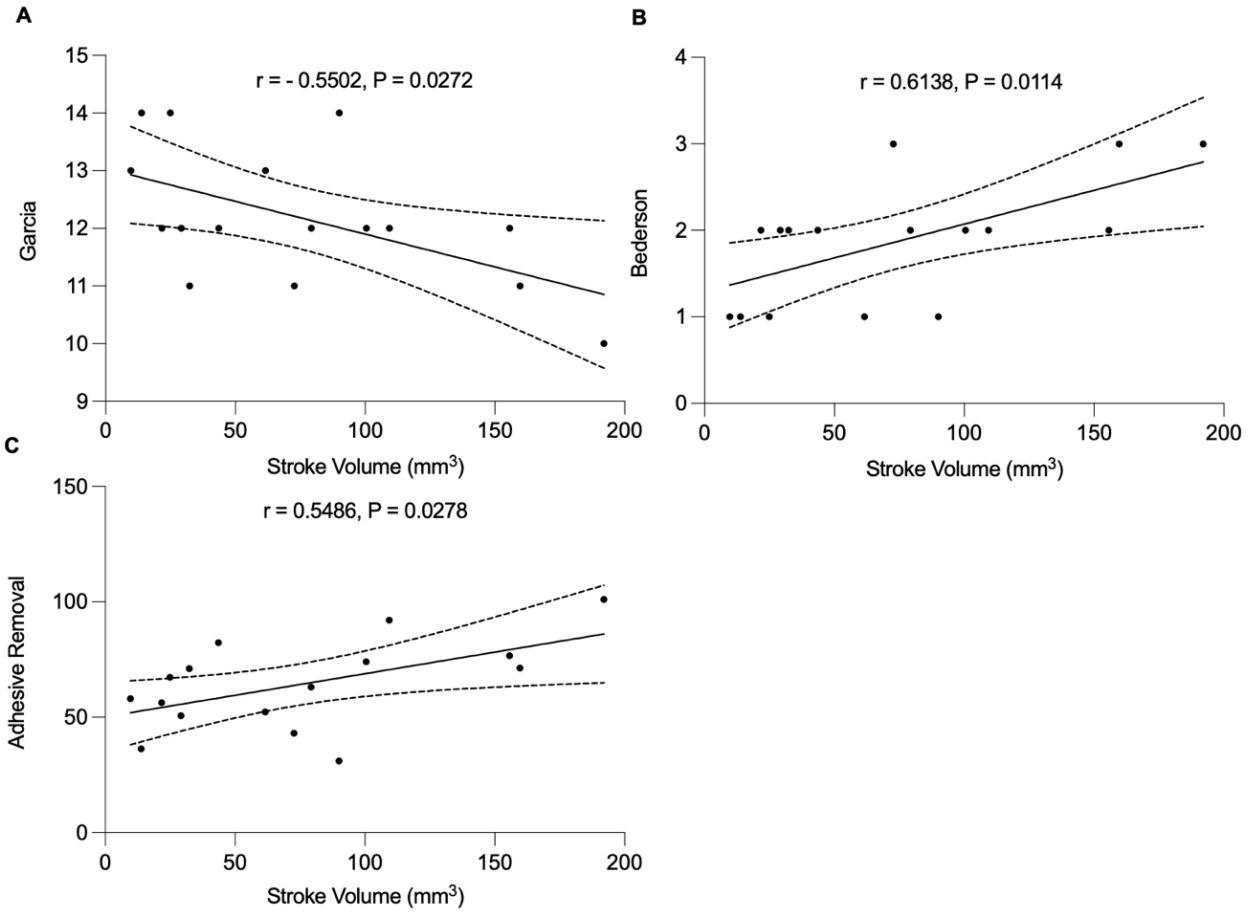

Figure 2.6 There is a modest correlation between stroke volume and neurological test results, with larger lesions leading to worse functional outcomes. **(A)** stroke volume vs. Garcia r=-0.5502, p=0.0272; **(B)** stroke volume vs. Bederson r=0.6138, p=0.0114; **(C)** stroke volume vs. time to notice of contralateral forepaw in adhesive removal test r=0.5486, p=0.0278. n=16 for all groups.

2.3.6 Rapamycin does not inhibit mTOR pathway activity at 3 days

For mTOR, the ratio of phosphorylated to total protein can indicate its level of pathway activity, where values over 1 indicate activation and values below 1 suggest an inhibitory effect. The ratio of phosphorylated mTOR (p-mTOR) to total mTOR did not differ significantly in the stroke animals treated with either vehicle or rapamycin (**Figure 2.7**; t-test; p=0.1880; vehicle: 0.9032 ± 0.1690; rapamycin: 0.5502 ± 0.1576).

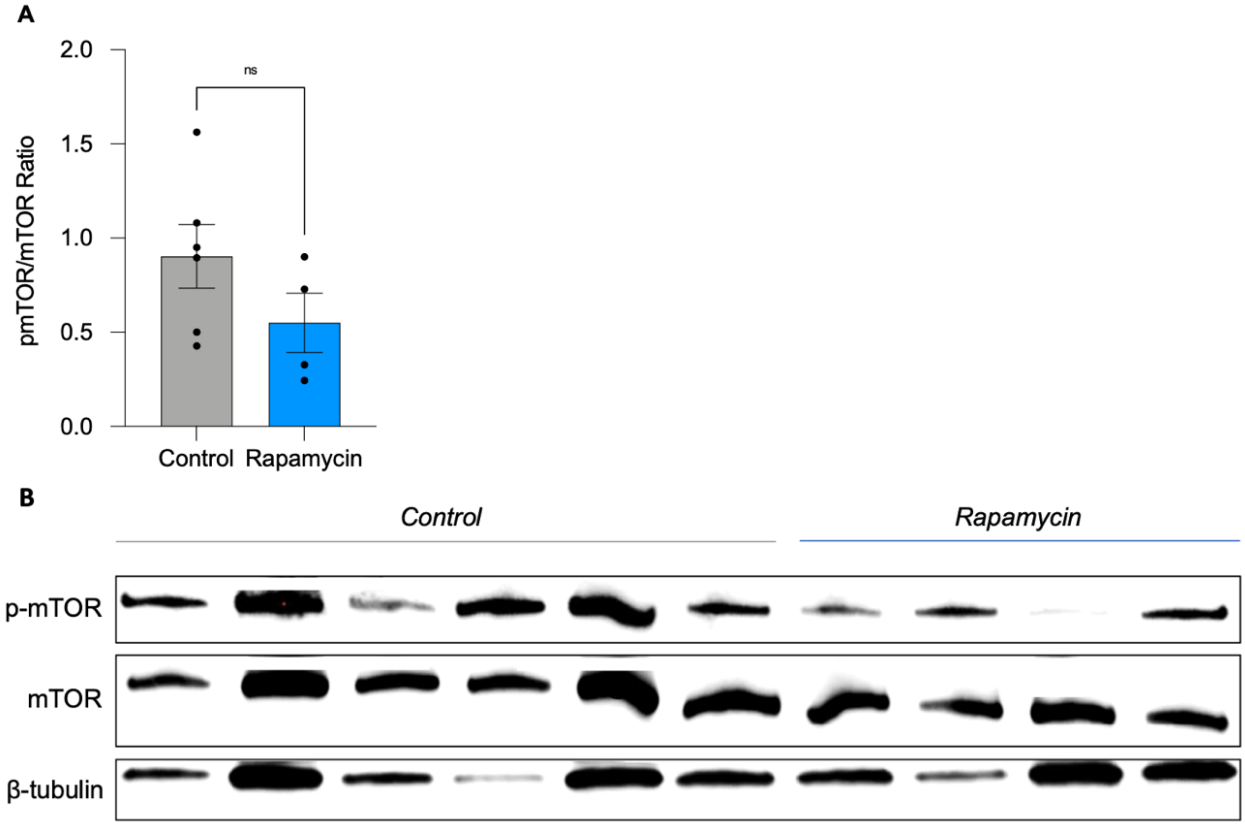

Figure 2.7 Rapamycin does not inhibit mTOR pathway activity at 3 days. At 3 days, brain tissue from the ipsilateral cortical lesion side from animals treated with rapamycin versus control was used to investigate mTOR activity (measured as pmTOR/mTOR ratio). Western Blot did not show a significant difference in mTOR activity in the lesion area 3 days following the rapamycin treatment. Data are mean ± SEM, n=6 for vehicle, and n=4 for rapamycin.

2.4 Discussion

This chapter explores the effects of post-ischemic mTOR inhibition on stroke outcome and BBB integrity in rats using MRI. The clinically approved mTORC1 inhibitor rapamycin improves reperfusion CBF immediately after recanalization and decreases stroke volume on day 3. Rapamycin also reduces somatosensory deficits in the stroke animals and tends to strengthen BBB breakdown, as shown by MRI 3 days following the insult, at which point mTORC1 activity is not downregulated anymore.

Rapamycin significantly increases CBF in the MCA territory immediately after recanalization of the occluded artery in rats. This result is in agreement with previous findings from our lab showing increased collateral perfusion in Wistar and spontaneously hypertensive rats following rapamycin administration 30 minutes following recanalization (Beard, Li et al., 2020). Similarly, Wang et al. showed that intraperitoneal rapamycin administration immediately after MCAo in Sprague Dawley rats increased the diameter of deep brain collaterals between the terminal branches of the PCA and MCA (Wang, Lin et al., 2019). Although these findings are encouraging, the timing of administration is of central importance, especially given the potential translational capacity of rapamycin, an already FDA-approved drug in clinical use. Therefore, administration of rapamycin at, as in this study, or after reperfusion, as done by Beard et al. (Beard, Li et al., 2020), is of greater clinical significance compared to studies in which the drug was administered before or at stroke induction (Guo, Feng et al., 2014, Sheng, Zhang et al., 2010, Su, Zhang et al., 2014, Yang, Zhong et al., 2015, Yin, Ye et al., 2012). The mechanism by which rapamycin exerts its beneficial vasodilatory effects is not fully elucidated, but some studies suggest an endothelial nitric oxide synthase (eNOS) dependent mechanism as seen in mouse models and isolated collateral vessels, a RhoA-dependent pathway, or direct reduction in calcium sensitivity

in smooth muscle cells (Beard, Li et al., 2020, Cipolla, Chan et al., 2014, Lin, Zheng et al., 2013, Palomares and Cipolla, 2011). Better understanding the pathway by which rapamycin exerts its beneficial effects, which cell types are primarily targeted, and which dose exerts optimal effects are essential questions for future studies.

In agreement with previous studies, T2w MRI showed that rats treated with rapamycin have a significantly smaller lesion volume at 3 days when compared to the vehicle-treated group (Meng, Fisher et al., 2004). The meta-analysis by Beard et al. on rapamycin treatment in rodent models of stroke included a global estimate of 30 comparisons and suggested that rapamycin significantly reduced stroke volume by 22% (Beard, Hadley et al., 2019). The current study exceeded the expected number with a mean reduction of 39% (P=0.0102).

MRI imaging didn't show a difference in diffusion or perfusion when rapamycin-treated animals were compared to control 3 days after the infarct. Further, no DPM was observed in either the treatment or control group, suggesting that there was no "salvageable" brain tissue at this time point, which might also explain why there was no effect in the treatment group. Literature suggests that DPM volume gradually decreases over time, with a stark decrease to a fourth of the initial penumbral region from 45 to 210 minutes after the occlusion (Bardutzky, Shen et al., 2005). The number of research papers determining a time-course of penumbral lesion evolvement in rat models after MCAo that goes beyond 24 hours is small (Bardutzky, Shen et al., 2005, Reid, Graham et al., 2012). Interestingly, studies have demonstrated substantial differences in acute ischemic lesion evolution between different rodent strains, which must be considered when assessing new therapeutic approaches on ischemic lesion evolution in an MCAo model.

Diagnostic stroke imaging aims to rapidly assess whether successful reperfusion would help the patient in functional recovery or whether the ischemic core is already too large, and

treatment would unnecessarily increase the risk of hemorrhagic transformation without making a clinical difference (Baron, 2018, Merino and Warach, 2010, Thrippleton, Backes et al., 2019). DWI is a commonly performed MRI sequence that assesses the diffusion movement of water molecules across the intracellular space, thereby identifying the core ischemic brain tissue (Duong and Fisher, 2004, Meng, Fisher et al., 2004). PWI imaging, on the other hand, allows estimation of CBF by using an intravascular tracer and serial imaging to quantify blood flow through the brain parenchyma (Canazza, Minati et al., 2014). While it may aid diagnosis and identification of the treatment target, its usefulness in the acute clinical setting has been under scrutiny, as PWI is time-consuming and data analysis can be challenging (Campbell, Weir et al., 2013, Hakimelahi, Yoo et al., 2012, Ma, Campbell et al., 2019).

The discrepancy between diffusion and perfusion (DPM) usually enlarges over time until it coincides with the perfusion deficit. Meng et al. characterized the evolution of mismatch in tMCAo-rats and found the first 2 hours after the reperfusion to be where the mismatch, and hence the potential to rescue potentially salvageable brain tissue, to be the greatest (Meng, Fisher et al., 2004). A study by Hakimelahi and colleagues showed that 100% of patients with DWI of less than 70ml had a major DPM of more than 100%, arguing that using DWI would suffice to identify patients that most likely benefit from reperfusion therapy without unnecessarily performing additional imaging sequences and eventually losing time to treatment (Hakimelahi, Yoo et al., 2012). For pre-clinical research, understanding how findings from different imaging modalities translate into animal models and how this relates to histological findings might allow us to draw more effective conclusions about the success of neuroprotective therapy and subsequent decisions on optimal treatment strategies.

BBB integrity shows a trend towards significance in being improved in rapamycin-treated animals versus control (P=0.0606). Post-hoc power calculations indicated that one additional animal would have been needed to observe a significant effect and reject the null hypothesis. Subtle impairment of BBB function has been reported as early as 30 minutes to 6 hours after ischemia-reperfusion (I/R) in a mouse model of t-MCAo, resulting in extravasation of small macromolecules (≤3kDa) from blood to brain parenchyma (Huang, Xue et al., 1999, Knowland, Arac et al., 2014, Shi, Zhang et al., 2016). After more than 3 hours, larger macromolecules (≥40kDa) leak through the barrier, contributing to high BBB leakage during this phase. Tight junction strands maintain their integrity during the hyperacute phase following the insult but lose their integrity at around 48 hours post-I/R (EA, H et al., 2018, Knowland, Arac et al., 2014, Rosenberg, Estrada et al., 1998) due to damage caused by cytokine-activated matrix-metalloproteinases MMP-3, MMP-9, and cyclooxygenase-2. The loss of tight-junction integrity during the acute phase of BBB breakdown is thought to be the leading cause of the development of vasogenic edema (Huang, Xue et al., 1999, Rosenberg, 2012). This study, however, did not find a significant difference in edema formation between the treatment and control group, as measured by T2w MR imaging. Post-hoc power calculations revealed that a sample size of 26 would have been required to observe a true effect.

Neurological and behavioral testing using the Bederson and Garcia scale and the adhesive removal test show significant improvements in the rapamycin-treated group versus control. Studying behavior is very important for evaluating the effectiveness of neuroprotective therapy to understand its impact on functional recovery. Three days is a sensible time point to assess potential long-lasting functional deficits and improvements with treatment, as it is not masked by acute deficits and weaknesses due to the surgery. The testing battery chosen in this chapter aimed to include both functional and neurological deficit scores that test broad motor control and overall

functional outcomes. Alternative tests to the selected battery of functional assessments include the cylinder test to assess asymmetry in spontaneous forelimb use, while the pasta-handling test determines fine motor skills that are expected to be asymmetrical after the stroke (Schaar, Brenneman et al., 2010). The Bederson and Garcia scales used in this study are the mainstay in composite scores, together with the modified Neurological Severity Score (mNSS) (Schaar, Brenneman et al., 2010).

Western blot of tissue from the ipsilateral cortical lesion shows that mTOR activity (as measured by pmTOR:mTOR ratio) at three days was not downregulated anymore, suggesting that rapamycin had already exerted the entirety of its effects. To the best of my knowledge, there is no information on mTOR activity after rapamycin treatment in rats after 3 days. However, my findings agree with Nalbandian et al.'s findings describing that rapamycin's half-life is 58 hours in mice (Nalbandian, Llewellyn et al., 2015). Conversely, Böttiger and colleagues reported rapamycin's half-life to be 79 hours in healthy males, suggesting a species-dependent difference in the biochemical effect and metabolism of the drug (Böttiger, Säwe et al., 2001). To test this, future studies should repeat the experiments but choose earlier study endpoints and compare the effects of rapamycin treatment on mTOR activity, the microvasculature, and stroke volume with MRI, histology, and functional outcome. Alternatively, to test whether the positive effects of rapamycin treatment are due to its mediating effects on the blood flow in the hyperacute phase, treatment could be started later to test whether this would lessen the impact. Better understanding the temporal pattern under which post-ischemic mTOR inhibition exerts its beneficial effects on stroke outcomes might increase our knowledge of the underlying physiological properties of rapamycin in the context of stroke and eventually optimize the treatment approach for a clinical setting.

In conclusion, these results show that inhibiting mTOR activity upon reperfusion with the FDA-approved drug rapamycin in an ischemic rat model immediately increases CBF. At 3 days, lesion volume was significantly smaller, and functional outcome improved. Interestingly, although rapamycin treatment tended to improve BBB integrity, it did not affect edema formation in the subacute stroke phase. Despite the lack of ongoing mTOR inhibition at 3 days rapamycin exerted a beneficial effect, suggesting that its effects are likely to be in the first hours post-stroke. This chapter confirms previous findings of rapamycin's positive impact on stroke outcome, reinforcing its potential as a neuroprotective drug for ischemic stroke patients. Further studies are required to investigate how rapamycin exerts its vasodilatory effect on the microvasculature.

Chapter 3: Effects of mTOR inhibition during ischemia *in vitro*

3.1 Introduction

The blood-brain barrier (BBB) - which is composed of brain endothelial cells (BECs), pericytes, astrocyte end-feet, and the basement membrane - regulates the passage of selected substances between the central nervous system (CNS) and circulatory system to maintain CNS homeostasis (Sharif, Jumah et al., 2018). Damage to the components and subsequent breakdown of the BBB is a consequence of stroke that exacerbates damage caused by the ischemic event (Haley and Lawrence, 2017, Iadecola, 2017). Thus, augmenting neurovascular health and BBB stability could slow disease progression and improve recovery. Until now, however, we only have a limited understanding of the temporal-spatial BBB alterations and the molecular, as well as functional effects of the different BBB components during and after ischemic stroke. Obtaining better insight is essential for developing new interventions to help recovery post-stroke.

Pericytes are vascular smooth muscle cells that share a basement membrane with the endothelium, where they help regulate the vascular compartment. Indeed, pericytes are involved in vessel maturation, BBB formation and maintenance, immune cell trafficking, and regulation of CBF (Beard, Brown et al., 2020, Beard, Li et al., 2020). Over the last decade, there has been an increasing interest in better understanding the physiological and pathological properties of pericytes in cerebral ischemia. Multiple studies have demonstrated pericyte contraction in response to the ischemic stroke (Hall, Reynell et al., 2014, Yemisci, Gursoy-Ozdemir et al., 2009). The reduced CBF despite recanalization, referred to as the “no-reflow” phenomenon, has been observed in both clinical stroke victims and various animal stroke models and is thought to be due to a combination of pericyte constriction and autoregulatory failure of the vasculature (Kloner, King et al., 2018, Yemisci, Gursoy-Ozdemir et al., 2009). Pericyte constriction and death in this

constricted ("in rigor") state significantly reduces vessel diameter and traps blood cells, such as erythrocytes and platelets, within the vessel lumen and is hypothesized to be caused by increased Ca^{2+} sensitivity during the early post-ischemic reperfusion phase (Hall, Reynell et al., 2014, Yemisci, Gursoy-Ozdemir et al., 2009). The pathways involved in this phenomenon are in part mediated by mTOR (Hadley, Beard et al., 2019). Cipolla et al. have shown that a rapid increase in intracellular Ca^{2+} due to hypoxia prompts the activation of the Rho GTPase/ROCK/myosin light chain (MLC) pathway, which amplifies calcium sensitivity and subsequent pericyte constriction (Cipolla, Chan et al., 2014). Correspondingly, a study from our group has recently shown that rapamycin treatment reduced pericyte constriction by a Rho-A-dependent mechanism (Beard, Couch et al., 2022). Further, Beard et al. have recently demonstrated that mTOR inhibition enhanced pericyte relaxation through an eNOS-dependent mechanism (Beard, Li et al., 2020). An additional pathway that is known to be responsive to hypoxic changes in smooth muscle cells is through the activation of protein kinase C (PKC), though no study so far has tested yet whether this is also mediated by mTOR and, therefore, whether the positive effects of rapamycin treatment on pericytes are also mediated through this pathway. Future research should examine the pathways leading to pericyte constriction in response to hypoxia and how they can be targeted pharmacologically to improve post-ischemic CBF and stroke outcomes.

In addition to functionality, hypoxic injury has also been shown to impact cellular viability and metabolism in pericytes, which is an indispensable aspect to consider for testing potential neuroprotective therapies. Only a few studies and the work in this thesis have focused on investigating the molecular effects of rapamycin treatment on cells of the BBB (Beard, Couch et al., 2022, Beard, Li et al., 2020, Sheng, Zhang et al., 2010), whereas the majority of literature examined the effects of rapamycin treatment on the viability of neurons (Dutta, Rutkai et al., 2015,

Fletcher, Evans et al., 2013). Mitochondrial function, which can be assessed through ATP generation, in addition to cellular viability, can give a reasonable estimate of the molecular health of cells (Sims and Muyderman, 2010). Hypoxia-inducible factor-1 (HIF1α), a master transcription factor that drives cellular adaptions to hypoxia, has been shown to have opposing effects on metabolic and functional outcomes. While a recent study has demonstrated that HIF1α stabilization improved post-ischemic recovery and reduced metabolic dysfunction in a diabetic heart (da Luz Sousa Fialho, Purnama et al., 2021), pericyte HIF1α has been shown to drive BBB disruption and worsen acute ischemic stroke outcome (Tsao, Baumann et al., 2021). Indeed, many *in vivo* and *in vitro* studies have shown that activated HIF1α signaling had undesirable vascular effects and disrupted endothelial function, increased BBB permeability, and modified BBB cell-cell interactions, respectively (Al Ahmad, Taboada et al., 2011, Engelhardt, Al-Ahmad et al., 2014, Xin, Rodrigues et al., 2013, Yan, Zhang et al., 2012, Yan, Zhou et al., 2011). Investigating the diverse and multicellular effects of cerebral ischemia and how downregulation of mTOR's metabolic function alters these effects is crucial.

The importance of intercellular communication and interactions between pericytes and BECs in health and disease has been described in detail, and pericyte loss has been shown to not only lead to BBB disruption but also endothelial barrier dysfunction (Armulik, Abramsson et al., 2005). Pericytes, for example, release angiopoietin-1 (Ang-1), which aids integrity but is also associated with increased occludin expression in BECs, which helps prevent endothelial dysfunction (Dohgu, Takata et al., 2005, Hori, Ohtsuki et al., 2004). BECs are essential for brain health by forming an integral part of the BBB, altering vascular tone, and having paracrine functions by releasing matrix metalloproteinases (MMPs), brain-derived neurotrophic factor (BDNF), insulin-like growth factor 1 (IGF-1), and vascular endothelial growth factor (VEGF)

(Andjelkovic, Xiang et al., 2019). During a stroke, BECs lose their tight junction proteins, release MMPs and drive a proinflammatory state with reduces cellular integrity and a weakens the BBB (Sandoval and Witt, 2008), which ultimately exacerbates parenchymal injury and contributes to worse stroke outcome (Andjelkovic, Xiang et al., 2019).

Therapeutic approaches aim to find treatment options that help restore endothelial function following stroke and address the increased risk of hemorrhagic transformation following reperfusion therapy, which is thought to be mainly mediated by disrupted endothelial cell function (Andjelkovic, Xiang et al., 2019). A range of studies have aimed to target endothelial cell survival and BBB integrity by strengthening the expression of tight junction proteins, such as occludin-5 (Cui, Zhang et al., 2013), reducing endothelial transcytosis (Haley and Lawrence, 2017, Knowland, Arac et al., 2014), and degeneration of the endothelial cells themselves (Arai, Lok et al., 2011, Hancock, Bennani et al., 2004).

The timing of therapy in *in vitro* stroke studies to investigate the neuroprotective properties of different agents varies significantly, making it harder to compare one study to another. Therefore, a more consistent approach in treatment administration, preferably after the insult to be of clinically translational value, has been largely missing. Furthermore, the importance of describing the effects of ischemic stroke on individual cell types and investigating potential treatment options to combat the adverse downstream effects, an optimal adjunct treatment to reperfusion would have protective effects on multiple cell types. This chapter will use a multimodal approach to study the molecular and functional effects of mTOR inhibition in an *in vitro* model of stroke of two central cellular components of the ischemic landscape.

3.1.1 Aims

The aims of this chapter are, therefore:

1. To determine the effects of rapamycin treatment on the contractility of pericytes subjected to OGD/R injury.

2. To examine whether the PKC pathway partly mediates the relaxing effect of mTOR inhibition on smooth muscle cells.

3. To investigate whether rapamycin changes the adhesion of endothelial cells that were subjected to OGD/R.

4. To understand how rapamycin affects the molecular health of pericytes and endothelial cells by investigating ATP production and survival.

5. To study the impact of the timing of the treatment in relation to the hypoxic injury by administering rapamycin before, at, or after the acute OGD intervention and comparing the results.

3.2 Materials and methods

3.2.1 Cell culture

All experiments were conducted under standardized incubation conditions (37°C, 5% CO_2 in humidified air). Cell culture flasks and multi-well plates were obtained from Corning (USA).

3.2.1.1 Human pericytes

Human brain vascular pericytes (HBVP; ScienCell Research Laboratories, USA) were grown on flasks and plates coated with 1% poly-l-lysine hydrobromide (MW >70.000) in pericyte medium (ScienCell) including 1% growth supplement (ScienC sell), 1% P/S, and 2% FCS. HBVPs were used before passage 10, and immunohistochemistry (IHC) showed no difference between earlier and later passage numbers.

3.2.1.2 Human endothelial cells

Human cerebral microvascular endothelial cells (hCMEC/D3; Millipore, USA) were obtained from Professor Ignacio Romero (The Open University, Milton Keynes, UK). hCMEC/D3 cells were cultured before passage number 35, cultured on flasks and plates coated with 6.25% rat-tail collagen, and grown in endothelial basal medium (EBM2, Lonza) supplemented with the following components that were obtained from the same manufacturer: 0.04% hydrocortisone, 0.1% gentamicin, and amphotericin-B (GA) cocktail, 0.1% ascorbic acid, 0.1% heparin, 0.1% recombinant human fibroblast growth factor β (rhFGFβ), 0.1% vascular endothelial growth factor (VEGF), 0.1% R3 insulin-like growth factor-1 (R3-IGF-1), 0.1% recombinant human epidermal growth factor (rhEGF). Heparin was not included in the growth factor reduced medium, and the following doses were adjusted: rhFGFβ to 0.1%, VEGF, R3-IGF, and rhEGF to 0.025%.

3.2.1.3 Oxygen glucose deprivation

For OGD experiments, cultures were transferred to an anaerobic chamber (Coy, USA) containing a gas mixture of 0% O_2, 5% CO_2, and 95% N_2. Plates were washed 3 times and immersed in the deoxygenated glucose-free medium for pericytes (ScienCell) or endothelial cells (Lonza), respectively, that was pre-equilibrated in the hypoxic chamber overnight to obtain a pO_2 of less than 10 mmHg. Controls were treated identically but under normoxic conditions and with the standard glucose-containing medium described above. The chosen length of OGD was 3 hours, followed by 24 hours of reperfusion (see **Figure 3.2**).

3.2.2 Rapamycin treatment

Cells were treated with rapamycin (Sigma Aldrich, diluted in laboratory grade ethanol) or vehicle (ethanol only). The standard dose used was 10 nM, equivalent to the concentration used in the *in vivo* experiments (see **Chapter 2**, 250 μg/kg), diluted in the corresponding media. First, a dose-response curve experiment was conducted comparing the doses of 1 nM, 10 nM, and 100 nM of rapamycin. Second, the effects of 10 nM rapamycin treatment at three different time points were studied, 1 hour before OGD, at the time of OGD, or immediately after the OGD experiment, respectively. The timeline of the experiment is outlined in **Figure 3.1**.

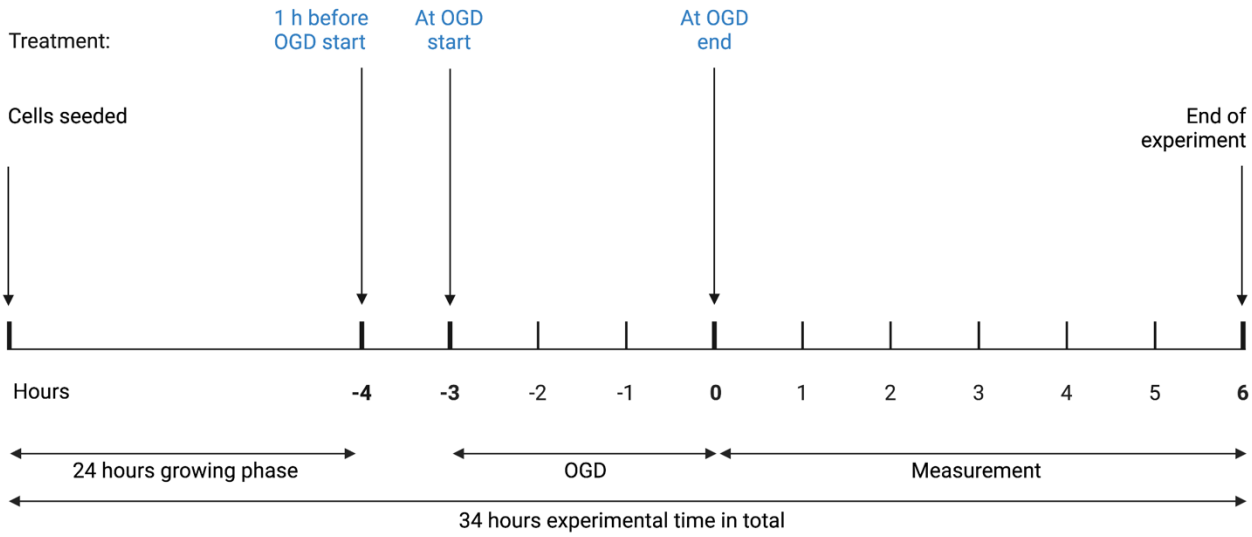

Figure 3.1 Experimental timeline of 10 nM rapamycin treatment. Cells were seeded and grown for 24 hours. To investigate how the timing of treatment affected pericyte contractility, 3 timings of rapamycin application were compared to the vehicle: 1 hour before the start of OGD (-4 hours); at the beginning of OGD (-3 hours); immediately after OGD (0 hours). Measurements of pericyte contractility were started at the end of OGD and lasted for 6 hours, after which the experiment was ended.

3.2.3 Pericyte contractility: iCelligence electrical impedance

The iCelligence electrical impedance assay was used to measure pericyte contractility (ACEA Biosciences, USA). This assay consists of cell plates with gold-coated electrodes (E-plates) and an iCelligence reading device. Cells grown on the surface form an electrical circuit that can be quantitatively assessed and changes upon cell proliferation or alteration in their contractility (contractility leads to increased pressure on the surface detected by the plate reader as an increase in electrical impedance, i.e., the opposition of a circuit to current, measured in ohm).

These changes were then expressed as a cell index (CI) based on the following formula:

$$CI\ (t) = \frac{\boldsymbol{I}t - \boldsymbol{I}t0}{\boldsymbol{Z}n}$$

where **I**t is the impedance measured at frequency fn and at time t, **I**t0 is the impedance measured at frequency fn and at time t0, thereby representing and controlling for background impedance in the absence of cells, and **Z**n is the frequency factor of fn in ohms. Therefore, the ohm units cancel out, and CI is a unitless parameter defining relative impedance. The impedance instrument was kept under standardized incubation conditions (37°C, 5% CO_2 in humidified air). In this particular experiment, pericytes were grown on 8-well E-plates coated with 1% poly-l-lysine hydrobromide (MW >70.000) in a pericyte medium (see above), with a seeding density of 10,000 cells/well (approximately 16,000 cells/cm^2) and left to adhere for 24 hours. OGD intervention and rapamycin treatment used the identical protocol as described above. iCelligence data were analyzed using the RTCA Software Lite (310100210, Agilent). Data are presented as normalized cell index (a unitless parameter, automatically derived from recorded impedance values in iCelligence software and normalized to the last time point immediately preceding reperfusion).

3.2.4 Endothelial cell adhesion: iCelligence electrical impedance

To measure endothelial adhesion, which is indicative of paracellular barrier strength as described by Hucklesby et al. (Hucklesby, Anchan et al., 2021), the impedance of an endothelial monolayer was measured, as previously described (Hucklesby, Anchan et al., 2021). hCMEC/D3 (The Open University, Milton Keynes, UK) cells were cultured before passage number 35 and grown in EBM2 as described above. Cells were plated onto 8 well E-plates with a seeding density of 120,000 cells/well (approximately 250,000 cells/cm^2) and left to adhere for 24 hours until CI had stabilized. As with pericytes, data of endothelial cells are presented as normalized cell index (a unitless

parameter, automatically derived from recorded impedance values in iCelligence software and normalized to the last time point immediately preceding reperfusion).

3.2.5 Lactate dehydrogenase assay

Using a lactate dehydrogenase (LDH) assay (CytoTox 96 Non-Radioactive Cytotoxicity Assay, Promega, UK), cell death was estimated by a fluorescent reaction between tetrazolium salt and LDH, an enzyme released upon cell lysis. Cells were plated and treated in duplicates, and the test kit was used according to the manufacturer's instructions. Briefly, supernatant samples were collected, and a tetrazolium salt LDH substrate was added and kept under constant agitation at room temperature for 30 minutes, at which point a stop solution was added. Within 30 minutes, the light absorption of the red formazan product was measured at 492nm using a SPECTROstar Omega microplate reader (BMG Labtech, Germany). Cell death was calculated as follows:

$$\%\ cell\ death = \frac{\boldsymbol{AB}Spent - \boldsymbol{BG}Spent}{(\boldsymbol{AB}Spnt - \boldsymbol{BG}Spnt) + (\boldsymbol{AB}Lys - \boldsymbol{BG}Lys)} = \frac{Released\ LDH}{Total\ LDH}$$

where AB is sample light absorbance, BG is background light absorbance (from cell culture medium or lysis buffer without cells), Spnt is supernatant, and Lys is lysate.

3.2.6 ATP production assay

Luminescent ATP Detection Assay Kit (abcam113849, Abcam, Cambridge, MA) was used to detect cellular adenosine triphosphate (ATP) levels, as the ATP's reaction with the added firefly's luciferase and luciferin produces a light signal that is proportional to the ATP concentration. Cells were plated in triplicates, and the assay kit was used according to the manufacturer's instructions. After the treatment, cells were treated with the compounds before the detergent was added, and cells were incubated for 5 minutes at room temperature (RT). After, substrate solution was added

and incubated for another 5 minutes at RT, before the plate was dark-adapted for 10 minutes before the luminescence was measured using SPECTROstar Omega microplate reader (BMG Labtech, Germany).

3.2.7 Protein kinase C assay

To assess rapamycin's effect on protein kinase C (PKC) activity, the assay kit ab139437 (Abcam, Cambridge, MA) was used according to the manufacturer's instructions. In brief, wells with three different kinase concentrations in the presence of 10 nM rapamycin or control (ethanol) were prepared. ATP was added for 90 minutes at 30°C to activate the kinase reaction. Phospho-specific antibody was added to each well for an incubation period of 60 minutes at RT, after which horseradish peroxidase (HRP) conjugated secondary antibody was added for 30 minutes at RT. The wells were then washed, and the 3,3',5,5'-tetramethylbenzidine (TMB) solution was added for 30-60 minutes, or until a color change was visible. Stop solution was added, and the absorbance was measured on a microplate reader at an optical density (OD) of 450 nm using SPECTROstar Omega microplate reader (BMG Labtech, Germany).

3.2.8 Immunocytochemistry

HBVP or hCMEC cells were fixed with 4% formaldehyde in phosphate-buffered saline (PBS) for 10 minutes, washed three times with PBS, permeabilized with 0.5% Tween in PBS for 5 minutes, and rewashed 3 times with PBS (all at room temperature). They were then blocked in 10% donkey serum (DkS; Life Technologies) in PBS for 1 hour at RT and incubated in primary antibody in 1% DkS in PBS at 4°C overnight (**Table 3.1**). Secondary antibody (donkey anti-primary species conjugated to Alexa Fluor 488) diluted in 1% DkS in PBS was applied for 1 hour at RT before

being counterstained with Alexa Fluor 594-conjugated phalloidin (approximately 30 nM; Life Technologies) and 4',6-diamidino-2-phenylindole (DAPI, 1 μM; Sigma). The microscope glass slides were mounted with glass coverslips using anti-fade fluorescence mounting medium (Dako, USA) and imaged immediately after with a Nikon Eclipse E1000 epifluorescence microscope with 40 x air objectives and appropriate excitation/emission filters (Nikon, Japan).

Table 3.1: Primary antibodies used for Immunocytochemistry

°1 Antibody	Manufacturer	Species	Concentration
PDGFRβ	R&D Systems (af385)	Goat anti-human	1:100
NG2	Abcam (ab20156)	Mouse anti-human	1:100
Desmin	Abcam (ab15200)	Rabbit anti-human	1:200
CD13	Abcam (ab498001)	Rabbit anti-human	1:200
CD31	R&D Systems (af3629)	Goat anti-human	1:100
GFAP	Abcam (ab53554)	Goat anti-human	1:500
Iba-1	Abcam (ab5076)	Goat anti-human	1:500
αSMA	Abcam (ab7817)	Mouse anti-human	1:200
HIF1α	Cell Signalling (3716S)	Rabbit anti-human	1:500
Claudin-5	Thermo Fisher (35-1600)	Rabbit anti-human	1:200
Occludin	Abcam (ab31721)	Rabbit anti-human	1:200
Talin	Abcam (ab71333)	Rabbit anti-human	1:200
ZO-1	Abcam (ab216880)	Rabbit anti-human	1:200
VE-cadherin	Abcam (ab33168)	Rabbit anti-human	1:200

3.2.8.1 HIF1α staining

The hypoxia-inducible factor-1 (HIF1) activity in response to OGD and with and without the presence of rapamycin treatment was assessed using fluorescent staining. Pericytes were subjected to 3 hours of OGD or normoxia. At the start of OGD, cells were either treated with 10 nM of rapamycin or control (ethanol). After 3 hours of OGD or control experiments, pericytes were immediately fixed with 4% formaldehyde in PBS for 10 minutes. Pericytes subjected to OGD were fixed in the hypoxic chamber to avoid confounding any uncontrolled oxygen in the treatment group. Pericytes were then washed with PBS 3 times, permeabilized with 0.5% Tween in PBS for 5 minutes, and rewashed 3 times with PBS (all at RT). Cells were blocked in 10% donkey serum in PBS for 1 hour at RT and incubated in HIF1α primary antibody (PA1-16610, Invitrogen) in PBS at 4°C overnight. Secondary antibody (donkey-anti rabbit conjugated to Alexa Fluor 488) diluted in PBS was applied for 1 hour at RT before counterstaining with DAPI (1 μM; Sigma) for

10min. The microscope glass slides were mounted with glass coverslips using anti-fade fluorescence mounting medium (Dako, USA) and imaged immediately after with a Nikon Eclipse E1000 epifluorescence microscope with 40 x air objectives and appropriate excitation/emission filters (Nikon, Japan). From every experimental group, four images each from two separate slides were taken (n=4 per group).

HIF1α staining was described as either being cytosolic or translocated to the nucleus. The fraction of nuclear/cytosolic HIF1α signal was averaged (n=8 per group), and the % of HIF1α nuclear translocation over DAPI was calculated.

3.2.9 Statistical analysis

Statistical analysis was carried out in Prism 6 (Graphpad, USA). For iCelligence results, a one-way ANOVA test was used for dose-response analysis, and unpaired Student's t-tests were used for comparing different treatment time points. For LDH, ATP, and PKC results, Student's t-test was used to compare rapamycin treatment to the vehicle group. If the D'Agostino revealed that normality was not met, the Mann-Whitney test was used instead. α of 0.05 was considered statistically significant, and the results are presented as mean ± standard error of the mean (SEM).

3.3 Results

3.3.1 The duration of OGD and reperfusion were chosen to be 3 hours and 24 hours, respectively

To determine the optimal duration for OGD and reperfusion in hCMECs, cells were subjected to different lengths of OGD and reperfusion. The dose-response curve of hCMECs shows that both increasing lengths of OGD and reperfusion proportionally increased cell death, with 3 hours of OGD and 24 hours of reperfusion producing a considerable amount of cell death that is not exceedingly high (**Figure 3.2**). For consistency, HBVPs were subjected to the same duration of OGD and reperfusion.

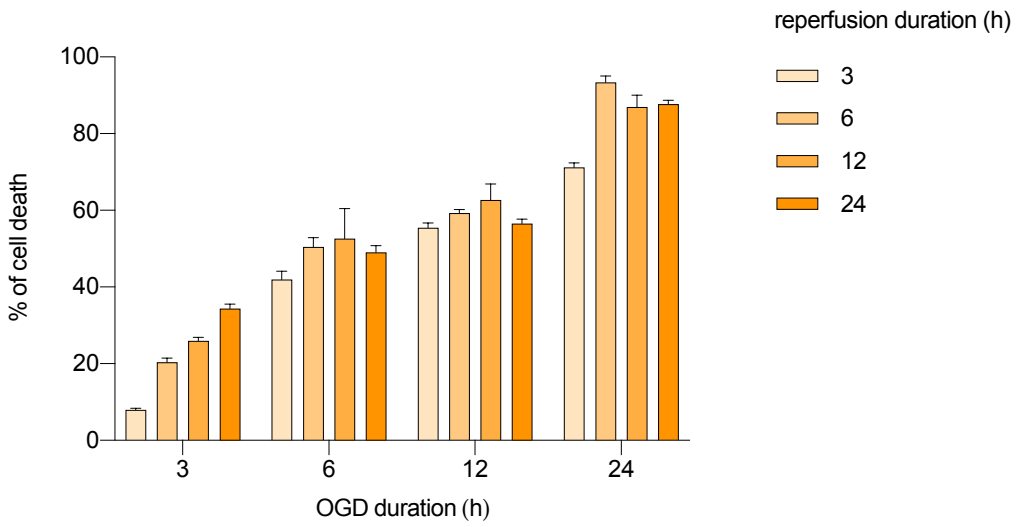

Figure 3.2 Determination of the optimal duration for OGD and reperfusion in hCMECs. The effect of different lengths of OGD and reperfusion on cell death in hCMECs was studied. Increasing lengths of OGD and reperfusion increased cellular death in a proportional manner. 3 hours of OGD and 24 hours of reperfusion were chosen for the experiment in this chapter for both hCMECs and HBVPs.

3.3.2 IHC staining of HBVPs confirms their pericyte lineage

Fluorescent microscopy showed that the HBVPs expressed clear staining for pericyte markers PDGFRβ, NG2, desmin, and CD13 (**Figure 3.3**). In contrast, HBVPs were negative for endothelial cell (CD31), astrocyte (GFAP), microglia (Iba-1), and epithelial (αSMA) markers, respectively, indicating that the pericyte population was not contaminated with non-pericyte cell lineages (**Figure 3.4**).

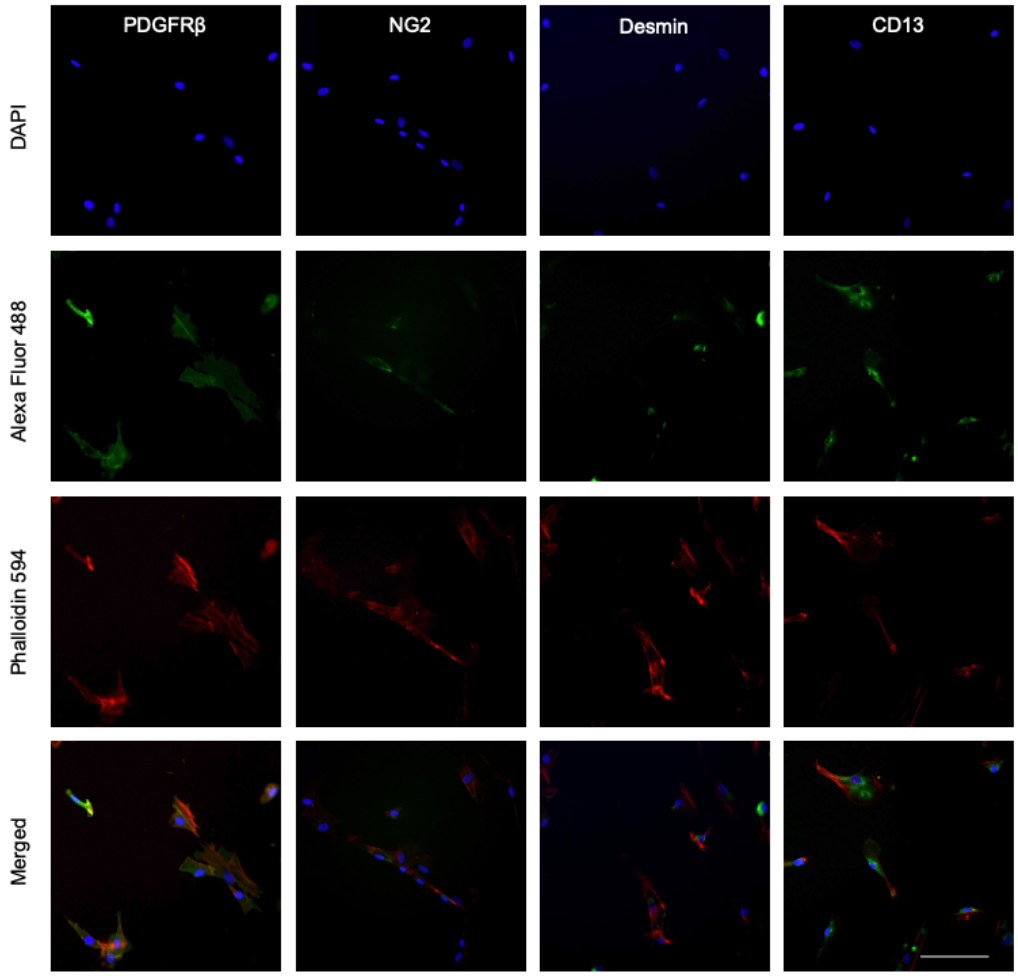

Figure 3.3 IHC staining of HBVPs confirms their pericyte lineage. Immunohistochemical characterization of HBVPs with pericyte markers shows that the used HBVP cells express typical pericyte markers. Immunocytochemistry for PDGFRβ, NG2, desmin, and CD13 in the green channel, nuclear (DAPI), and cytoskeletal (phalloidin 594) counterstaining in the blue and red channels, respectively. Scale bar represents 100 µm.

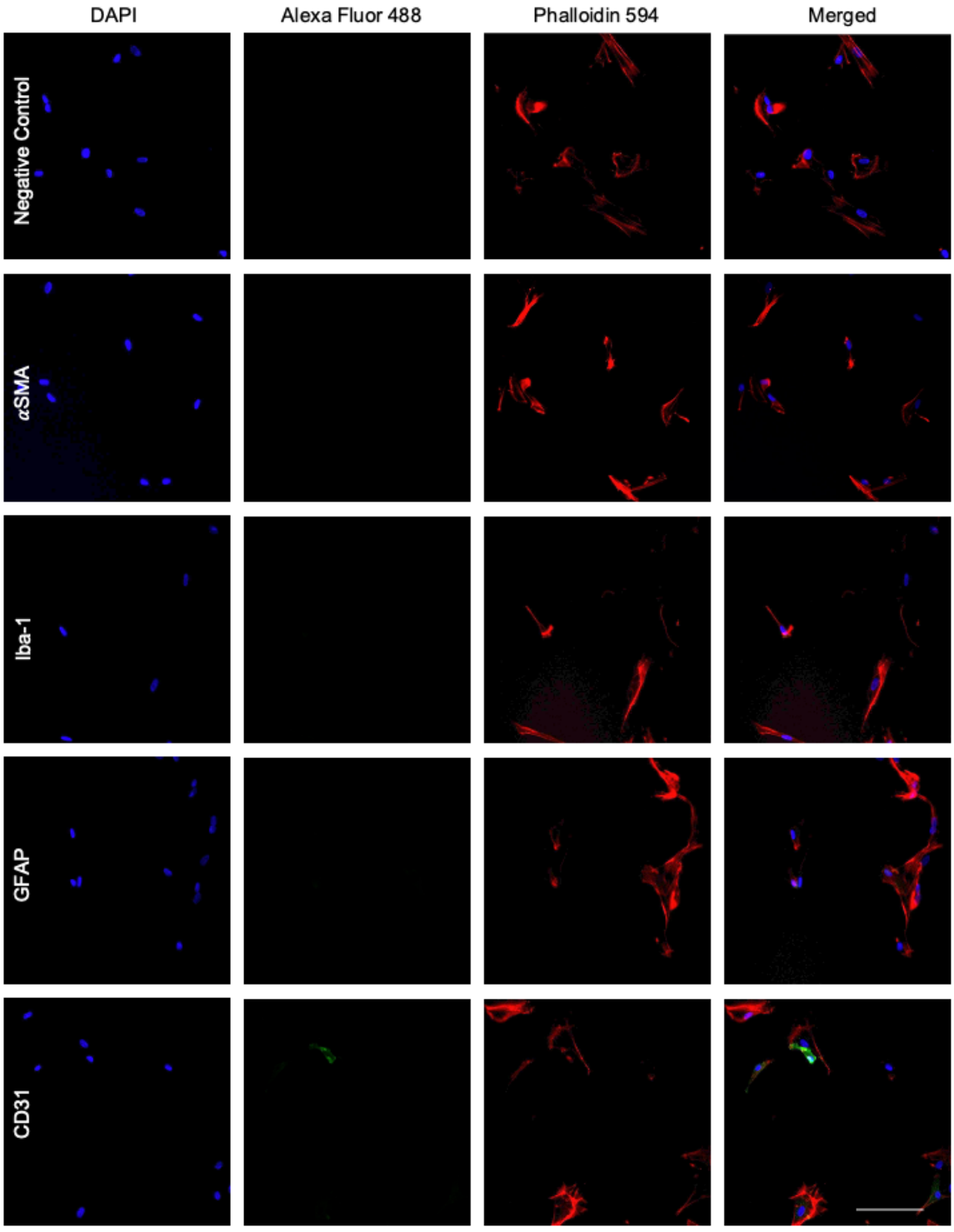

Figure 3.4 IHC shows that the used HBVPs are negative for non-pericyte marker expression. Immunocytochemistry for CD31, GFAP, Iba-1, αSMA in the green channel, nuclear (DAPI), and cytoskeletal (phalloidin 594) counterstaining in the blue and red channels, respectively. Scale bar represents 100 µm.

3.3.3 Rapamycin induces a dose-dependent relaxation of pericytes

The findings from chapter 2, which showed that rapamycin improved CBF post-ischemia (see **Chapter 2, Figure 2.1**), were taken further to better understand rapamycin's effect on individual cells of the BBB, specifically pericytes and endothelial cells. HBVP were grown on the iCelligence device for 24 hours before treatment with either a medium containing rapamycin (1 nM, 10 nM, 100 nM) or a vehicle-containing medium, and the cellular response during the first 6 hours following drug application from hours 24–30 was measured (**Figure 3.5 (A)**). Calculation of the relative slope, which was normalized and compared to vehicle, shows that rapamycin induces a dose-dependent relaxation of pericytes (**Figure 3.5 (B)**; one-way ANOVA; relative slopes of cells treated with 1 nM, 10 nM, 100 nM of rapamycin: 1.082 ($p=0.0012$), 1.102 ($p<0.0001$), 1.149 ($p<0.0001$), respectively).

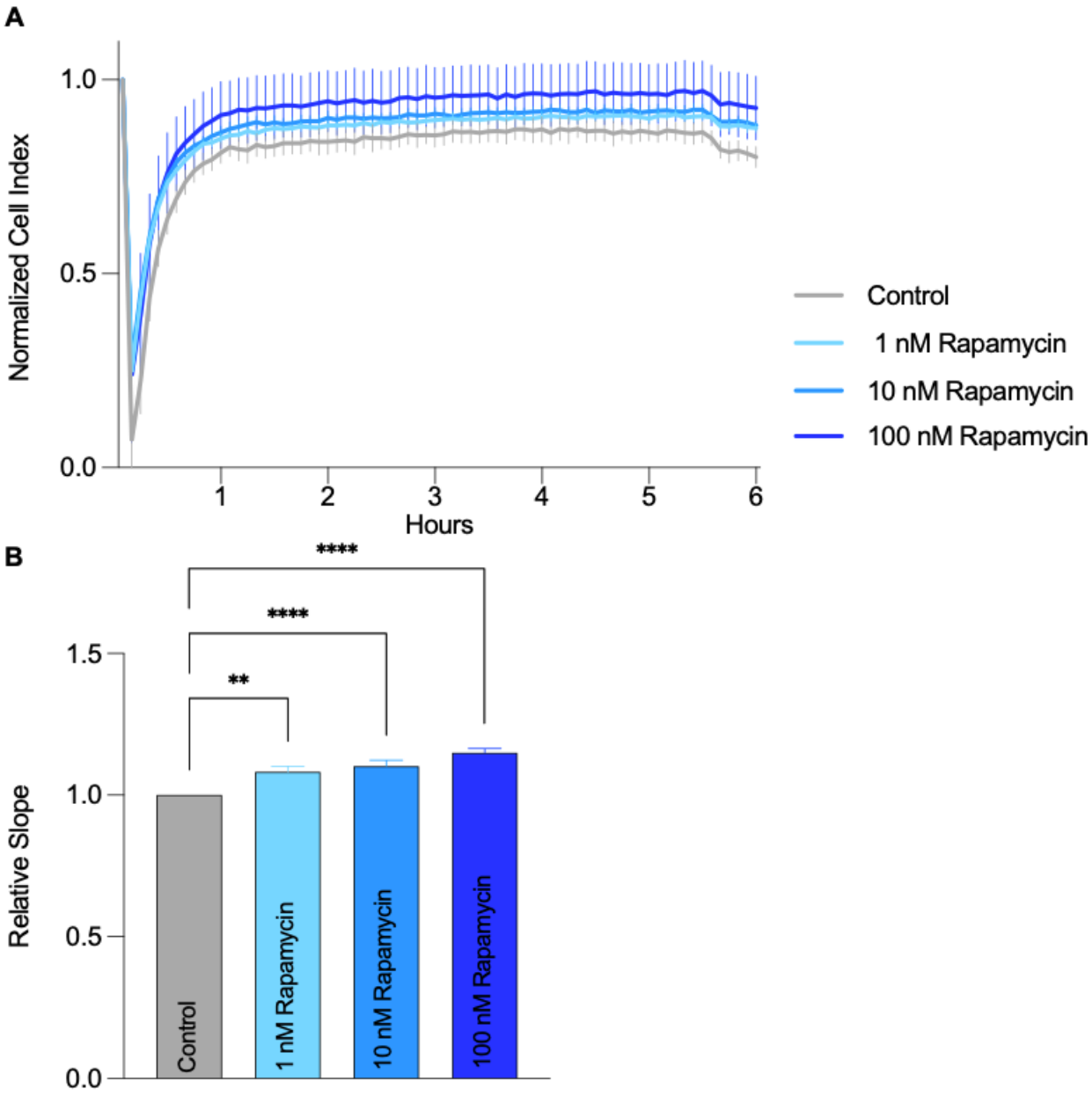

Figure 3.5 Electrical impedance measurement of relaxation of HBVP in response to rapamycin. HBVP were grown on the iCelligence device for 24 hours before treatment with either a medium containing rapamycin (1 nM, 10 nM, 100 nM) or a vehicle-containing medium at 24 hours. **(A)** Measurement during the first 6 hours following drug application shows a prolonged relaxation in response to rapamycin. **(B)** Calculation of the relative slope from the time of drug administration at 24 hours for the following 6 hours was normalized and compared to vehicle. Data are mean ± SEM, n=3-4; **p<0.01, ****p<0.0001, when compared to vehicle controls. n=8 wells/treatment group.

3.3.4 Rapamycin treatment after OGD relaxes pericytes

Next, electrical impedance measurements of the contractile state of HBVP in response to OGD deprivation (OGD) and 10 nM rapamycin were taken. To investigate how the timing of treatment affected pericyte contractility, 3 timings of rapamycin application were compared to the vehicle: 1 hour before the start of OGD; at the beginning of OGD; immediately after OGD. Calculation of the relative slope, which was normalized and compared to the vehicle, shows that rapamycin treatment before and at the start of OGD induced pericyte contraction. Contrary to that, rapamycin treatment immediately after OGD, at the point of "reperfusion", induced pericyte relaxation compared to pericytes treated with vehicle (**Figure 3.6 (B), (D), (F)**; t-test; relative slopes of cells treated with 10 nM rapamycin pre, at, and post OGD: 0.9186 ($p<0.0001$), 0.6502 ($p<0.0001$), 1.118 ($p<0.0001$), respectively).

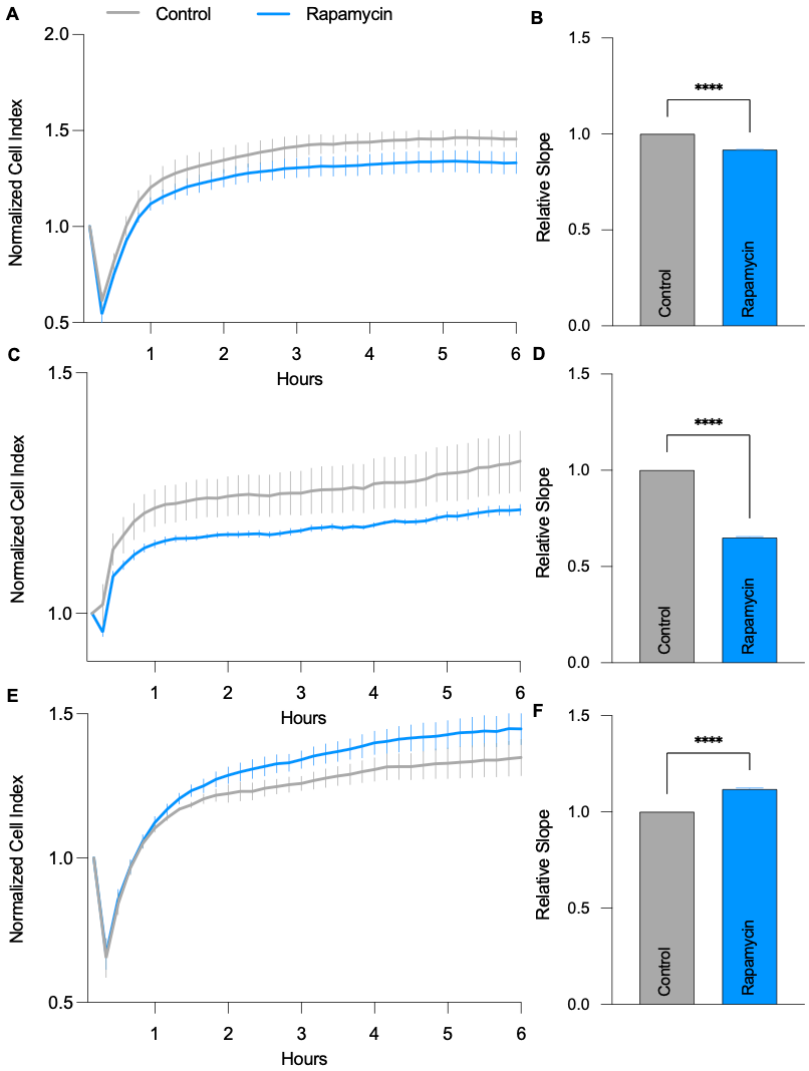

Figure 3.6 Electrical impedance measurement of relaxation of HBVP in response to OGD/R and 10 nM rapamycin. HBVP were grown on the iCelligence device for 24 hours before the intervention and treatment with either 10 nM rapamycin or a vehicle-containing medium. Measurements start immediately preceding the end of OGD at 28 hours and last for 6 hours. Relative slopes were normalized and compared to the vehicle-treated cells. **(A)** Rapamycin was applied 1 hour before OGD. **(B)** Calculation of the relative slope shows increased pericyte contractility in rapamycin-treated cells compared to vehicle-treated cells. **(C)** Rapamycin was applied at the start of OGD. **(D)** Calculation of the relative slope shows increased pericyte contractility in rapamycin-treated cells compared to vehicle-treated cells. **(E)** Rapamycin was applied immediately after OGD at the start of reperfusion. **(F)** Calculation of the relative slope shows relaxation of pericytes treated with rapamycin compared to vehicle-treated cells. Data are mean, ****$p<0.0001$, when compared to vehicle controls. n=4 wells/treatment group.

3.3.5 Rapamycin reduces PKC activity

The next step was to test the hypothesis of whether rapamycin induces its relaxing effect on pericytes to post hypoxia in part by blocking PKC activity, which is essential for calcium sensitization and further smooth muscle cell contraction. Serial dilutions of PKC were treated with either 10 nM of rapamycin or control before PKC was chemically activated with ATP. The absorbance, which is proportional to the activity level of PKC, was then measured using a plate reader. Wells containing 1 μl of PKC treated with 10 nM rapamycin yielded significantly lower PKC activation than control. Wells containing 0.048 and. 0.0023 μl of PKC, 10 nM of rapamycin treatment did not show an effect (**Figure 3.7**; t-test; vehicle vs 10 nM rapamycin at 1 μl PKC ($p=0.0238$; vehicle: 0.3351 ± 0.02514; rapamycin: 0.2241 ± 0.02701), 0.048 μl PKC ($p=0.5793$), and 0.0023 μl PKC ($p=0.3696$)).

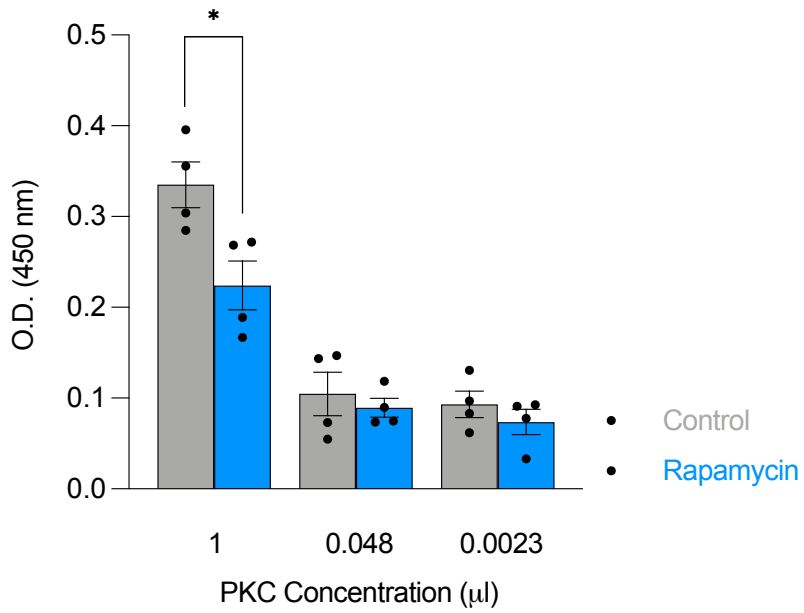

Figure 3.7 Rapamycin reduces PKC activity. Wells containing 1 µl of PKC treated with 10 nM rapamycin yielded significantly lower PKC activation than control, while no effect was observed at lower PKC concentrations. Serial dilutions of PKC were treated with either 10 nM of rapamycin or control, and the absorbance, which is proportional to the activity level of PKC, was then measured using a plate reader at an optical density (OD) of 450 nm. Data are mean ± SEM, * $p<0.05$, when compared to vehicle-treated cells. n=4/group in all groups.

3.3.6 Rapamycin negatively impacts HBVP survival and ATP production in response to OGD/R injury

To investigate the effect of rapamycin treatment on metabolic health, LDH and ATP assays were performed. Cells were subjected to 3 hours of OGD and treated with 10 nM of rapamycin either before (labeled as “pre”), at the start of (labeled as “at”), or after (labeled as “post”) the OGD intervention. After OGD, cells underwent 24 hours of reperfusion, at which point measurements were taken. Rapamycin treatment 1 hour before OGD induction did not show any effect on cell death (**Figure 3.8 (A)**; t-test; p=0.0827) or ATP production (**Figure 3.8 (B)**; t-test; p=0.5149). Rapamycin treatment at the start of OGD reduced ATP production (**Figure 3.8 (B)**; t-test; p=0.0304; vehicle: 0.4222 ± 0.02558; rapamycin: 0.3346 ± 0.007617) but did not affect cellular survival (**Figure 3.8 (A)**; t-test; p=0.5871). Rapamycin treatment after OGD increased cell death (**Figure 3.8 (A)**; t-test; p=0.0085; vehicle: 18.48 ± 0.5926; rapamycin: 21.59 ± 0.2522) while not affecting ATP production (**Figure 3.8 (B)**; t-test; p=0.6838**)**.

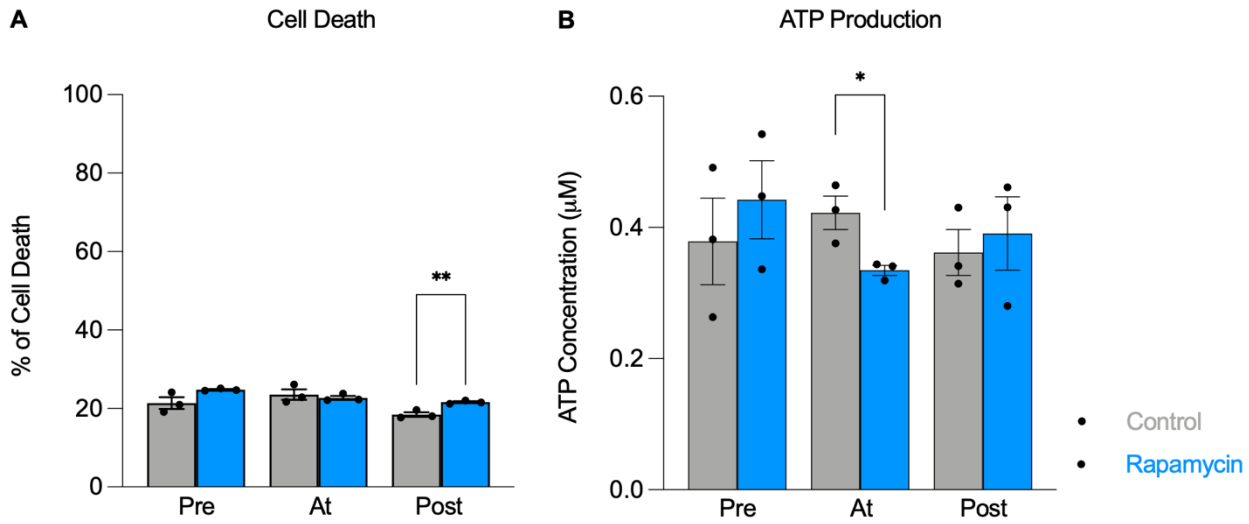

Figure 3.8 Rapamycin negatively impacts HBVP survival and ATP production in response to OGD/R injury. The effect of rapamycin on pericyte cell death and ATP production in response to OGD/R intervention was examined. Pericytes were treated with rapamycin at 3 distinct time points: 1 hour before, at the start of, or immediately after the OGD intervention, which lasted for 3 hours. After OGD, cells underwent 24 hours of reperfusion, at which time point measurements were taken. (**A**) % of cell death, (**B**) ATP concentration. Data are mean ± SEM, *p<0.05, **p<0.01, when compared to vehicle-treated cells. n=3/group in all groups.

3.3.7 Nuclear translocation of HIF1α in response to OGD is halted by rapamycin treatment

To determine the molecular effects of OGD and rapamycin treatment on the translocation and subsequent activity of HIF1α in pericytes, fluorescent staining was performed. Pericytes were subjected to either 3 hour-OGD or normoxia, and at the start of OGD, cells were either treated with 10 nM of rapamycin or control (ethanol). After the OGD or control intervention, cells were immediately fixed and stained for HIF1α. HIF1α staining was described as either being cytosolic or translocated to the nucleus, whereby the fraction of nuclear/cytosolic HIF1α signal was averaged (n=8 per group), and the % of HIF1α nuclear translocation over DAPI was calculated.

3-hour OGD but not the control normoxia intervention induced the translocation of HIF1α to the nucleus (**Figure 3.9 (B)**; t-test; p=0.0286; normoxia; 0.000 ± 0.000; rapamycin: 98.64 ± 1.358). Treatment with 10 nM rapamycin but not the control treatment halted the nuclear translocation of HIF1α in response to hypoxia (**Figure 3.9 (B)**; t-test; p=0.0286; vehicle: 98.64 ± 1.358; rapamycin: 9.243 ± 5.803).

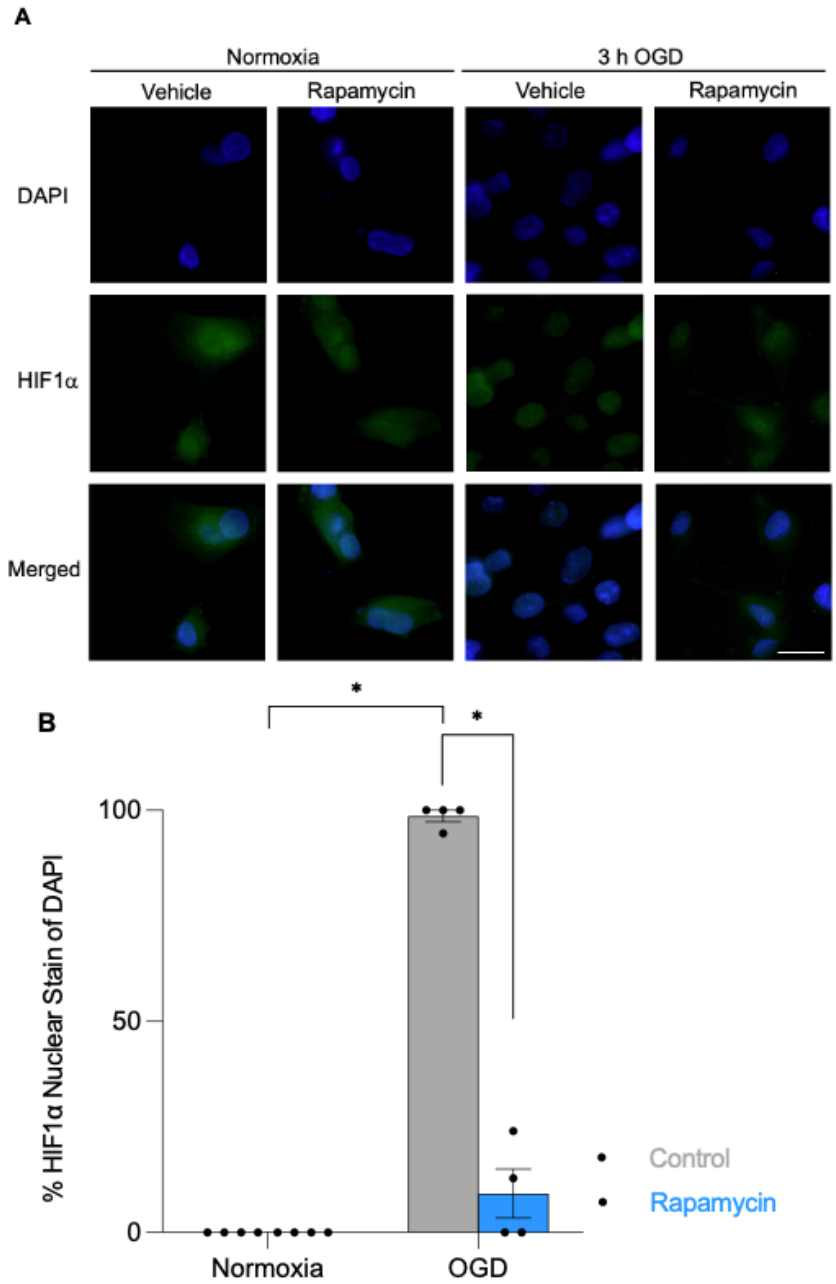

Figure 3.9 Nuclear translocation of HIF1α in response to OGD is halted by rapamycin treatment. Pericytes were subjected to either 3 hour-OGD or normoxia, and at the start of OGD, cells were either treated with 10 nM of rapamycin or control (ethanol). After the OGD or control intervention, cells were immediately fixed and stained for HIF1α. **(A)** Representative image showing the expression of HIF1α in the cytosol or translocated to the nucleus. Scale bar represents 400 μm. **(B)** The fraction of nuclear/cytosolic HIF1α signal was averaged, and the % of HIF1α nuclear translocation over DAPI was calculated. Data are mean ± SEM, *$p<0.05$, when compared to vehicle-treated cells. n=4/group for all groups.

3.3.8 IHC staining of hCMECs identifies typical endothelial cell markers

Fluorescent microscopy showed that the hCMECs expressed clear staining for endothelial cell markers and their tight junction proteins claudin-5, occludin, talin, desmin, ZO-1, and VE-cadherin (**Figure 3.10)**.

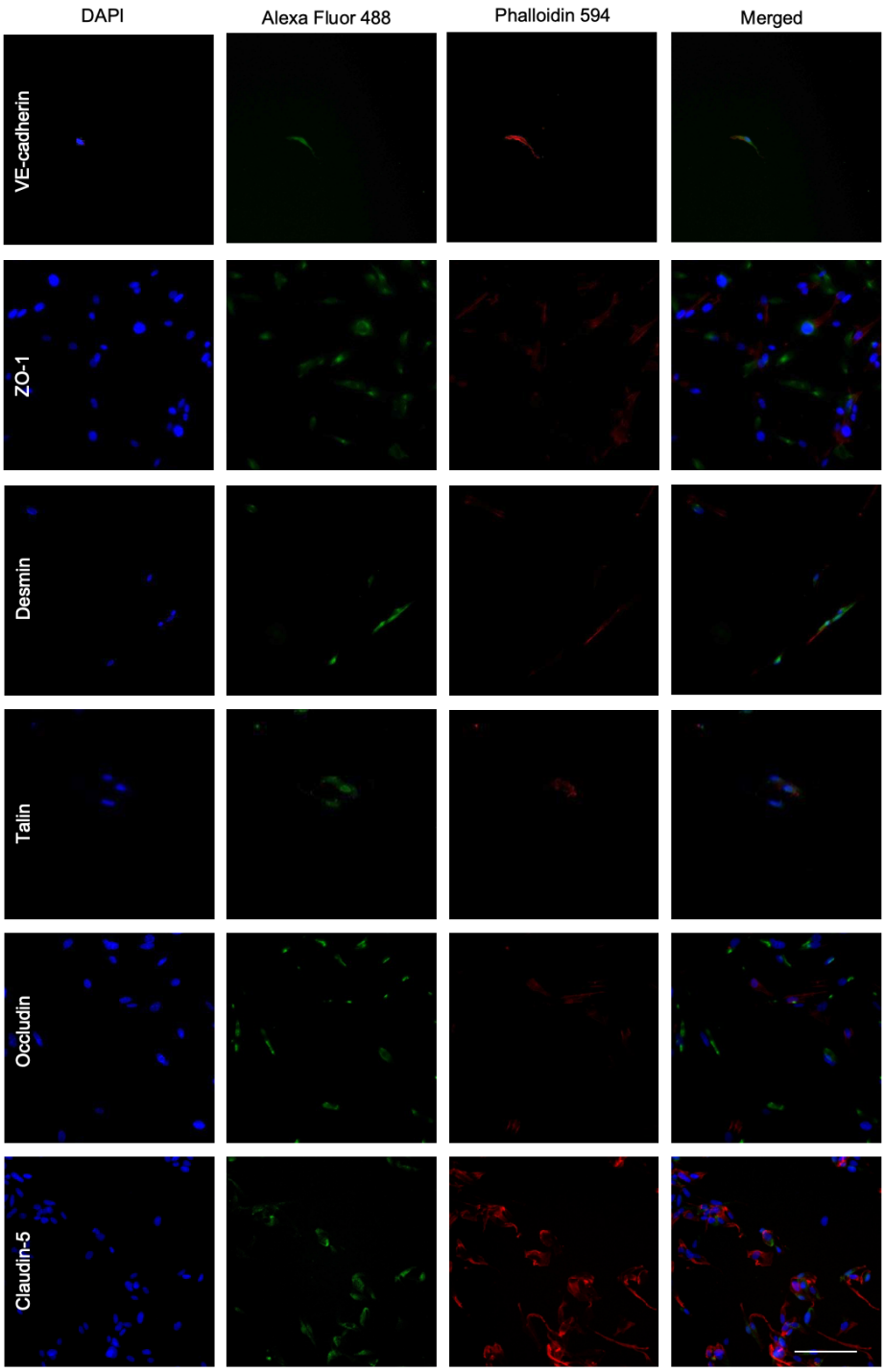

Figure 3.10 IHC staining of hCMECs identifies typical endothelial cell markers. Immunohistochemical characterization of hCMECs and their tight junction proteins: Claudin-5, occludin, talin, desmin, ZO-1, VE-cadherin in the green channel, nuclear (DAPI) and cytoskeletal (phalloidin 594) counterstaining in the blue and red channels, respectively. Scale bar represents 100µm.

3.3.9 High-dose rapamycin treatment strengthens hCMEC adhesion

The iCelligence device was used to evaluate rapamycin's effect on the integrity of the endothelial monolayer, where an increased resistance reflects increased adhesion of the endothelial cells. hCMEC were grown on the iCelligence device for 24 hours before treatment with either a medium containing rapamycin (1 nM, 10 nM, 100 nM) or a vehicle-containing medium, and the cellular response during the first 6 hours following drug application from hours 24–30 was measured (**Figure 3.11 (A)**). Calculation of the relative slope, which was normalized and compared to vehicle, suggests that rapamycin induces a dose-dependent increase in hCMEC adhesion, although only the application of 100 nM rapamycin produced a large enough effect to be significantly different (**Figure 3.11 (B)**; one-way ANOVA; relative slopes of cells treated with 1 nM, 10 nM, 100 nM of rapamycin: 1.111 ($p=0.9300$), 1.190 ($p=0.7408$), 1.707 ($p=0.0058$), respectively)).

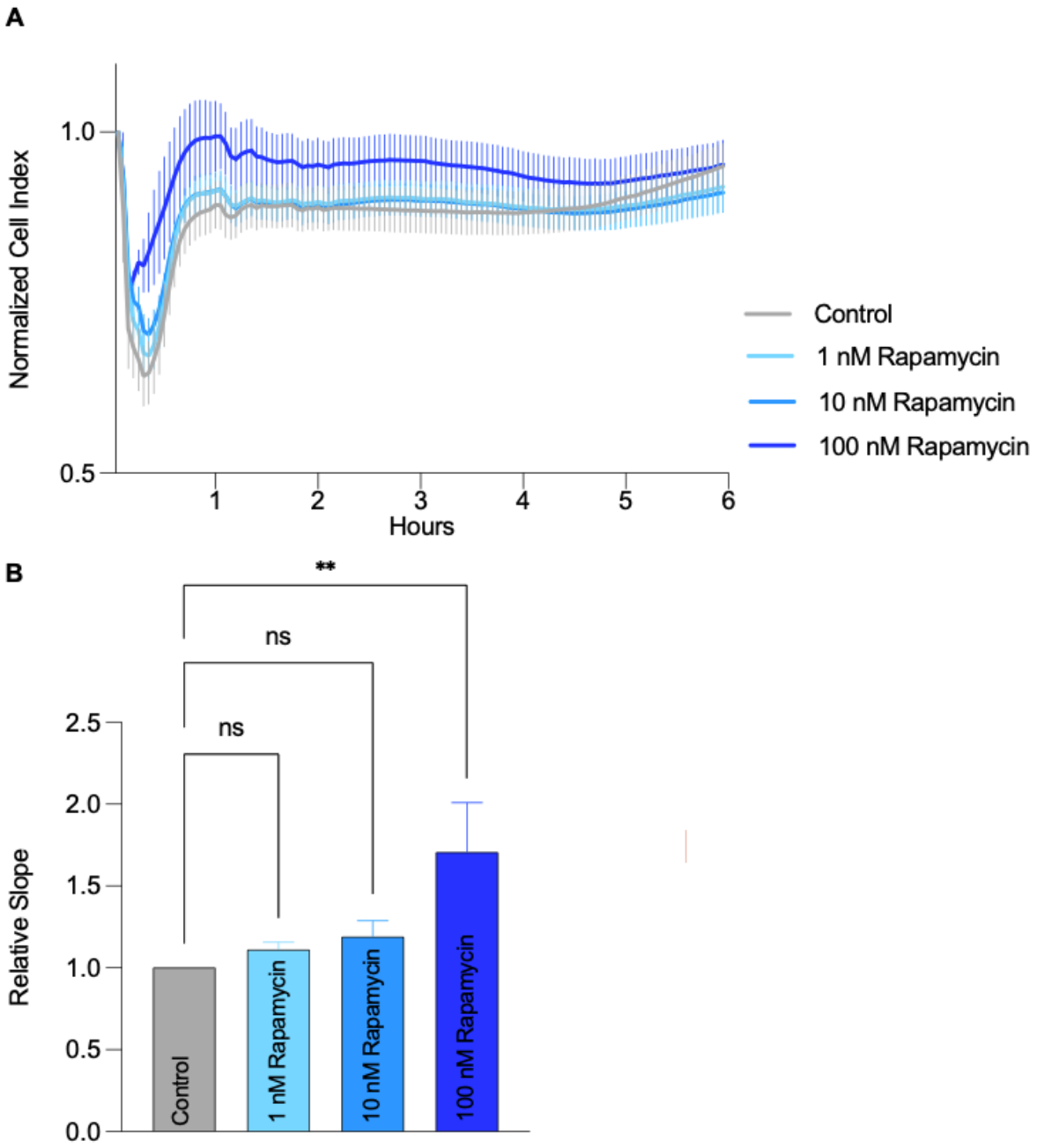

Figure 3.11 Electrical impedance measurement of adhesion of hCMEC in response to rapamycin. hCMEC were grown on the iCelligence device for 24 hours before treatment with either a medium containing rapamycin (1 nM, 10 nM, 100 nM) or a vehicle-containing medium at 24 hours. **(A)** Measurement during the first 6 hours following drug application shows increased adhesion of hCMEC in response to rapamycin. **(B)** Calculation of the relative slope from the time of drug administration at 24 hours for the following 6 hours was normalized and compared to vehicle. Data are mean ± SEM; n=4; **p<0.01, when compared to vehicle controls. n=8 wells/treatment group.

3.3.10 Rapamycin treatment at and after OGD increases adhesion of hCMEC

Next, electrical impedance measurements of the hCMEC adhesion in response to OGD deprivation (OGD) and 10 nM rapamycin were taken. To investigate how the timing of treatment affected hCMEC adhesion, 3 timings of rapamycin application were compared to the vehicle: 1 hour before the start of OGD; at the beginning of OGD; immediately after OGD. Calculation of the relative slope normalized and compared to the vehicle shows that rapamycin treatment at the start of and following OGD enhanced endothelial cell adhesion. Contrary to that, rapamycin treatment 1 hour before OGD, reduced endothelial cell adhesion compared to vehicle (**Figure 3.12 (B), (D), (F)**; t-test; relative slopes of cells treated with 10 nM rapamycin pre, at, and post OGD: 0.7412 ($p<0.0001$), 3.346 ($p<0.0001$), 1.239 ($p<0.0001$), respectively).

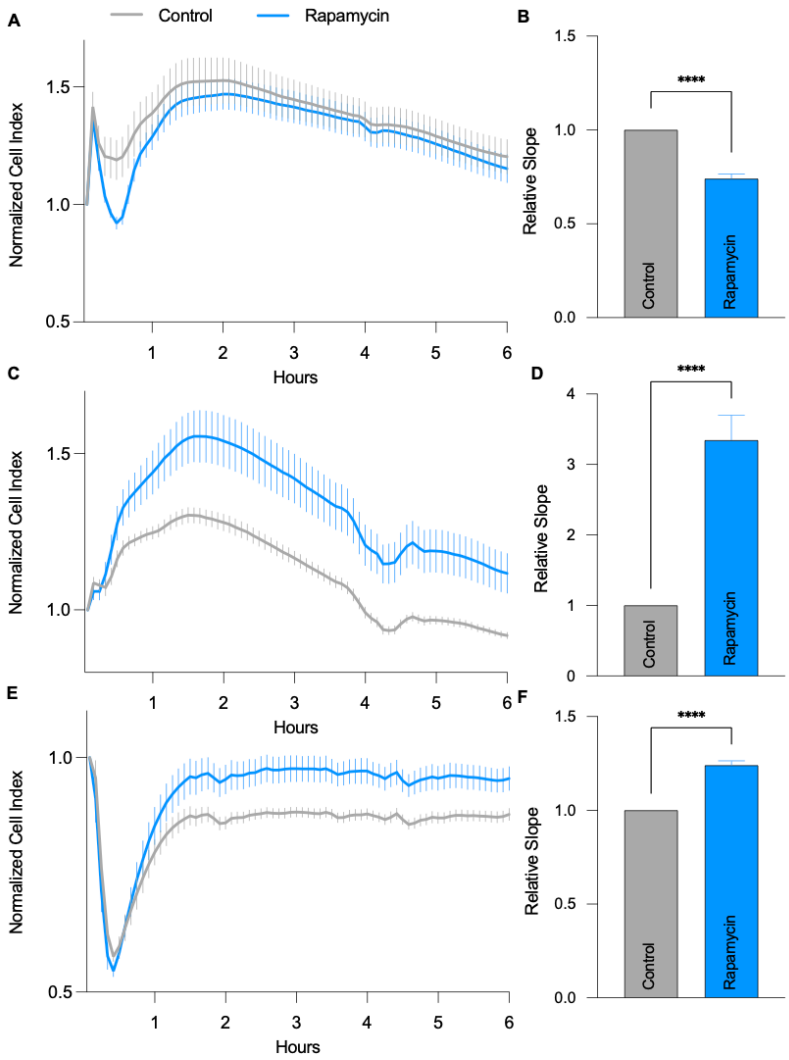

Figure 3.12 Electrical impedance measurement of adhesion of hCMEC in response to OGD/R and 10 nM rapamycin. hCMEC were grown on the iCelligence device for 24 hours before the intervention and treatment with either 10 nM rapamycin or a vehicle-containing medium. Measurements start immediately preceding the end of OGD at 28 hours and last for 6 hours. Relative slopes were normalized and compared to the vehicle-treated cells. **(A)** Rapamycin was applied 1 hour before OGD. **(B)** Calculation of the relative slope shows reduced adhesion in rapamycin-treated cells compared to vehicle-treated cells. **(C)** Rapamycin was applied at the start of OGD. **(D)** Calculation of the relative slope shows increased adhesion in rapamycin-treated cells compared to vehicle-treated cells. **(E)** Rapamycin was applied immediately after OGD at the start of reperfusion. **(F)** Calculation of the relative slope shows increased adhesion in rapamycin-treated cells compared to vehicle-treated cells. Data are mean ± SEM, ****p<0.0001, when compared to vehicle controls. n=8 wells/treatment group.

3.3.11 Rapamycin reduces survival of hCMEC in response to OGD/R injury

To investigate the effect of rapamycin treatment on metabolic health, LDH and ATP assays were performed. Cells were subjected to 3 hours of OGD and treated with 10 nM of rapamycin either before (labeled as "pre"), during (labeled as "at"), or after (labeled as "post") the intervention. After OGD, cells underwent 24 hours of reperfusion, at which time point measurements were taken. Rapamycin treatment 1 hour before OGD induction, at the start of OGD, as well as after OGD increased cell death (**Figure 3.13 (A)**; t-test; "pre" p=0.0082; vehicle: 49.07 ± 3.064; rapamycin 71.02 ± 3.309; "at" p=0.0170; vehicle: 60.19 ± 2.218; rapamycin 71.22 ± 1.707; "post" p=0.0003; vehicle: 46.42 ± 1.517; rapamycin 65.26 ± 0.5893). Rapamycin treatment showed no effect on ATP production when treated either pre, at, or post the OGD/R intervention (**Figure 3.13 (B) "**pre" p=0.9715; "at" p=0.0572; "post" p=0.0952).

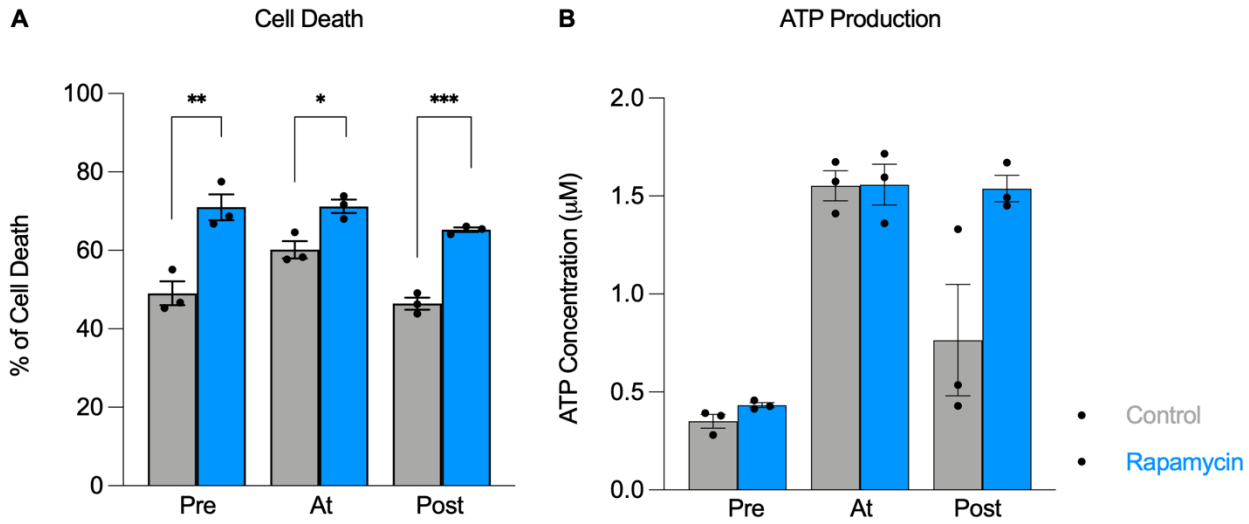

Figure 3.13 Rapamycin reduces survival of hCMEC in response to OGD/R injury. The effect of rapamycin treatment on endothelial cell death and ATP production in response to OGD/R was examined. Endothelial cells were treated with rapamycin at three different time points: 1 hour before, at the start, or immediately after the OGD intervention that lasted for 3 hours. After OGD, cells underwent 24 hours of reperfusion, at which time point measurements were taken. (**A**) % of cell death. (**B**) ATP concentration. Data are mean ± SEM, *p<0.05, **p<0.01, ***p<0.001, when compared to vehicle-treated cells. n=3/group for all groups.

3.4 Discussion

There is a pressing need for treatment options that target the BBB after cerebral ischemia as it plays a significant role in the pathogenesis of the disease. This chapter shows that the clinically approved mTORC1 inhibitor rapamycin exerts significant effects on the functional and molecular health of both pericytes and endothelial cells, which are two major components of the BBB.

Importantly, this chapter highlights the fact that rapamycin treatment of BBB cells in culture can result in both beneficial and detrimental effects. Specifically, that treatment at the end of OGD exerted a beneficial effect, and pre-treatment exerted harmful effects in both cell types, while treatment applied at the same time as OGD resulted in pericyte constriction while increasing endothelial cell adhesion. The importance of treatment timing was further reinforced with the ATP and LDH assays describing the metabolic health of the respective cell types in response to OGD/R and rapamycin treatment, showing more harmful than beneficial effects of mTORC1 inhibition.

These findings support the existing literature suggesting that mTORC1 activity under non-hypoxic conditions is essential to cellular health, and inhibition can lead to disease (Liu and Sabatini, 2020), while under austere conditions, such as those occurring during an ischemic stroke, mTORC1 inhibition might be beneficial (Hadley, Beard et al., 2019). During phases of overall cellular health with enough nutrient supply, mTORC1 is upregulated, promoting an anabolic cellular state and fulfilling critical cellular functions such as the production of proteins, lipids, nucleotides, and ATP while limiting autophagic breakdown of cellular components (Liu and Sabatini, 2020). It is under times of starvation when mTOR is downregulated, and its resulting catabolic state signaling energy deficiency and a state of emergency, where remaining efforts are shifted towards autophagy, cellular defense, and reducing the loss of surplus energy, all to the expense of reduced metabolic functioning and overall cellular health (Liu and Sabatini, 2020).

This energy-sensing switch is naturally switched into a 'catabolic' state during an ischemic insult, promoting cellular self-defense, and rapamycin is known to further support this catabolic state although, prolonged phases of cellular deficiency prohibit normal cellular functioning (Sabatini, 2017). Here, rapamycin treatment of cells before OGD induction led to worse cellular function and molecular health – presumably as the cells were in a state of relatively good health - while augmenting mTOR downregulation at or after OGD led to overall protective effects – when the cells were metabolically struggling. This highlights the importance of translational considerations about neuroprotective stroke therapy and the optimal timing of the treatment.

Studies have shown that pericytes contribute to stroke pathogenesis by impacting BBB integrity and regulating CBF (Gautam and Yao, 2018). Prior research found that ischemia-induced pericyte contraction contributes to incomplete reperfusion following recanalization due to pericyte-constriction in response to ischemia (termed "no-reflow phenomenon"), thereby aggravating ischemic injury (Cipolla, Chan et al., 2014, Hall, Reynell et al., 2014, Yemisci, Gursoy-Ozdemir et al., 2009). Additionally, pericytes have immunological properties and contribute to angiogenesis, scar formation, and fibrosis, highlighting the critical roles that pericytes play in ensuring normal brain functioning (Gautam and Yao, 2018). Treatment options focusing on pericytes for brain health have therefore the difficult job of targeting the negative aspects of pericyte functions in disease while promoting the beneficial (Beard, Brown et al., 2020, Beard, Li et al., 2020, Hall, Reynell et al., 2014, Yemisci, Gursoy-Ozdemir et al., 2009) . Work in chapter 2 confirmed findings by Beard and colleagues showing that treating rats that had undergone stroke surgery with rapamycin significantly improved blood perfusion to the brain (Beard, Li et al., 2020). The current results build on these data by showing on the effect of rapamycin on pericyte contraction in real-time in a controlled environment.

The mechanism by which rapamycin reduces pericyte constriction is still under debate and may be due to a RhoA- dependent pathway, enhancement of eNOS activation, or direct reduction in Ca^{2+} sensitivity in smooth muscle cells (Cipolla, Chan et al., 2014, Liu, Zhang et al., 2010, Palomares and Cipolla, 2011) (see **Figure 3.14**). Cipolla et al. compared the vasoactive response of arterioles with both ROCK and PKC inhibition and found that the conventional PKC inhibitor Go6976 had little effect on the basal tone of parenchymal arterioles (PAs), irrespective of ischemia and reperfusion (Cipolla, Chan et al., 2014). This might suggest that PKC activation is not involved in the Ca^{2+} sensitization of the PAs themselves, but it could be that the pericytes, which wrap around PAs, regulate their tone through a PKC-dependent mechanism (Khalil, 2010, Sukriti, Tauseef et al., 2014, Webb, 2003). A recent study has shown PKC downregulation upon rapamycin treatment in the mitochondrial disease (Martin-Perez, Grillo et al., 2020), and results in this chapter demonstrate that rapamycin treatment of pericytes results in decreased PKC activity. This is a known phenomenon in other cell types and, considering the role of PKC in smooth muscle contractility, may explain the relaxant effect of rapamycin on the pericytes (Martin-Perez, Grillo et al., 2020). However, PKC inhibition during and after OGD would need to be carried out to confirm this fully. Understanding the mechanisms by which rapamycin exerts its effects is vital for developing novel mTOR drugs with reduced side-effect profiles.

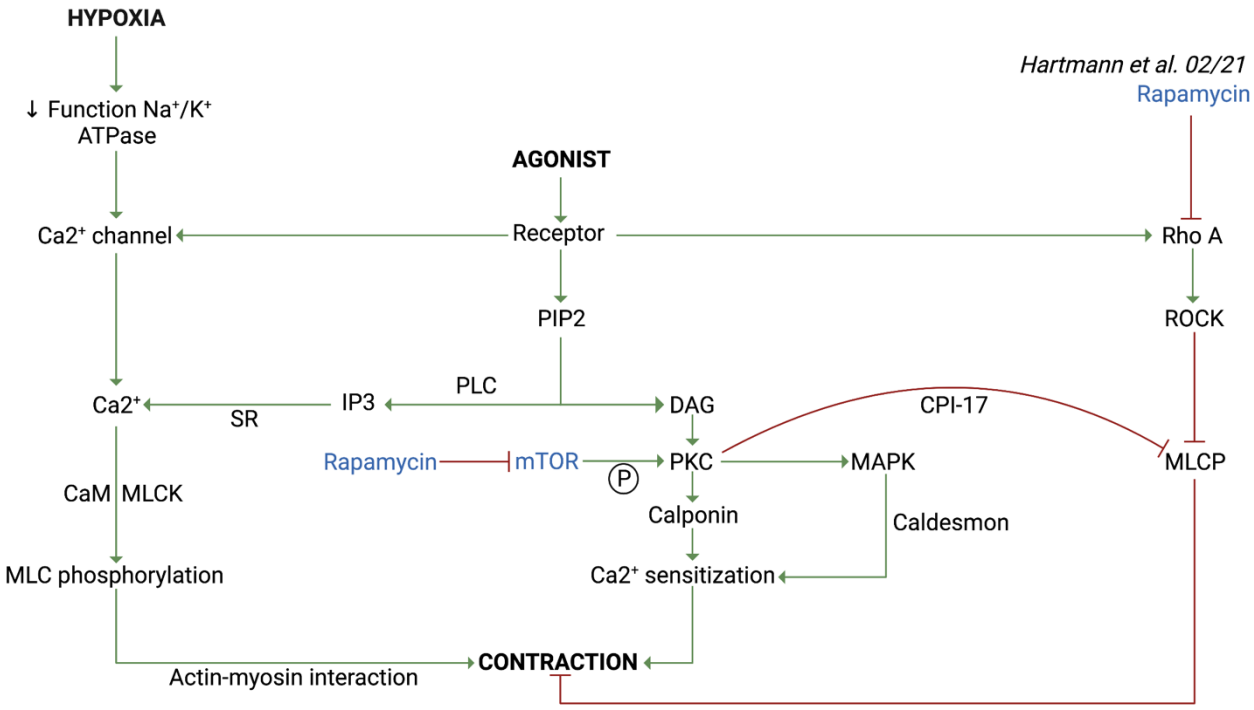

Figure 3.14 Pathways contributing to smooth muscle cell contraction. Pericyte contraction is mediated through increased intracellular Ca2+ concentration, leading to a calcium-calmodulin-dependent activation of the myosin light chain kinase (MLCK), and subsequent actin-myosin interaction. Contraction can also be elicited through Rho-A, which activates Rho-associated protein kinase (ROCK), subsequently downregulating myosin light chain phosphatase (MLCP), thereby increasing acting-myosin interaction. In addition to that, the activation of phospholipase C-beta cleaves the membrane phospholipid phosphoatidylinositol-4,5-biphosphate (PIP2) into diacylglycerol (DAG) and inositol triphosphate (IP3), which both act as second messengers. While IP3 stimulates the opening of Ca2+ channels on the sarcoplasmic reticulum, DAG remains in the membrane and activates protein kinase C (PKC). PKC activates calponin, which in turn enhances Ca2+ sensitization and contraction. mTOR has recently been described as a potential upstream promoter of PKC, enhancing the contractile effects of PKC downstream. This chapter showed that mTOR inhibition through rapamycin treatment reduced PKC activity, which, at least in part, may explain the relaxing effect of rapamycin treatment on pericytes.

This chapter demonstrates that rapamycin increases the adhesion of hCMECs following OGD. Further, under hypoxic conditions, rapamycin has been shown to help maintain endothelial cell adhesion when given either at the start or immediately after the completion of OGD. At the time of writing, only two studies have used biosensor technology devices to study the adhesion and barrier properties of endothelial cells. A study by Johnson and colleagues used the xCelligence Biosensor technology to examine the effects of Toll-Like Receptor (TLR) agonists on endothelial cell function in real-time, showing increased inflammation and varying effects on endothelial barrier strength contingent upon the TLR-agonist used (Johnson, Kho et al., 2018). Further, Hucklesby et al. compared different biosensor technologies to measure endothelial adhesion and barrier properties and concluded that their sensitivities and ability to infer cellular processes, such as contraction or adhesion, from the biosensor data varied consider (Hucklesby, Anchan et al., 2021). To gain further insight into the impact of mTOR inhibition on endothelial cell adhesion, the experiments presented in this study should be considered in tandem with other technologies, such as those designed to measure barrier function specifically

Multiple studies have shown that stress conditions and extracellular stimuli such as OGD and proinflammatory cytokines increase the monolayer permeability of endothelial cells, which form an essential part of the BBB (Chen, Sun et al., 2019, Lin, Wang et al., 2018, Weksler, Romero et al., 2013). One mechanism by which this occurs is MMP-mediated degradation of tight junction integrity, leading to a loss of BBB function (Kim, Kim et al., 2020, Liu, Jin et al., 2012). It has also been suggested that autophagy, a downstream effect of mTORC1 inhibition, plays a central role in the regulation of endothelial cell integrity, but the literature on this is discordant: Some studies suggest that autophagy is one of the mechanisms by which BBB integrity is disrupted,

while others describe the strengthening of BBB integrity by autophagy (Kim, Kim et al., 2020, Li, Gao et al., 2014).

For example, studies have shown that ischemia-induced autophagy-mediated degradation of junctional proteins such as claudin and occludin (Kim, Kim et al., 2020, Li, Gao et al., 2014, Liu, Jin et al., 2012). However, work by Li suggests that autophagy reversed barrier disruption following I/R injury (Li, Gao et al., 2014). Rapamycin has been shown to upregulate junctional proteins (Yang, Hawkins et al., 2019) as well as downregulating MMP activity (Van Skike, Jahrling et al., 2018). The discrepancies in data presented here and data within the literature are likely to be due to the considerable variation in techniques applied and outcomes measured. Consistency in our approaches to the study of autophagy, particularly whether it is directly measured or inhibited, will enable more effective conclusions about its contribution to BBB breakdown after stroke.

The findings of this chapter point toward the possibility that rapamycin improves stroke outcomes by not only protecting the neuron itself from dying but also ameliorating the downstream effects of hypoxia on the BBB. These results consolidate previous research describing the negative impact of OGD on BBB integrity and describe potential beneficial effects of rapamycin treatment when given following the stroke induction. Considering the above, further research is needed to establish the optimal timing for rapamycin treatment relative to the hypoxic injury.

Chapter 4: The Effects of Fasting on Acute Post-Stroke Recovery

4.1 Introduction

One of the main determinants of post-stroke recovery is inflammation (Fang, Zhong et al., 2019, Lambertsen, Finsen et al., 2019). Emerging data suggest that inflammatory cells play complex and multiphasic roles after ischemic stroke, and interestingly most cell types display both beneficial *and* adverse effects (Jin, Yang et al., 2010). The brain responds to ischemic injury with a rapid inflammatory response that is initiated by the release of damage-associated molecular patterns (DAMPs), rapid activation of resident microglia, and production of pro-inflammatory mediators, followed by the infiltration of leukocytes, including neutrophils, macrophages and different subtypes of T-cells to the site of injury (Jin, Yang et al., 2010). Proteolytic enzymes and reactive oxygen species (ROS) released by many of these cells cause secondary brain damage by further disrupting brain tissue and the BBB (Jin, Yang et al., 2010).

There is a growing body of evidence that inflammatory cell infiltration is predominantly deleterious in the early phase after ischemic stroke and therefore decreasing inflammation in the acute phase of stroke is likely to be neuroprotective (Jin, Yang et al., 2010, Lambertsen, Finsen et al., 2019). But all attempts to translate anti-inflammatory agents in ischemic stroke have so far remained unsuccessful at reducing lesion progression (Chamorro, Lo et al., 2021, Neuhaus, Couch et al., 2017, Savitz, Baron et al., 2017, Tymianski, 2017).

The majority of these interventions have been targeted at a specific cytokine, chemokine, or inflammatory process (Schreuder and Cliteur, 2021). However, the inflammatory cascade is multifaceted with a significant amount of inherent redundancy (Dyer, 2020), while also being context-dependent, and the inflammatory response at the start of ischemia will not be the same as that at 3 days. Single targets are likely not to be expressed long-term and, therefore, targeting

systems like mTOR, which is ubiquitous and adaptive, is a more practical approach. If we were to add to this practicality, non-pharmacological interventions have several benefits, including reduced side-effect profiles. One such choice may be altering diet to have downstream effects on mTOR signaling and the outcomes of ischemia.

Fasting, defined as the abstinence from food intake for a set period, has been shown to be a successful intervention to lower inflammation in different species (Duregon, Pomatto-Watson et al., 2021, Gabandé-Rodríguez, Gómez de Las Heras et al., 2019, Mattson, Longo et al., 2017). Fasting is a form of time-restricted eating, and together with calorie-restricted eating and changing the dietary content, make up the nutritional interventions. In humans, fasting has been shown to reduce levels of C-reactive protein (CRP) (Wang, Yang et al., 2020, Wei, Brandhorst et al., 2017), pro-inflammatory cytokines, such as tumor necrosis factor-α (TNFα), interleukin-1β (IL1β) (Johnson, Summer et al., 2007, Moro, Tinsley et al., 2016, Shang, Weiss et al., 2006), as well as the number of circulating monocytes (Jordan, Tung et al., 2019). Furthermore, fasting has been shown to increase the anti-inflammatory hormone adiponectin (Moro, Tinsley et al., 2016, Shang, Weiss et al., 2006) and brain-derived neurotrophic factor (BDNF) in humans and primates (Johnson, Summer et al., 2007, Maswood, Young et al., 2004, Vasconcelos, Yshii et al., 2014). In the brain, fasting has been shown to attenuate both oxidative stress and microglial activation suggesting it may be a useful way of reducing inflammation in the context of brain injuries such as stroke (Radler, Hale et al., 2014, Vasconcelos, Yshii et al., 2014) and in a rat a model of cortical injury (Loncarevic-Vasiljkovic, Pesic et al., 2012).

Reports have found that the effects of fasting are likely to be due, at least in part, to changes in the AMPK/mTOR signaling cascade (Jordan, Tung et al., 2019) via the promotion of autophagy (Kume, Uzu et al., 2010). mTOR is activated by the PI3K/Akt pathway and promotes cell

proliferation, growth, cytokine production, and signaling, all of which are essential for an efficient immune response (Liu and Sabatini, 2020). Like the pharmacological compound rapamycin, fasting downregulates mTOR activity, thereby decreasing inflammation and immune cell activation (Delgoffe and Powell, 2009). Studies have found that a suppressed mTORC1 pathway not only decreased lesion size and improved motor function in a focal stroke model, but also ameliorated the production of pro-inflammatory cytokines and chemokines (Li, Wang et al., 2016).

This data suggests that non-pharmacological approaches such as fasting, which act on the mTOR pathway, may also successfully decrease inflammation post-stroke. Indeed, studies on the effect of dietary interventions on post-stroke inflammation are limited but so far show promising results, suggesting that caloric restriction (CR) and time-restricted eating before ischemia suppress the overproduction of cytokines following the ischemic stroke (Arumugam, Phillips et al., 2010, Lakhan, Kirchgessner et al., 2009). Arumugam and colleagues restricted food intake before MCAo in mice and showed that reduced dietary intake modulated neurotrophic and inflammatory pathways to protect neurons against ischemic injury (Arumugam, Phillips et al., 2010). Similarly, Varendi and colleagues found that preoperative fasting in a rat focal stroke model is neuroprotective while suppressing the pro-inflammatory response (Varendi, Airavaara et al., 2014). Indeed, TNFα, its receptor TNFRSF1A, and downstream target intercellular adhesion molecule-1 (ICAM-1) were upregulated in the lesioned hemisphere of the control group but not in the fasted group (Varendi, Airavaara et al., 2014). However, all of these studies introduced fasting before stroke induction, which, from a translational perspective, is irrelevant although helpful in target discovery. Only one study so far has examined the effects of a hypocaloric diet following focal stroke in mice and found that after 56 days, mice that were kept on a calorically reduced diet during this period had smaller stroke volumes, improved neuronal function, and neuronal survival

(de Carvalho, Sanchez-Mendoza et al., 2021). Further, the treatment group exhibited increased brain capillary density in the striatal peri-infarct region, together with increased BDNF and SIRT1, suggesting improved neuroprotection and promotion of peri-infarct remodeling.

4.1.1 Aims

The aims of this chapter are, therefore:

1. To introduce fasting after a focal model of cerebral ischemia in rats and investigate its acute effects on inflammation, BBB integrity, and stroke volume after 24 hours.

2. To benchmark the observed effects to rapamycin, a well-described neuroprotective drug with a similar mechanism of action.

3. To understand how reduced glucose medium post-OGD affects the molecular health of pericytes and endothelial cells by investigating ATP production and survival.

4.2 Materials and methods

4.2.1 Ethics and animal care

All experimental procedures were approved by the UK Home Office (1986 Animal Act, Scientific Procedures), conducted in accordance with local ethical guidelines at the University of Oxford, and where possible conformed to the ARRIVE and IMPROVE guidelines for animal and pre-clinical stroke work (Kilkenny, Browne et al., 2010, Percie du Sert, Alfieri et al., 2017). Male Wistar Han rats (250g - 320g, Envigo Research Model Services in Blackthorn, England) were housed in individually ventilated cages under a 12-hour light/12-hour dark cycle with *ad libitum* access to water. Before the intervention, access to food was unrestricted and strictly controlled or restricted in the first 24 hours after the stroke. The principal investigator began daily animal handling and weighing the animals three days before the surgery. No animal had to be excluded from the study.

4.2.2 Sufficient statistical power

Preliminary data on the effects of fasting after stroke are limited. Power calculations were based on the rapamycin intervention in **Section 2.2.2**, which significantly reduced lesion volume compared to control. A sample size of 10 rats per group was used, which was thought to be sufficient to detect biologically significant effects while minimizing the number of animals required to achieve the research objectives of this study.

4.2.3 Controls

Appropriate control groups were included in all experiments. To minimize the number of animals used, one control group was used for both the fasting and rapamycin cohorts. These animals had

ad libitum access to food and water and did not receive any pharmacological treatment. To control for the stroke itself, sham animals with the respective treatment (fasting, n=10/rapamycin, n=10/control, n=10) were included. Sham surgery followed the identical protocol to the endothelin-1 (ET-1) model but with sterile saline injection rather than ET-1.

Further, to control for the surgical intervention itself, naïve animals that did not undergo surgery were included (fasting, n=5/rapamycin, n=5/control, n=5). Throughout the chapter, the different study groups will be referred to as "stroke", "sham" and "naïve", respectively. An overview of the various study groups and analyses performed in each group is outlined below (**Figure 4.1**).

Study groups	Analysis	Body weight	Blood glucose and ketone bodies	Stroke volume	BBB breakdown	Brain neutrophil infiltration	Microglia and astrocyte quantification	Full blood count	Western Blot mTOR activity
Stroke surgery	Stroke + Fasting (10) / Stroke + Rapamycin (10)	✓	✓	✓	✓	✓	✓	✓	
	Stroke + Control (10)	✓	✓	✓	✓	✓	✓	✓	
Sham surgery	Sham + Fasting (10) / Sham + Rapamycin (10)	✓	✓	✓	✓	✓	✓	✓	
	Sham + Control (10)	✓	✓	✓	✓	✓	✓	✓	
Naïve	Naïve + Fasting (5) / Naïve + Rapamycin (5)	✓	✓					✓	✓
	Naïve + Control (5)	✓	✓					✓	✓

Figure 4.1 Overview of the study groups and analyses performed. For the intervention, there are naïve animals (no surgery), sham (surgery, but no stroke), and stroke (surgery, stroke) animals. These animals are either treated with control (normally fed and vehicle), fasting (fasting treatment, no rapamycin), or rapamycin (normally fed and rapamycin).

The effects of rats that underwent stroke surgery and subsequent fasting (*Stroke + fasting*) or rapamycin (*Stroke + rapamycin*) treatment were compared to stroke rats that did not receive either treatment (*Stroke + control*). To account for the effects of the stroke itself, rats underwent sham surgery and subsequent fasting (*Sham + fasting*) or rapamycin (*Sham + rapamycin)* treatment, and the results were compared to rats that did not receive either treatment (*Sham + control*). The study size for the abovementioned study groups was 10 rats each. Brain tissue was utilized to study brain inflammation. One additional study group, termed naïve, was used to investigate the effects of fasting (*Naïve + fasting*) or rapamycin (*Naïve + rapamycin*) without any surgical intervention. The study size for the naïve group was 5 rats each. Brain tissue was utilized to study mTOR activity in the striatum of those animals.

4.2.4 Excluded animals

1 control animal was excluded from the stroke volume analysis because no lesion volume was detectable.

4.2.5 Randomization and blinding

To prevent accidental bias in the *in vivo* experiments, tissue was randomized after collection by the main investigator (AMS), and blinding was continued throughout the whole experiment wherever possible and until data acquisition was complete.

4.2.6 Endothelin-1 surgery

During the surgery, the core body temperature of all animals was maintained at 37.0 ± 0.5°C using a rectal thermometer connected to a feedback-controlled heating pad (Harvard Apparatus, Cambourne, UK). Physical parameters, including body temperature and respiratory rate, were checked and recorded every 5 minutes throughout the surgical intervention. Respiration was kept between 50 and 60 breaths per minute by adjusting isoflurane concentration. Focal brain ischemia was induced by ET-1 injection into the area of the right striatum, similar to a method previously described (Abeysinghe and Roulston, 2018). Briefly, the rat was deeply anesthetized with 5% isoflurane in 70% N_2 and 30% O_2 and maintained at 1-2% isoflurane throughout the intervention. After weighing, blood glucose and ketone bodies were measured before the head was shaved and disinfected using a 70% ethanol and 30% chlorhexidine solution. The animal was secured in a stereotaxic frame before a midline incision at the top of the head was made, and the needle navigated to the coordinates of the MCA territory in the striatum of the right hemisphere (AP +1.0, ML -3.0, SI -4.0 mm). A small hole was drilled in the skull, through which a needle was inserted, and 1 µl of ET-1 (25 pmol) or saline (for the control group) was slowly injected over the time course of 2 minutes. The head wounds were cleaned and closed (4-0 Vicryl Rapide Undyed 1x18" P-3, Somerville, US). Animals received 0.05 mg/kg marcaine into the wound to alleviate pain and 2 ml of saline solution subcutaneously. The rectal thermometer was removed, isoflurane turned

off, and the gases changed to 0% N_2O and 100% O_2. Upon awakening, the animal was put in a pre-warmed cage, using a heating mat underneath. The animal was closely monitored for an additional 3 hours after awakening with post-surgical check-ups every 30 minutes.

4.2.7 Treatment

Animals in the fasting group had no access to food for 24 hours from the point of suture closure, with *ad libitum* access to water (n=10). Animals allocated to the drug-treatment group received rapamycin (Sigma Aldrich, 250 μg/kg, n=10) once the sutures were closed. The control group had *ad libitum* access to food and water and did not receive any pharmacological treatment (n=10).

4.2.8 Welfare assessment

A welfare assessment was performed every 30 minutes for the first 3 hours after the surgery and then every 12 hours, using the scoring system previously described in **Table 2.1**. Scores of less than 4 were considered mild, whereas 7 and above were considered a severe impairment, respectively.

4.2.9 Tissue processing

After 24 hours from the start of treatment, rats were deeply anesthetized with 5% isoflurane in 70% N_2 and 30% O_2. Rats were weighed, blood glucose and blood ketone bodies were measured (On Call GK Dual Blood Glucose & Ketone Monitoring System, Acon Laboratories, San Diego, CA, USA), and then killed by intraperitoneal pentobarbital injection (800 mg/kg). 5 ml of blood was drawn from the heart into EDTA tubes, and full blood count was analyzed on the same day (Laboratory Haematology, John Radcliffe Hospital, Oxford OX3 9DU, UK). Animals were

transcardially perfused using heparinized saline and 4% PFA in PBS. Brains were collected, post-fixed in 4% PFA in PBS overnight, and changed into a 30% sucrose solution in PBS. For the naïve group, fresh non-perfused brains were collected and sliced into 2 mm thick coronal sections with an ice-cold stainless-steel matrix (Kent Scientific). 1 mm^2 tissue samples of the striatum and cortex of both hemispheres were snap-frozen on dry ice.

4.2.10 Immunohistochemistry

Perfused brains were dehydrated through graded ethanol solutions and embedded in OCT mounting medium before snap-frozen on dry ice. Using a cryostat, 10 µm-thick serial sections in the coronal place were collected 0.5 mm anterior to posterior of the lesion on gelatinized slides and stored at -80°C until further use. Brain sections were rehydrated through graded ethanol solutions. Nonspecific binding was blocked using 10% of serum of the species the secondary antibody was raised in (diluted in PBS) for 1 hour at RT and incubated in primary antibody in PBS at 4°C overnight (**Table 4.1**). After that, sections were rinsed in PBS, and a secondary antibody was added at 1:500 in PBS for 45 minutes at RT. Antibody binding was visualized with 3,3'-diaminobenzidine. Sections were dehydrated through graded ethanol solutions and cleared with Histo-Clear II (National Diagnostics, HS2021GLL). The slides were mounted with glass coverslips using an anti-fade fluorescence mounting medium (Dako, USA) and imaged with a microscope scanner (Manual Whole Slide Imager 2017b-31, Olympus Life Science) with 10 x magnification.

Table 4.1 Antibodies used for Immunohistochemistry

Antibody	Manufacturer	Species	Concentration
GFAP (°1)	Abcam (ab53554)	Goat anti-rat	1:500
Iba-1 (°1)	Abcam (ab5076)	Goat anti-rat	1:500
Neutrophil (°1)	In house	Rabbit anti-rat	1:10000
IgG (°2)	Abcam (ab182931)	Goat anti-rat	1:100

4.2.11 Stroke volume

Cresyl violet was used to stain five brain sections per animal which were +1.28 mm, +0.6 mm, +0.12 mm, -0.12, and -0.48 mm away from the bregma, respectively. To obtain the lesion volume, areas of infarct were multiplied by the distance between the brain. Lesion volume was then presented as a percentage of the ipsilesional hemisphere.

4.2.12 Western blotting

4.2.12.1 Whole-cell homogenization

Whole-cell homogenization was performed as outlined in **Section 2.2.11.1**.

4.2.12.2 Protein quantification

Protein quantification was performed as outlined in **Section 2.2.11.2**.

4.2.12.3 Gel electrophoresis

Gel electrophoresis was performed as outlined in **Section 2.2.11.3**.

4.2.12.4 Protein detection

All steps were performed under gentle agitation. To detect 3 proteins with distinct molecular weights, the membrane onto which proteins were transferred from a gradient gel was cut between the molecular weight ladders 37 and 50 kDa and 75 and 100 kDa. Membrane pieces were then blocked in PBS containing 5% BSA and 0.1% Tween-20 for 1 hour at room temperature before being incubated in primary antibody (**Table 4.2**) in 5% PBS-T solution overnight. After 3 x 5-minute-washes in PBS-T, the membrane was incubated in secondary antibody goat anti-rabbit (IgG H&L (HRP), ab6721, Abcam, dilution 1:2000) in 5% BSA PBS-T for 1 hour at RT. After 3 x 5-minute-washes in PBS-T, the membrane was developed using enhanced chemiluminescence (ECL; 12644055, Fisher Scientific) for 5 minutes and immediately imaged after that. Western Blot analysis and quantification were performed using densitometry and corrected for loading using β-tubulin as the housekeeping protein (**Table 4.2**). The membrane was probed for antibodies twice, using the following mild antibody-stripping protocol: The membrane strips were incubated in stripping solution (7.5 g glycine, 0.5 g SDS, 5 ml Tween-20, pH to 2.2, and diluted up to 500 ml distilled water) for 2 x 7 minutes, followed by 2 x 10-minute-washes in PBS, and 2 x 5-minutes washes in PBS-T, before blocking in 5% BSA and 0.1% Tween-20.

Table 4.2 Primary antibodies used for Western Blotting

Antigen	**Molecular weight (kDa)**	**Source**	**Manufacturer**	**Dilution**
mTOR	289	Rabbit	Cell Signaling (#2972)	1:1000
Phospho – mTOR (Ser2448)	289	Rabbit	Cell Signaling (#2971)	1:1000
β-tubulin	55	Rabbit	Cell Signaling (#2146)	1:1000

4.2.13 Blood analysis

For full blood count analysis, 5 ml of whole blood was drawn directly out of the heart in EDTA tubes and analyzed on the same day (Laboratory Haematology, John Radcliffe Hospital, Oxford OX3 9DU, UK).

4.2.14 Cell culture

All experiments were conducted under standardized incubation conditions (37°C, 5% CO2 in humidified air). Cell culture flasks and multi-well plates were obtained from Corning (USA).

4.2.14.1 Human pericytes

Human brain vascular pericytes were grown and kept under conditions as outlined in **Section 3.2.1.1.**

4.2.14.2 Human endothelial cells

Human endothelial cells were grown and kept under conditions as outlined in **Section 3.2.1.2.**

4.2.14.3 Oxygen glucose deprivation

Oxygen glucose deprivation was performed as described in **Section 3.2.1.3**.

4.2.15 Glucose intervention

The impact of different glucose concentrations over 24 hours following OGD was evaluated. The different glucose concentrations were 0, 1, 5, and 10 mM, whereby 5 mM was used as the control

group, representing the standard glucose concentration in most cell culture media, including the standard media for the HBVP and hCMEC used.

4.2.16 Molecular analysis

4.2.16.1 Lactate dehydrogenase assay

Lactate dehydrogenase assay was performed as outlined in **Section 3.2.5.**

4.2.16.2 ATP production assay

ATP production assay was performed as outlined in **Section 3.2.6.**

4.2.17 Statistical analysis

Statistical analysis was carried out in Prism 6 (Graphpad, USA). For analysis of stroke volume, BBB breakdown, neutrophil infiltration into the brain, Western Blot on mTOR activity, one-way ANOVA was used with Dunnett's multiple comparison test. For weight, blood glucose and ketone bodies, microglia and astrocyte count, full blood cell count, and *in vitro* LDH and ATP data analysis, two-way ANOVA was used with Dunnett's multiple comparisons test and Bonferroni's multiple comparisons test for LDH and ATP data. When the interaction term between surgery and treatment was insignificant, I opted for an additive two-way ANOVA model. α of 0.05 was considered statistically significant, and the results are presented as mean ± standard error of the mean (SEM). *p<0.05, **p<0.01, ***p<0.001, ****p<0.0001.

4.3 Results

4.3.1. Fasting but not rapamycin decreases body weight

Bodyweight measurements were recorded immediately before the surgical intervention and at 24 hours, marking the experiment's end. The aim was to determine whether fasting or rapamycin treatment affects body weight in animals that have experienced a stroke. There was no main effect of the surgery ($p=0.3382$; two-way ANOVA), but a main effect of treatment ($p<0.0001$) and an interaction between the two effects ($F(4, 67)=3.064$, $p=0.0222$). Post-hoc testing revealed that fasting significantly reduced body weight in naïve, sham, and stroke animals ($p<0.0001$ for all, Dunnett's multiple comparisons test). Rapamycin, on the other hand, did not affect body weight in any group (naïve ($p=0.4428$), sham ($p=0.8743$), stroke ($p=0.7733$)) (**Figure 4.2**).

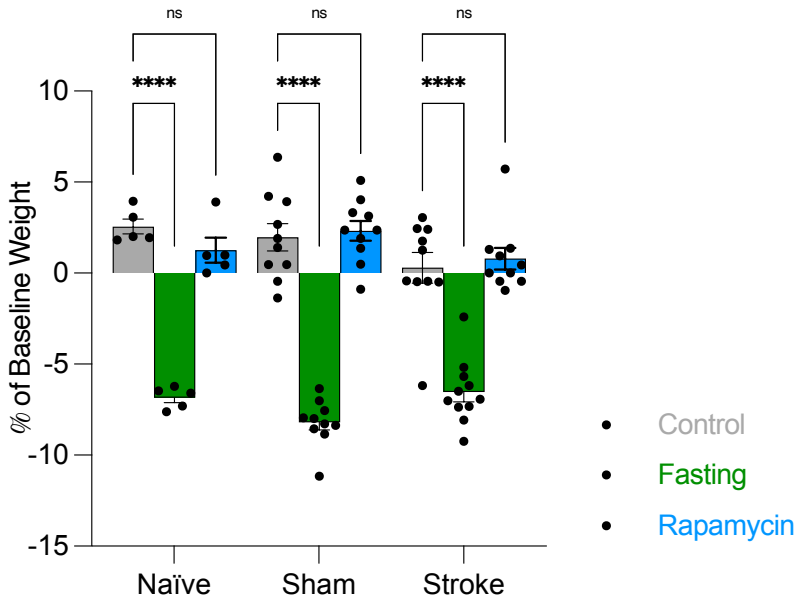

Figure 4.2 Fasting but not rapamycin decreases body weight. The effect of 24 hours of fasting and rapamycin treatment on relative weight change was examined. Fasting reduced the bodyweight of naïve, sham-operated, and stroke animals. Rapamycin treatment did not lower body weight in either group compared to control animals. Results are presented mean ± SEM. ****$p<0.0001$. n=5 in naïve groups, n=10 in sham and stroke groups.

4.3.2 The effects of fasting or rapamycin treatment on blood glucose levels and ketone bodies

The next aim was to investigate whether fasting or rapamycin significantly affects blood glucose and ketone levels in animals that have experienced a stroke. At 24 hours post-stroke, blood glucose, and ketone body levels were measured.

There was a main effect of treatment ($p<0.0001$; two-way ANOVA), but no main effect of the surgery ($p=0.0562$) on blood glucose levels, and no interaction between the two effects ($F(4,67)=2.454$, $p=0.0541$). Post-hoc testing revealed that in naïve animals, fasting significantly reduced, and rapamycin significantly increased blood glucose levels compared to control (fasting: $p=0.0019$; rapamycin: $p=0.0073$; Dunnett's multiple comparisons test). This was not reflected in sham animals, where only fasting ($p<0.0001$) but not rapamycin ($p=0.9513$) significantly reduced blood glucose levels. Similarly, in stroke animals fasting ($p<0.0001$) but not rapamycin ($p=0.7844$) resulted in significantly lower blood glucose levels compared to control (**Figure 4.3 (A)**).

For ketone body levels, there was a main effect of the surgery ($p=0.0410$) and a main effect of treatment ($p<0.0001$) but no interaction between the two effects ($F(4,67)=2.058$, $p=0.0962$). Post-hoc testing revealed that fasting increased ketone bodies in all groups (naïve ($p<0.0001$), sham ($p<0.0001$), stroke ($p<0.0001$)) compared to control animals. Rapamycin did not affect blood ketone levels when compared to control animals (naïve ($p=0.5610$), sham ($p=0.1562$), and stroke ($p=0.5583$)) (**Figure 4.3 (B)**).

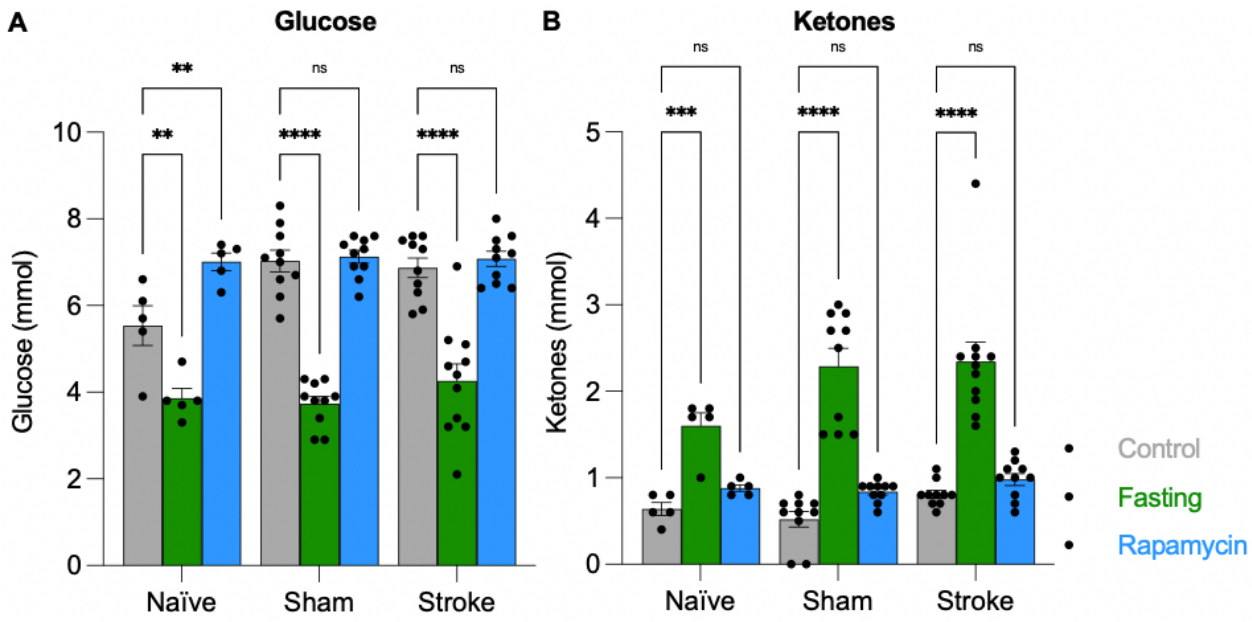

Figure 4.3 The effects of fasting or rapamycin treatment on blood glucose levels and ketone bodies. **(A)** Blood glucose levels following fasting or rapamycin treatment. **(B)** Blood ketone body levels following fasting or rapamycin treatment. Results are presented mean ± SEM., **p<0.01, ***p<0.001, ****p<0.0001. n=5 in naïve groups, n=10 in sham and stroke groups.

4.3.3 Fasting but not rapamycin reduces stroke volume

To investigate and compare the effects of fasting and rapamycin treatment on stroke volume, lesions were stained for cresyl violet 24 hours post-stroke. Stroke volume for each brain was calculated using the determined infarcted areas and multiplying it by the corresponding distance from bregma and presenting it as a percent of the volume of the ipsilateral hemisphere. Relative percentages of all brain sections from the fasting or the rapamycin-treated group were pooled and compared to the control group. There was a statistically significant difference in stroke volume between the groups (one-way ANOVA, $F(2, 27)=4.34$, $p=0.0232$). Dunnett's multiple comparisons test found that the mean value of stroke volume was significantly lower in fasted animals versus the control group ($p=0.0123$; fasting: 2.685 ± 0.7762; control: 7.114 ± 1.307). There was no statistically significant difference between the rapamycin-treated animals and the control group ($p=0.1841$; rapamycin: 4.557 ± 1.121 control: 7.114 ± 1.307) (**Figure 4.4**).

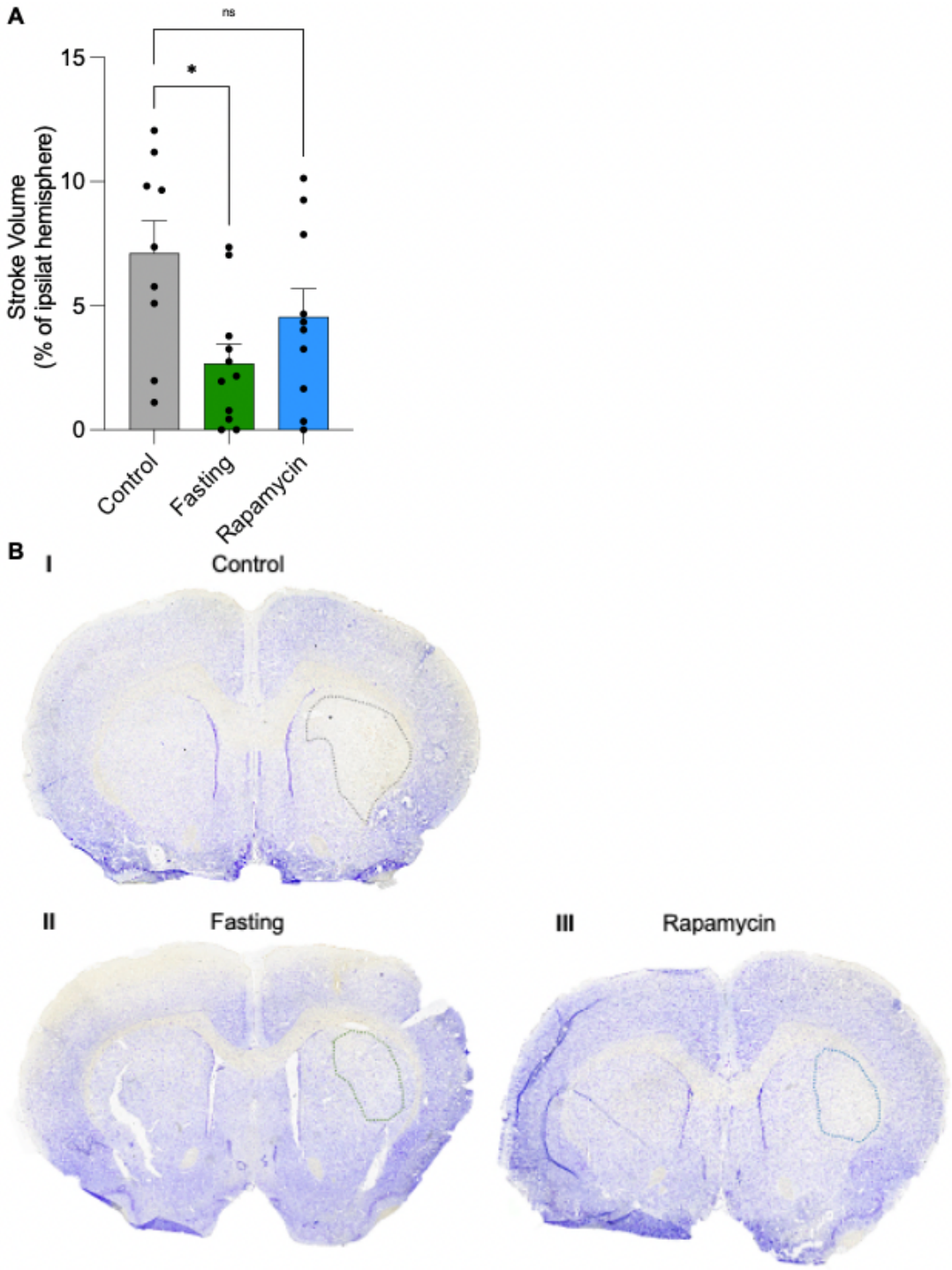

Figure 4.4 Fasting but not rapamycin reduces stroke volume. The effect of fasting or rapamycin treatment on stroke volume was examined. **(A)** Animals that were fasted for 24 hours following the stroke had a significantly lower stroke volume than the control group. **(B)** Representative images of **(I)** Control, **(II)** Fasting, and **(III)** Rapamycin-treated animals. Data are mean ± SEM. *p<0.05. n=9 for the control group, and n=10 for the fasting and rapamycin group.

4.3.4 Fasting and rapamycin reduce BBB breakdown

Next, the effect of fasting or rapamycin treatment on BBB integrity was investigated. At 24 hours, brains were processed for IHC, and BBB compromise was studied by using an antibody against the animal's own IgG to visualize serum proteins that passed through the leaky BBB. 10 animals per group were studied, of which 3 sections per brain were visualized, which were at 1.28 mm, 0.12 mm, and -0.48 mm away from bregma, respectively. IgG-positive staining was identified as apparent brown staining, and the IgG-positive area was then calculated as a percentage of the ipsilateral hemisphere. Relative percentages of all brain sections from each group were pooled and compared to the fed control group. There was a statistically significant difference in BBB breakdown between at least two groups (one-way ANOVA, $F(2, 81)=26.65$, $p<0.0001$). Dunnett's multiple comparisons test found that the mean value of BBB breakdown was significantly lower in fasted animals versus the control group ($p<0.0001$; fasting: 4.911 ± 0.4734; control: 9.423 ± 0.8885). There was also a statistically significant difference between the rapamycin-treated animals and the control group ($p<0.0001$; rapamycin: 3.380 ± 0.3127; control: 9.423 ± 0.8885) (**Figure 4.5**).

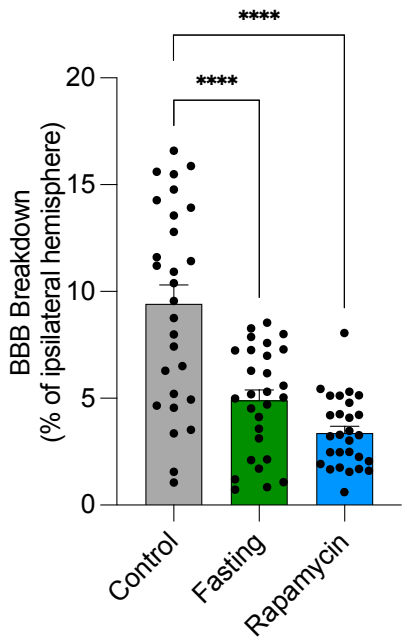

Figure 4.5 Fasting and rapamycin reduce BBB breakdown. The effect of fasting or rapamycin treatment on BBB integrity was examined. Animals that were fasted for 24 hours following the stroke had significantly less IgG-positive staining than the control group. Similarly, animals that received rapamycin treatment following the ischemic stroke had considerably less IgG-positive staining than the control group. Data are mean ± SEM. ***p<0.0001. n=10/group for all groups.

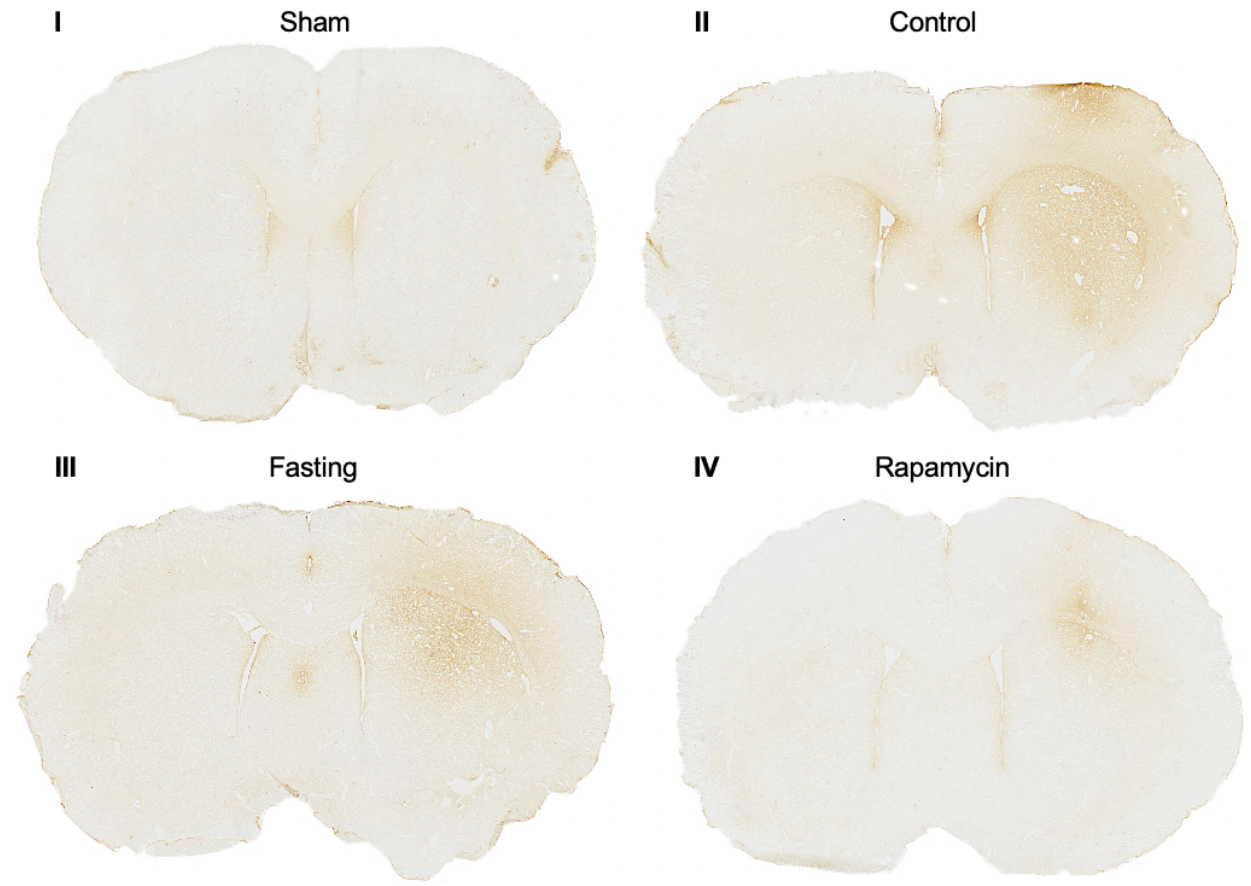

Figure 4.6 Representative images of BBB breakdown visualized with IgG staining. BBB compromise was studied by using an antibody against the animal's own IgG to visualize serum proteins that could pass through the leaky BBB. Note that IgG staining in the normal brain shows some tincture in periventricular structures and other areas known to have leaky BBB, such as the median eminence and area postrema. **(I)** Sham, **(II)** Control, **(III)** Fasting, **(IV)** Rapamycin.

4.3.5 The effects of fasting or rapamycin treatment on neutrophil infiltration into the striatum

The next aim was to investigate how fasting or rapamycin treatment influenced the number of infiltrating neutrophils into the striatum. To do this, neutrophils were visualized by antibody staining in the same five sections per brain as the cresyl staining. The mean number of neutrophils of the five brain sections was calculated, and the relative neutrophil numbers from each group were pooled and compared to the control group. There was a statistically significant difference between at least two groups (one-way ANOVA, $F(2, 28)=4.231$, $p=0.0248$). However, Dunnett's multiple comparisons found that the number of neutrophils was not significantly different between the fasting and control groups ($p=0.0925$; fasting: 50.91 ± 16.01; control: 145.7 ± 36.92). There was also no statistically significant difference between the rapamycin-treated and control group ($p=0.6748$; rapamycin: 181.5 ± 43.28; control: 145.7 ± 36.92) (**Figure 4.7**).

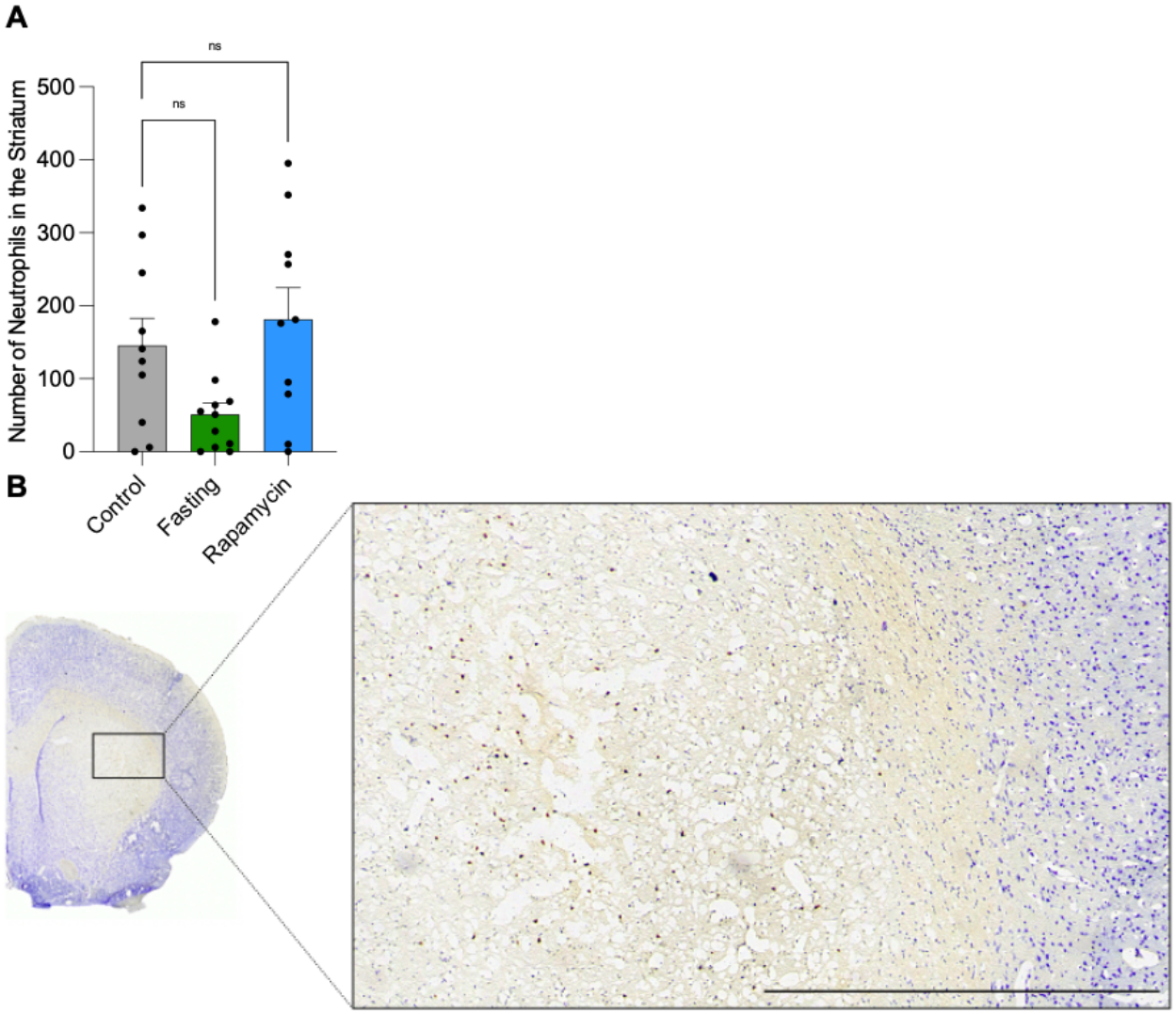

Figure 4.7 The effects of fasting or rapamycin treatment on neutrophil infiltration into the striatum. **(A)** Neither fasting nor rapamycin treatment affected infiltrating neutrophils in the striatum of post-ischemic rats. Data are mean ± SEM. n=10/group for all groups. **(B)** Representative image of neutrophil infiltration into the striatum. Scale bar represents 1 mm.

4.3.6 Fasting or rapamycin treatment does not affect microglia numbers

The effect of fasting or rapamycin treatment on microglia numbers (identified as Iba-1-positive cells) in stroke animals was studied. To do this, Iba-1 positive cells were counted at 24 hours in an area of 1 mm^2 within the cortex and striatum. In the cortex, there was no main effect of stroke ($p=0.2220$, two-way ANOVA), or treatment ($p=0.4347$), and also no interaction between the effects ($F(2,52)=0.3575$, $p=0.7011$) **Figure 4.8 (A)**). In the striatum, there was a main effect of stroke ($p=0.0201$), but no main effect of treatment ($p=0.6064$), and also no interaction between the effects ($F(2,52)=1.021$, $p=0.3675$). However, post-hoc testing revealed that neither fasting nor rapamycin treatment significantly affected microglial numbers in the striatum (fasting: sham ($p=0.7492$), stroke ($p=0.2895$); rapamycin: sham ($p=0.9611$), stroke ($p=0.3671$); Dunnett's multiple comparisons test) (**Figure 4.8 (B)**).

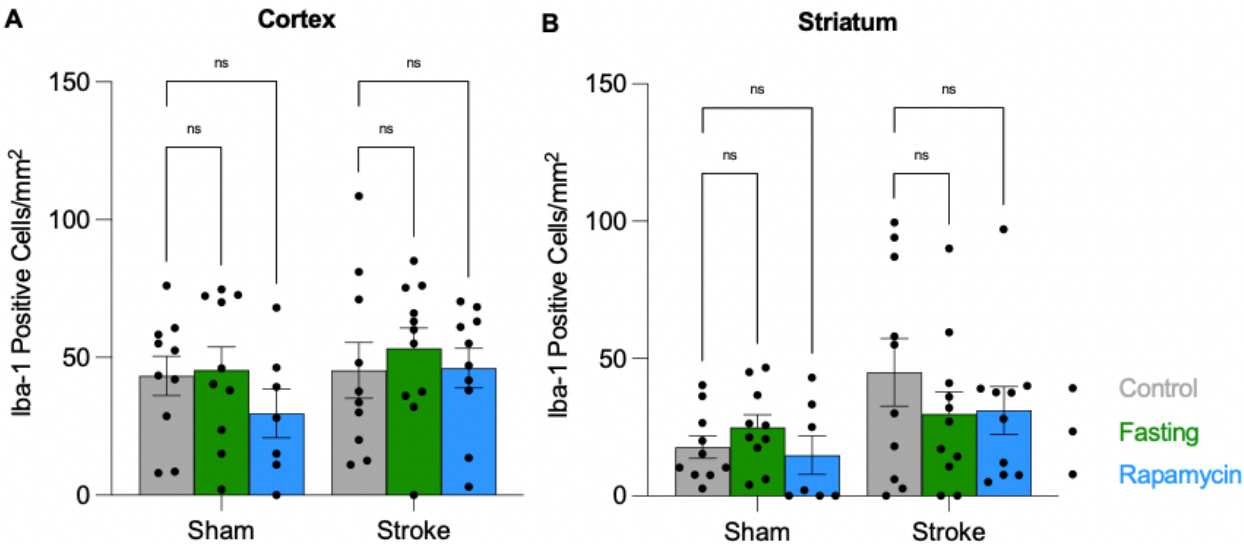

Figure 4.8 Fasting or rapamycin treatment does not affect microglia numbers. The number of microglia (identified as Iba-1-positive cells) was quantified in a 1 mm^2 area within the ipsilateral cortex and striatum of sham- and stroke-operated animals. **(A)** Microglial numbers in the cortex of fasted and rapamycin-treated animals. **(B)** Microglial numbers in the striatum of fasted and rapamycin-treated animals. Data are mean ± SEM. *$p<0.05$. n=10/group for all groups.

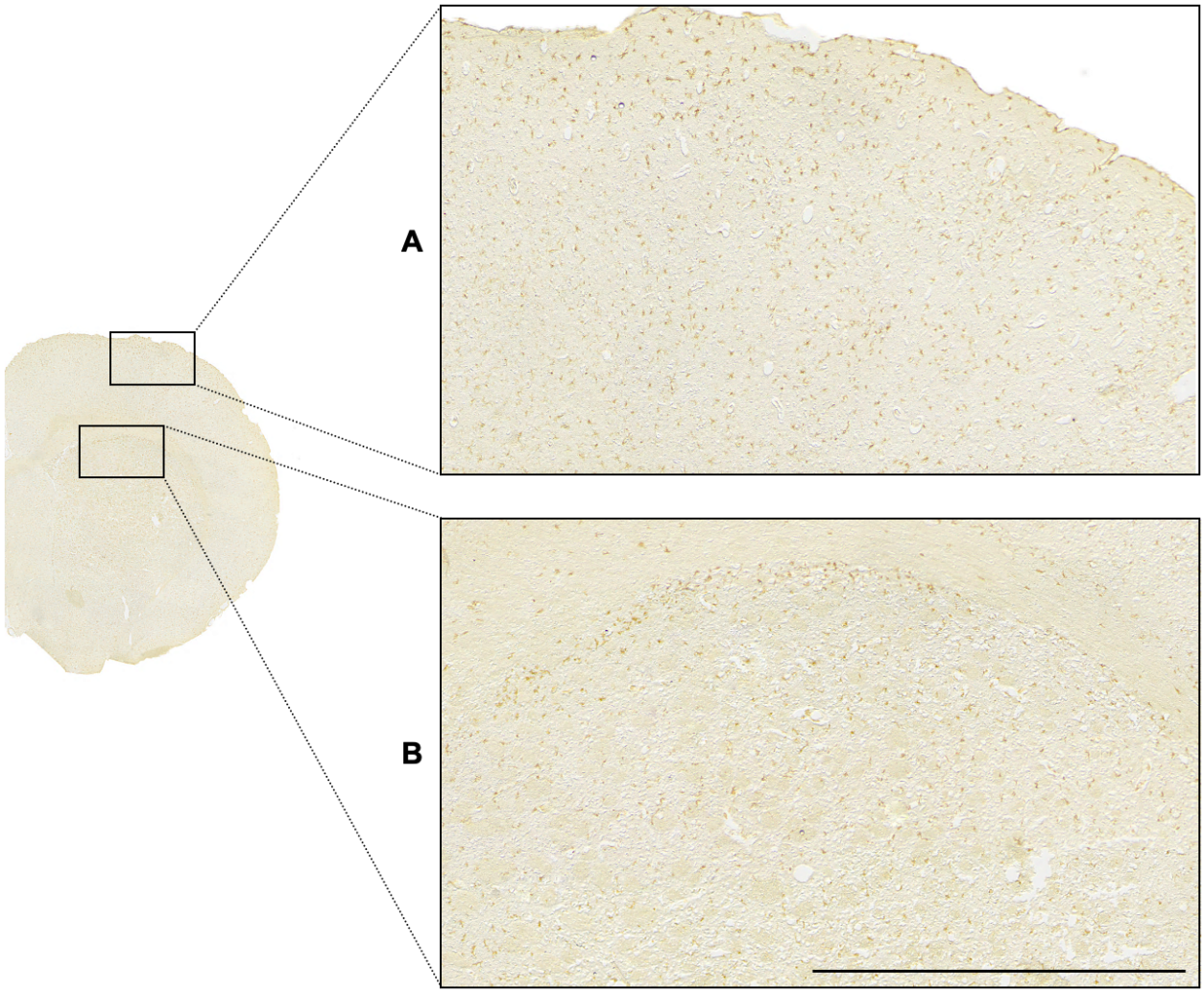

Figure 4.9 Representative image of microglia in **(A)** the cortex and **(B)** the corpus callosum and striatum in the ipsilesional hemisphere of a control rat that underwent stroke surgery. There are abundant numbers of microglia present in both the ipsilesional cortex and the striatum. The neuroimmune cells are not solely concentrated in the striatal area of the infarct. Scale bar represents 1 mm.

4.3.7 Fasting or rapamycin treatment does not affect astrocyte numbers

The effect of fasting or rapamycin treatment on astrocyte numbers (identified as GFAP-positive cells) in stroke animals was studied. To do this, GFAP-positive cells were counted at 24 hours in an area of 1 mm^2 within the cortex and striatum. In the cortex, there was no main effect of stroke ($p=0.1430$; two-way ANOVA), or treatment ($p=0.2966$), and also no interaction between the effects ($F(2,55)=0.7227$, $p=0.4900$) **Figure 4.10 (A)**). Similarly, in the striatum, there was no main effect of stroke ($p=0.2063$), or treatment ($p=0.6315$), and also no interaction between the effects ($F(2,55)=0.7129$, $p=0.4947$) **Figure 4.10 (B)**).

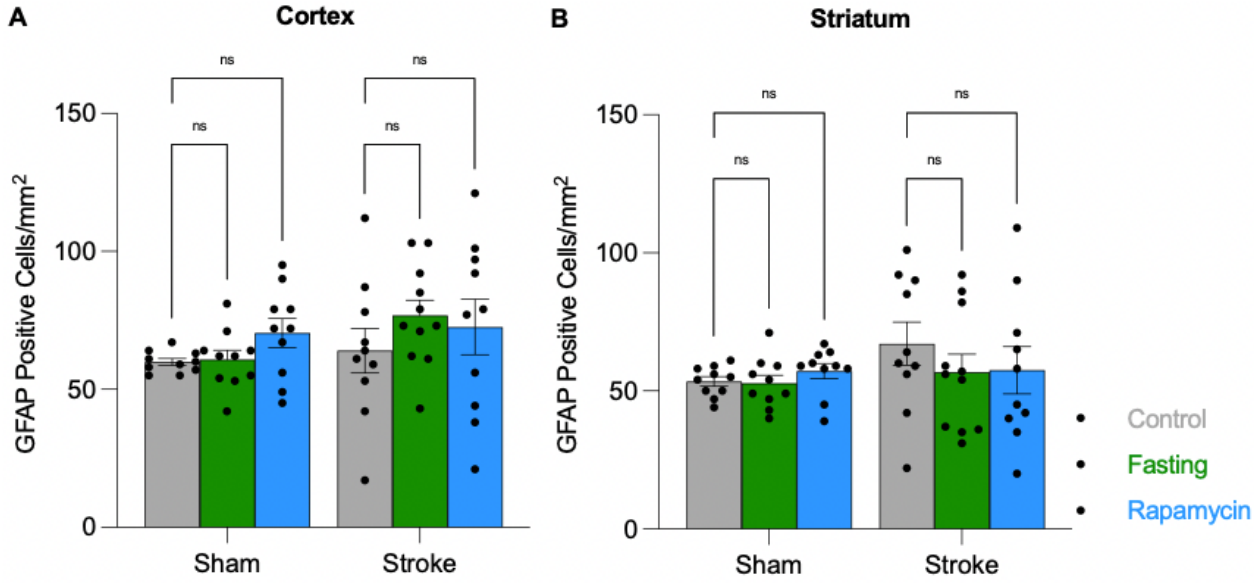

Figure 4.10 Fasting or rapamycin treatment does not affect astrocyte numbers. The effects of 24 hours of fasting or rapamycin treatment on the number of astrocytes (identified as GFAP-positive cells) in an area of 1 mm^2 within the ipsilateral cortex and striatum of stroke and sham-operated animals were quantified. **(A)** Astrocyte numbers in the cortex of fasted and rapamycin-treated animals. **(B)** Astrocyte numbers in the striatum of fasted and rapamycin-treated animals. Data are mean ± SEM. *$p<0.05$. n=10/group for all groups.

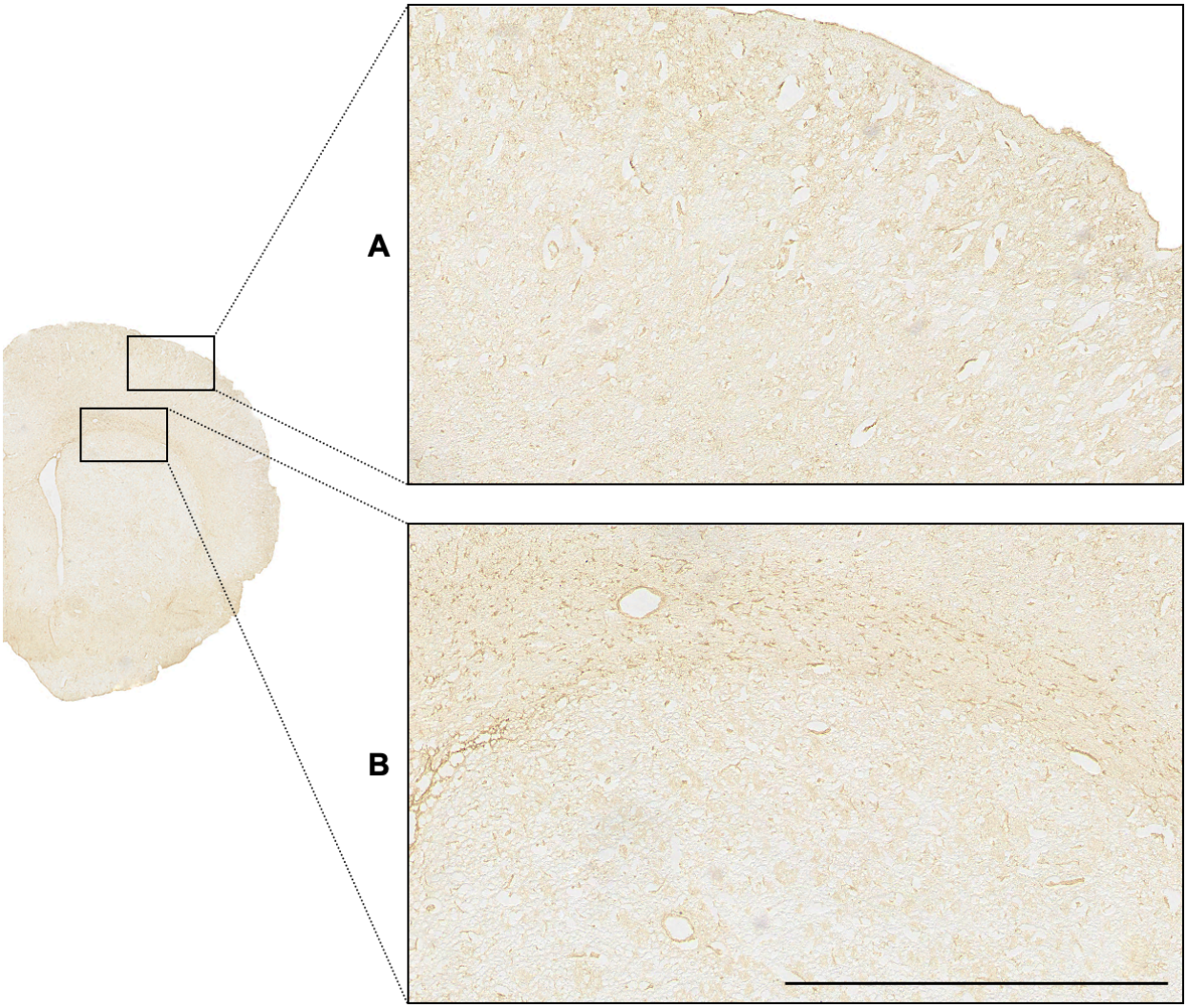

Figure 4.11 Representative image of astrocytes in **(A)** the cortex and **(B)** the corpus callosum and striatum in the ipsilesional hemisphere of a control rat that underwent stroke surgery. There are astrocytes present in the cortex and striatum, and the highest number of astrocytes is concentrated in and around the area of the ipsilesional corpus callosum. Scale bar represents 1 mm.

4.3.8 Fasting reduces neutrophils, and rapamycin reduces the neutrophil-to-lymphocyte ratio

Following the histological analysis, the next aim was to determine whether fasting or rapamycin affects blood inflammation markers in animals that have experienced a stroke. At 24 hours post-stroke, a full blood count was performed, and white blood cells (WBC), neutrophil numbers, lymphocyte numbers, and the neutrophil/lymphocyte (N/L) ratio were analyzed.

WBC: There was a main effect of the surgery ($p=0.0126$; two-way ANOVA), but no main effect of treatment ($p=0.5021$) on the WBC, and no interaction between the two effects ($F(4,67)=1.990$, $p=0.1061$). However, post-hoc testing revealed that neither sham nor stroke operation has a significant impact on WBC (sham ($p>0.9999$), stroke ($p=0.3630$); Dunnett's multiple comparisons test) (**Figure 4.12 (A)**).

Neutrophils: There was no main effect of the surgery ($p=0.3090$), but a main effect of treatment ($p=0.0149$) on the number of neutrophils, and no interaction between the two ($F(4,67)=0.9316$, $p=0.4510$). Post-hoc testing revealed that in stroke animals, only fasting significantly reduced neutrophils ($p=0.0079$), whereas rapamycin had no effect ($p=0.0730$), although post-hoc power calculations revealed these experiments were slightly underpowered (+4 animals). In both, naïve and sham-operated animals, neither fasting nor rapamycin significantly affected neutrophil numbers (fasting: naïve ($p=0.9543$), sham ($p=0.2581$)); rapamycin: naïve ($p=0.8375$), sham ($p=0.2669$)) (**Figure 4.12 (B)**).

Lymphocytes: There was a main effect of the surgery ($p=0.0019$), but no main effect of treatment ($p=0.1739$) on lymphocyte numbers, and no interaction between the two effects ($F(4,67)=0.6050$, $p=0.6604$). However, post-hoc testing revealed that sham nor stroke operation

has a significant impact on lymphocyte numbers (sham (p=0.9995), stroke (p=0.8696)) (**Figure 4.12 (C)**.

N/L ratio: There was a main effect of the surgery (p=0.0001) and a main effect of treatment (p=0.0215) on the N/L ratio, but no interaction between the two effects (F(4,67)=0.9622, p=0.4341). Post-hoc testing revealed that only in stroke animals, rapamycin significantly reduced the N/L ratio (p=0.0068), while fasting did not have an effect (p=0.0541). Naïve and sham animals were not affected by fasting or rapamycin treatment (fasting: naïve (p=0.8962), sham (p=0.6230); rapamycin: naïve (p=0.9968), sham (p=0.2861)) (**Figure 4.12 (D)**.

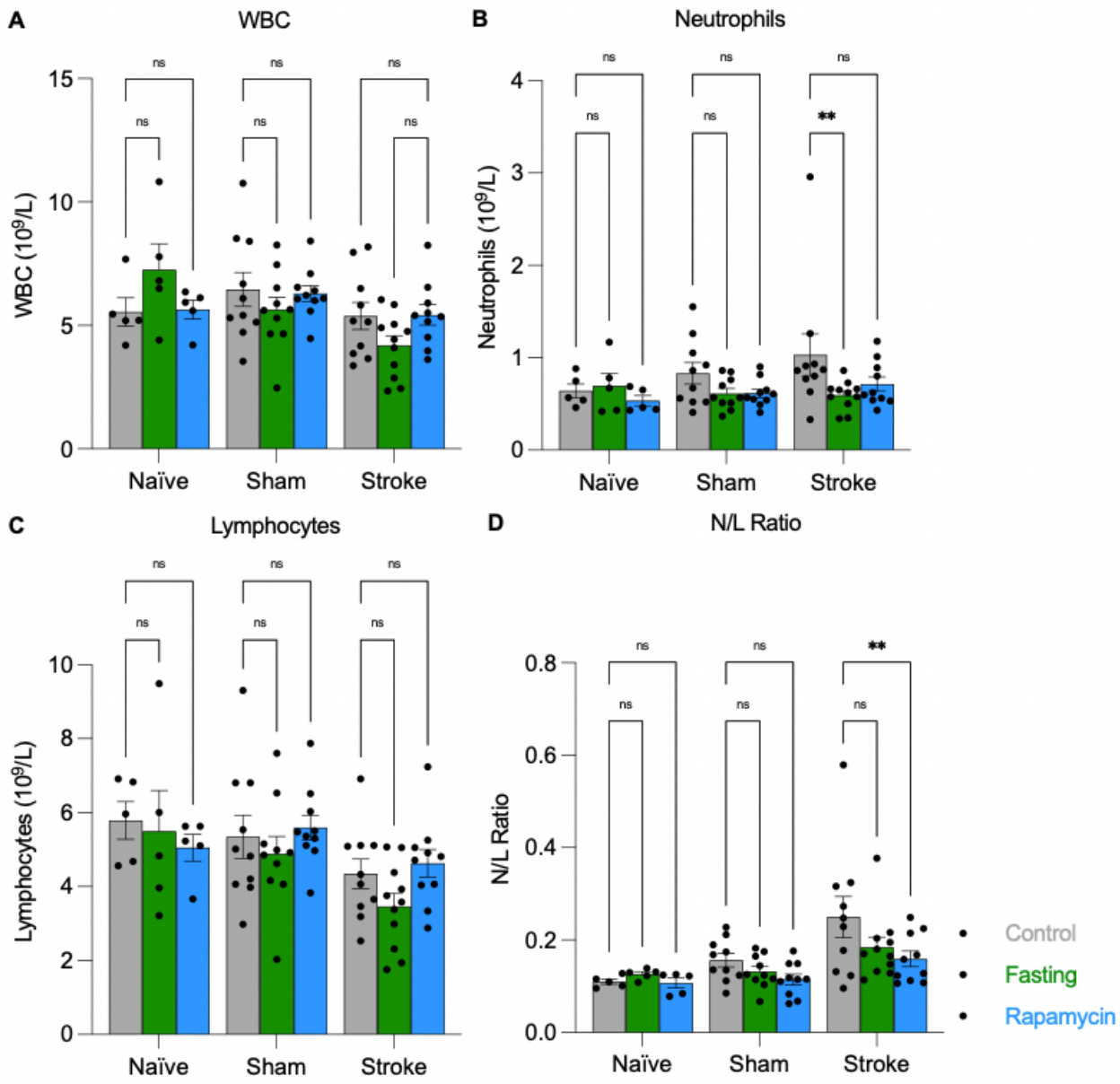

Figure 4.12 Fasting reduces neutrophils, and rapamycin reduces the neutrophil-to-lymphocyte ratio. The effect of 24 hours of fasting or rapamycin treatment on blood immune cells in naïve, sham-operated, and animals that had undergone stroke surgery was analyzed. Blood was drawn 24 hours following the initiation of either treatment and studied for WBC, neutrophils, leukocytes, and the N/L-ratio. **(A)** WBC, **(B)** Neutrophil numbers, **(C)** Leukocyte numbers, **(D)** N/L ratio. Results are presented in mean ± SEM. **p<0.01. n=5 in naïve groups, n=10 in sham and stroke groups.

4.3.9 Fasting or rapamycin does not significantly reduce mTOR activity

To investigate the effect of 24 hours of fasting or rapamycin treatment on mTOR activity, naïve animals that did not undergo surgery underwent either a 24-hour fasting period or received rapamycin treatment as described above, and either effect was compared to a control group that received vehicle treatment and did not undergo fasting. At 24 hours, striatal tissue was processed for Western Blotting. To study the activity of the mTOR pathway, phosphorylated mTOR (p-mTOR) and mTOR activity were examined, and the results were displayed as a ratio of phosphorylated to naïve mTOR protein presence, normalized to β-tubulin as the housekeeping protein. There was no statistically significant difference in the p-mTOR:mTOR ratio between the groups ($F(2, 12)=0.8500$, $p=0.4516$; one-way ANOVA) (**Figure 4.13**).

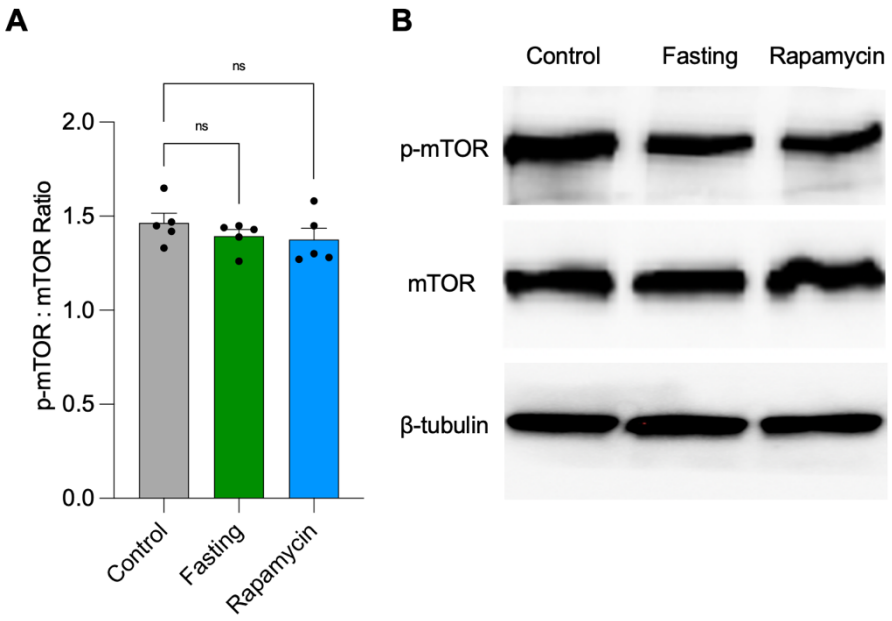

Figure 4.13 Fasting or rapamycin does not significantly reduce mTOR activity. The effect of rapamycin treatment on mTOR activity in the striatum of the right hemisphere in rats was investigated and compared to a control group. At 24 hours, WB was performed to study the activity of p-mTOR and mTOR proteins. mTOR activity was determined as the ratio of p-mTOR versus naïve mTOR protein quantity. **(A)** Quantification of mTOR activity based on p-mTOR to mTOR ratio, normalized to β-tubulin. **(B)** Representative Western Blots depict p-mTOR, mTOR, and β-tubulin activity. Results are presented in mean ± SEM. *p<0.05. n=5/per group in all groups.

4.3.10 The effects of glucose alterations following OGD on pericyte death and ATP concentration

Next, the effects of fasting and rapamycin treatment on cellular components of the BBB, particularly pericytes and endothelial cells were investigated. To examine whether glucose alterations following OGD affect pericyte death, once HBVP reached 70% confluency, cells were subjected to either 3 hours of normoxia or OGD, after which they were kept in media with distinct concentrations of glucose (0, 1, 5, 10 mM).

After 24 hours, cell death and cell proliferation were evaluated. Cell death was then normalized to cell proliferation in each intervention group. There was a main effect of OGD ($p<0.0001$; two-way ANOVA) and a trend of glucose concentrations ($p=0.0515$) on HBVP cell death, but no interaction between the two ($F(3,8)=0.8340$, $p=0.5119$). However, post-hoc testing revealed that, following OGD, there was no significant difference in cell death in cells kept in 0 mM glucose when compared to 1-, 5- or 10-mM glucose-containing media (0 vs. 1 mM ($p>0.9999$), 0 vs. 5 mM ($p>0.9999$), 0 vs. 10 nM ($p=0.1187$); Bonferroni's multiple comparisons test) (**Figure 4.14 (A)**).

Additionally, evaluating the ATP concentration at 24 hours showed that there was a main effect of OGD ($p=0.0003$), no main effect of glucose concentrations ($p=0.1279$) on HBVP ATP production, and also no interaction between the two ($F(3,8)=1.524$, $p=0.2813$). Post-hoc testing showed that, following OGD, there was no significant difference in ATP concentration in cells kept in 0 mM glucose when compared to 1-, 5- or 10-mM glucose-containing media (0 vs. 1 mM ($p=0.4932$), 0 vs. 5 mM ($p=0.1660$), 0 vs. 10 nM ($p=0.1568$)) (**Figure 4.14 (B)**).

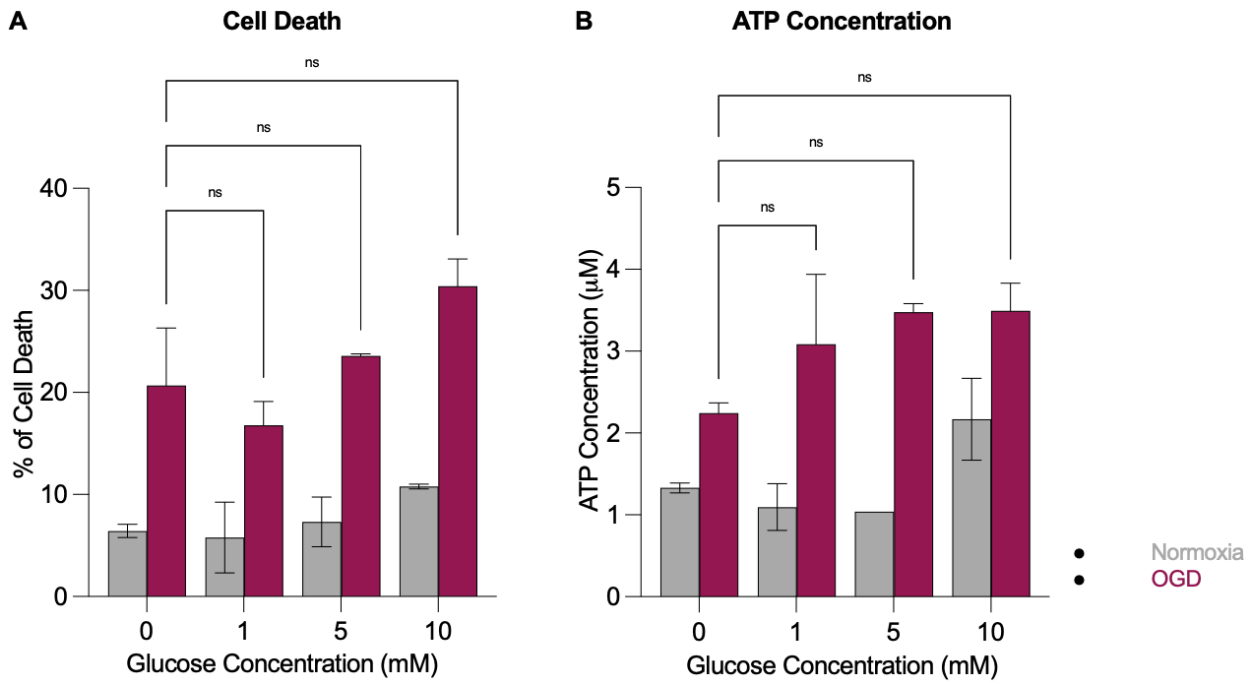

Figure 4.14 The effects of glucose alterations following OGD on pericyte death and ATP concentration. **(A)** Percentage of cell death normalized to cell proliferation of pericytes that, after 3 hours of OGD or normoxia (control) intervention, were kept in different glucose concentrations for 24 hours. **(B)** The concentration of ATP present in pericytes that, after 3 hours of OGD or normoxia (control) intervention, were kept in different glucose concentrations for 24 hours. Results are presented in mean ± SEM. *$p<0.05$. n=3 per group; all experiments were repeated twice.

4.3.11 The effects of glucose alterations following OGD on endothelial cell death and ATP concentration

The experiments were then performed in endothelial cells to investigate the effects of glucose alterations following OGD on cell death and ATP concentration on this cell type. There was a main effect of glucose concentrations ($p=0.0447$), but no main effect of OGD ($p=0.2839$) on hCMEC cell death, and also no interaction between the two effects ($F(3,8)=1.023$, $p=0.4321$). However, post-hoc testing revealed that, following OGD, there was no significant difference in cell death in cells kept in 0 mM glucose when compared to 1-, 5- or 10-mM glucose-containing media (0 vs. 1 mM ($p>0.9999$), 0 vs. 5 mM ($p>0.9999$), 0 vs. 10 nM ($p=0.4479$); Bonferroni's multiple comparisons test) (**Figure 4.15 (A)**).

Additionally, evaluating the ATP concentration at 24 hours showed that there was a main effect of both, OGD ($p=0.0001$), and glucose concentrations ($p=0.0064$) on hCMEC ATP production, but no interaction between the effects ($F(3,8)=1.839$, $p=0.2182$). Post-hoc testing showed that, following OGD, there was no significant difference in ATP concentration in cells kept in 0 mM glucose when compared to 1-, 5- or 10-mM glucose-containing media (0 vs. 1 mM ($p=0.2308$), 0 vs. 5 mM ($p=0.3822$), 0 vs. 10 nM ($p=0.7535$) (**Figure 4.14 (B)**).

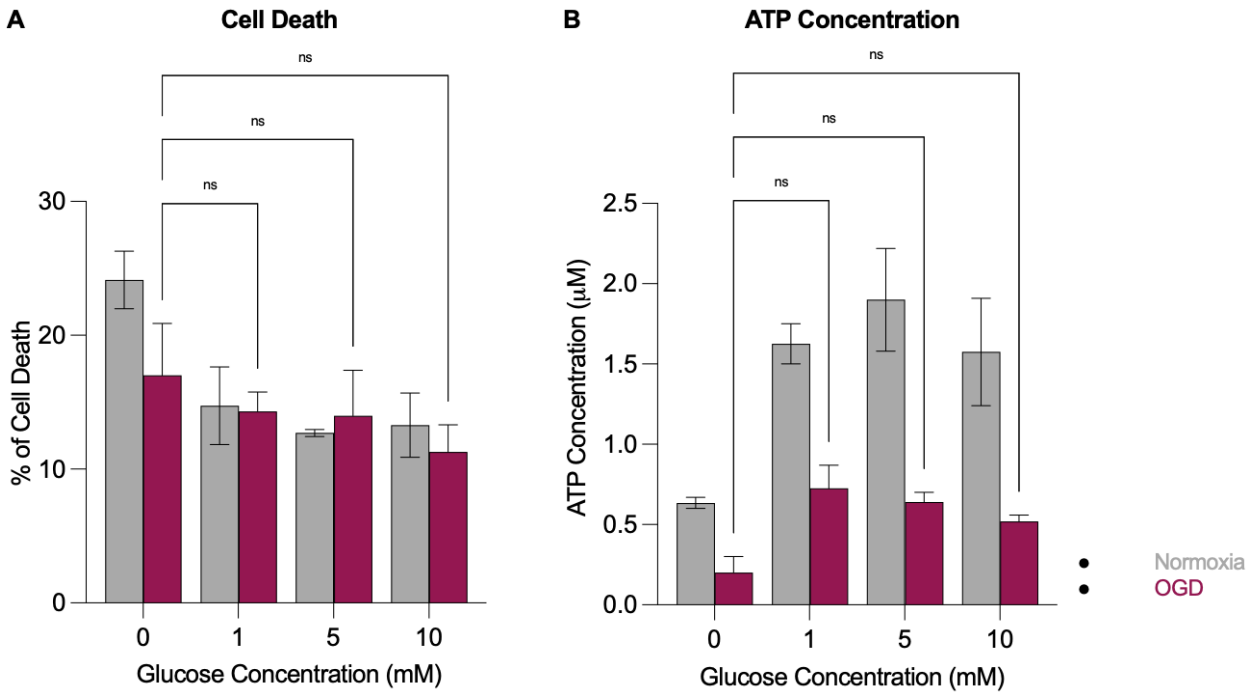

Figure 4.15 The effects of glucose alterations following OGD on endothelial cell death and ATP concentration. **(A)** Percentage of cell death normalized to cell proliferation of endothelial cells that, after 3 hours of OGD or normoxia (control), were kept in different glucose concentrations for 24 hours. **(B)** The concentration of ATP present in endothelial cells that, after 3 hours of OGD or normoxia (control), were kept in different glucose concentrations for 24 hours. Results are presented in mean ± SEM. *$p<0.05$. n=3 per group; all experiments were repeated twice.

4.4 Discussion

In this chapter, fasting was introduced as a treatment option for stroke. Fasting has been shown to have beneficial effects on metabolic health in times of cellular stress, in part by downregulating mTOR activity and reducing inflammation (Brandhorst, Harputlugil et al., 2017, Longo and Mattson, 2014, Mattson, Longo et al., 2017, Pak, Haws et al., 2021). It was established that fasting significantly reduces lesion volume and BBB breakdown 24 hours after the injection of ET-1. In comparison, while rapamycin reduces BBB leakiness, it does not affect stroke volume in this model. It was found that stroke induction with ET-1 minimally increases circulating inflammatory cells and that fasting but not rapamycin reduces neutrophil numbers in the blood and tends to reduce neutrophil infiltration into the brain. Further, an *in vitro* approach was used to study the cellular effects of OGD and the response to the amount of glucose present in the media of pericytes and endothelial cells. It was shown that OGD and varying glucose concentrations affect pericyte cell death, while ATP concentration is only affected by OGD. In endothelial cells, only glucose concentrations induce a main effect on cell death, whereas both OGD and glucose intervention impact cellular ATP concentrations. Together these results demonstrate that fasting is a promising way of mitigating stroke injury by reducing inflammation and ameliorating the breakdown of the BBB.

In addition to lesion volumes, inflammation is an essential aspect of the post-stroke landscape. Here, fasting was found to trend towards a reduction in neutrophil infiltration in the striatum, although post-hoc power calculations revealed these experiments were slightly underpowered (+4 animals). A previous study by Weston and colleagues investigated the temporal relationship between ischemic damage and neutrophil numbers in the ET-1 stroke model (Weston, Jones et al., 2007). They found that both stroke volume and neutrophil infiltration into the brain

peaked at three days and that the number of neutrophils was positively correlated with the volume of the infarcted tissue (Weston, Jones et al., 2007). Considering this, future work should aim to find the optimal dose-response relationship between the fasting intervention and its effects on post-ischemic inflammation and infarct progression (Weston, Jones et al., 2007). For example, it would be valuable to extend the current experiment and investigate the effects of a 24-hour fasting period immediately after the stroke and subsequent refeeding on the immunological and physiological outcome on day 3. Data from the cardiac field suggests this strategy would be beneficial (Lescano de Souza, Malfitano et al., 2015), but would also benefit from a comparison to more sustainable longer-term options such as caloric restriction or timed feeding (intermittent fasting). Given the fluid nature of the inflammatory response post-stroke it's even possible that altering the feeding strategy over the immediate post-stroke period would be beneficial to maintain a lower inflammatory response, starting with fasting, followed by timed feeding, followed by caloric restriction.

Current research suggests that fasting might work in various ways to provide health benefits independent of mTOR (de Cabo and Mattson, 2019). A recently published paper comprehensively reviewed data on the effects of rapamycin and caloric restriction and found strong evidence for different effects of the two interventions on lifespan extension and glucose metabolism (Unnikrishnan, Kurup et al., 2020). The effects of rapamycin on stroke outcome using the MCAo model (**Chapter 2**) were not replicated in this chapter, and rapamycin as an interventional strategy post-ischemia had a minimal impact on infarct volumes in the ET-1 model used here. This is likely due to the different physiological pathways that result in ischemia in the two models. Beard et al. demonstrated that rapamycin is expected to work via eNOS, which is not a pathway activated in the ET-1model of ischemia (Beard, Li et al., 2020). This suggests that any

positive effects of fasting in this model are independent of mTOR. Data from elsewhere have suggested that some degree of fasting is beneficial in the MCAo model, and that this appears to act via the induction of productive autophagy (Jeong, Yu et al., 2016).

Fasting may be beneficial in terms of translational potential as it does not suffer from a significant side-effect profile, unlike many pharmacological treatments, and therefore there is unlikely to be a mismatch between species, as is the case with some drugs. However, it should be said that rodent models used for stroke research may not display the same degree of inflammation as humans, and therefore fasting studies might not adequately mimic the biochemical and immunological complexities of the human pathophysiological cascade and metabolic pathways (Emerich, Dean et al., 2002). The dietary pattern of stroke patients in the first days to weeks after the insult is considerably influenced by the clinical outcome of the stroke and surrounding clinical settings whereas in rodents there is a pressure to make sure the animals are adequately eating and often those that do not because of severe injury are excluded from the studies. In patients, swallowing problems associated with stroke, known as post-stroke dysphagia, have been reported in 39-81% of patients (Martino, Foley et al., 2005, Steinhagen, Grossmann et al., 2009). However, no studies so far have investigated in a controlled environment whether altered dietary intake due to dysphagia is correlated with post-stroke outcome. To investigate potential underlying mechanisms for any observed correlation between dietary intake and stroke outcome, inflammation, and mTOR activity could be analyzed using blood samples (Dekter, Romijn et al., 2010, Nemes, Sebestyén et al., 2013).

In conclusion, this chapter sought to examine the effects of fasting on stroke volume, BBB integrity, and post-stroke inflammation at 24 hours and benchmarked the results against the effect of rapamycin. It was found that fasting, but not rapamycin treatment, reduced stroke volume,

reduced neutrophils in the blood, and tended to reduce neutrophil infiltration into the brain ($p=0.0925$), while both fasting and rapamycin improved BBB integrity at 24 hours. *In vitro,* it was demonstrated that OGD and varying glucose concentrations show varying effects on cell death and ATP concentration. These results are promising and suggest fasting as a potential treatment option to reperfusion therapy and other neuroprotective treatment options in ischemic stroke. While further research is needed to further explore the effects of fasting and the optimal dose-response relationship, this initial experiment yields promising results for fasting to be used as an additional treatment option that does not bear the risk of pharmacological side effects is low cost and widely accessible.

Chapter 5: Discussion

Principal findings

The unifying theme of my thesis is the neuroprotective effect of metabolic interventions in the setting of acute ischemic stroke. The principal findings are:

1. Post-stroke rapamycin treatment increases cerebral perfusion in the hyperacute phase, decreases lesion volume, and improves functional outcome after MCAo in the rat (**Chapter 2**).

2. *In vitro* rapamycin application after OGD intervention significantly affects the functional and molecular health of both pericytes and endothelial cells, two central components of the BBB (**Chapter 3**).

3. Fasting decreases inflammation, stabilizes the BBB, and reduces infarct volume after ET-1injection (**Chapter 4**).

5.1 Cerebral blood flow and the blood-brain barrier

As shown in this thesis and by others, rapamycin treatment immediately following reperfusion reduces infarct volumes and improves functional outcomes at both an acute (24 hours) and later time point (72 hours) (Beard, Li et al., 2020). The mechanisms by which rapamycin exerts its effects are not yet entirely understood, but there is a robust increase in CBF at the time of administration, a phenomenon known to improve brain health after a stroke (Brugnara, Herweh et al., 2022). Given Beard et al.'s demonstration of the eNOS dependency of this effect, inhibiting eNOS to prevent the vascular effects of rapamycin would establish whether CBF is a causal factor in the improvements seen here (Beard, Li et al., 2020). The eNOS dependency of rapamycin's pharmacodynamics might also help explain the absence of effectiveness in the ET-1 model, which

does not act via eNOS, suggesting that any positive effects of dietary restriction (DR) seen in this vasoconstrictive model are likely to be independent of mTOR (Beard, Li et al., 2020, Grunewald, Jurrissen et al., 2019). Given data in endothelial cells suggesting that dietary restrictions might dilate blood vessels, the benefits of fasting may still be via improved blood flow, but via an eNOS-independent mechanism (Headland, Clifton et al., 2018). In addition to improved CBF, there may also be changes to BBB mediated by rapamycin's effect on endothelial cells, pericytes, and their interaction with each other and similar mechanisms may exist for fasting (Chi, Kiss et al., 2017, Chi, Mellender et al., 2016, Teunissen-Beekman, Dopheide et al., 2015, Van Skike, Jahrling et al., 2018).

Endothelial cells, essential for maintaining BBB integrity and angiogenesis, and pericytes, important for endothelial cell support and CBF regulation, respond to ischemic injury by losing their structural integrity and increasing their contractile tone, leaving the BBB impaired and effective microcirculation reduced (Beard, Brown et al., 2020, Beard, Li et al., 2020, Sandoval and Witt, 2008, Sharif, Jumah et al., 2018, Yemisci, Gursoy-Ozdemir et al., 2009). mTOR inhibition using rapamycin affects both cell types in a way that is mainly dependent on the timing of the treatment in relation to the hypoxic injury, being largely beneficial when given post-stroke and harmful when given before or at the time of the stroke (see **Chapter 3**). This has also been confirmed in previous studies concerning the BBB, showing that rapamycin treatment before versus after the ischemic injury disrupted or improved its integrity, respectively (Chi, Mellender et al., 2016, Van Skike, Jahrling et al., 2018).

There is ample evidence for crosstalk between endothelial cells and pericytes, dictating the effectiveness of molecular mediators of vascular remodeling and stability, and stroke has shown to cause aberrations in this interaction (Geevarghese and Herman, 2014, Ozerdem and Stallcup,

2003). Despite increased recognition of rapamycin's crucial role in impacting both cell types individually, no research so far has been published that sought to understand how mTOR inhibition affects endothelial cell-pericyte crosstalk following ischemic stroke, thereby omitting potential opportunities for cerebroprotective intervention. Future research could investigate how rapamycin, in a stroke setting, impacts growth factors, direct endothelial cell-pericyte contact, and extracellular matrix modulation, identified as the three main ways of their interaction (Geevarghese and Herman, 2014, Sweeney and Foldes, 2018).

Outside the scope of this thesis was studying the specific function of endothelial cells post-stroke and rapamycin's modulatory role in this context. Primarily owing to ophthalmology and cancer research, there is scientific consensus that mTOR inhibition with rapamycin interferes with angiogenesis in part by inhibiting the signaling molecule VEGF in a time-dependent manner (Asani, Siedlecki et al., 2022, Faes, Santoro et al., 2017, Petővári, Hujber et al., 2018, Stahl, Paschek et al., 2008). Early in the post-ischemic process, VEGF induces vascular leakiness and permeability, while at later time points, it drives angiogenesis by enhancing endothelial cell migration and proliferation, thereby allowing the formation of a more efficient collateral network that can help circumvent the damaged area and rescue the penumbra (Adamczak and Hoehn, 2015, Geiseler and Morland, 2018). Therapeutically, the goal should be to deploy rapamycin in such a way that it reduces VEGF signaling in the hyperacute and acute post-stroke phase, and fosters VEGF activity at a later timepoint, thereby minimizing BBB breakdown, and maximizing blood vessel restoration, respectively (Geiseler and Morland, 2018). Indeed, a study by Apelo et al. found that, in mice, a one-time 1mg/kg (low-dose) rapamycin treatment within six hours after stroke, which is consistent with the treatment approach used in this thesis, suppressed mTORC1 acutely and was cleared from the brain by three days, allowing critical angiogenic and neuronal

proliferation necessary for stroke recovery (Arriola Apelo, Neuman et al., 2016, Hadley, Beard et al., 2019, Huang and Manning, 2008, Lo, 2008). It is known that fasting protocols increase VEGF activity and therefore one possibility could involve early adjunct therapy for the permeable BBB and later dietary interventions for the inflammatory response and angiogenesis (Kim, Kim et al., 2017).

Another essential aspect of endothelial cell function in the post-stroke environment is its impact on neuroinflammation and how it can be modulated by mTOR inhibition. The recruitment of circulating leukocytes through the neurovascular endothelium into the ischemic brain parenchyma requires adhesion molecule expression on the endothelial cell surface (Yilmaz and Granger, 2008, Yilmaz and Granger, 2010). Studies have shown that rapamycin treatment reduces ICAM-1 expression on endothelial cells, thereby inhibiting neuroinflammation and promoting BBB integrity (Daniel, Dutzmann et al., 2017, Mejia, Treviño-Villarreal et al., 2017, Sun, Yin et al., 2018, Wang, Qin et al., 2014). While there is also evidence for improved stroke outcomes in ICAM-1 knockout mice, no studies have investigated whether rapamycin therapy in a stroke model leads to improved outcomes in part by reduced ICAM-1 expression (Connolly, Winfree et al., 1996). Adhesion molecules are also altered by fasting regimens, suggesting that mTOR is a key regulator of adhesion molecule expression and that targeting it via either a pharmacological, or non-pharmacological mechanism, is likely to be beneficial in reducing post-stroke immune cell migration (Chen, Su et al., 2021).

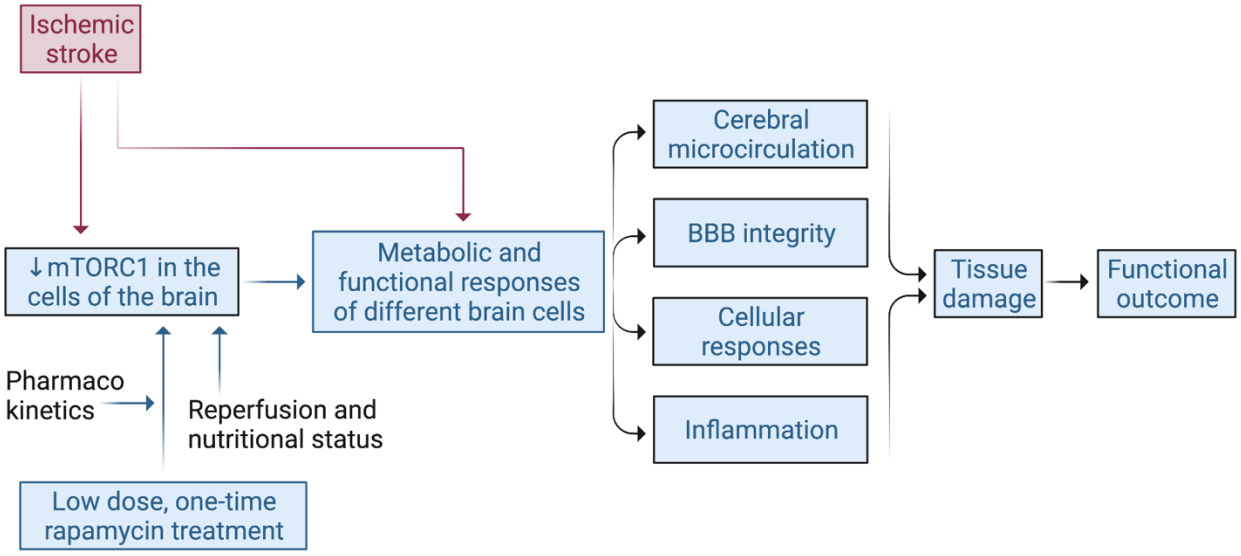

Figure 5.1 Conceptual model of ischemic stroke and the impact of low-dose, one-time rapamycin treatment effect, tissue damage, and functional outcome with influencing factors. Created with BioRender.com.

5.2 Inflammation

Building upon the previously discussed role of rapamycin in endothelial cell activation and leukocyte migration, and considering data from this thesis and others, it is becoming increasingly clear that mTOR inhibition with rapamycin is not only neuroprotective after ischemia through directly inducing neuronal autophagy and improving cerebrovascular function but also through positively affecting other systemic post-stroke processes, such as the downregulation of inflammation (Hadley, Beard et al., 2019, Li, Wang et al., 2016, Wu, Zhang et al., 2018).

While consistent with what I have found in this thesis, it has been generally accepted that, in the brain, mTOR downregulation following ischemia mitigates inflammation as evidenced by reduced pro-inflammatory cytokine expression and astrocyte activation, the effects are contrasting in other organ systems such as the liver and the heart (Aoyagi, Kusakari et al., 2012, Beard, Couch et al., 2022, Beard, Hadley et al., 2021, Beard, Li et al., 2020, Gao, Wei et al., 2020). In the liver, mTOR activation rather than inhibition reduces immune-cell activity through a mechanism dependent on the NF-κB proinflammatory cytokine pathway (Li, Zhang et al., 2017). Similarly, in the heart, it has been shown that mTOR overexpression might protect against ischemia/reperfusion (I/R) injury in part by reducing pro-inflammatory cytokines as measured in the cardiac effluent (Aoyagi, Kusakari et al., 2012). The opposing impact of mTOR activity has been previously addressed by *in vitro* experiments reporting tissue and sex-specific effects of mTOR-modulatory therapies (Rodriguez, Dodds et al., 2014, Zhang, Bokov et al., 2014). This Janus-faced effect of mTOR activity on post-ischemic inflammation in different organs suggests that mTOR activity is not only good or bad after ischemia and that its functional impact depends on the organ's cellular milieu.

In the brain, various inflammatory processes are involved in the post-ischemic environment. For example, early activation of microglia and astrocytes produces pro-inflammatory cytokines, which mobilize systemic immune cells such as macrophages and neutrophils to the site of injury (Iadecola, Buckwalter et al., 2020). mTOR inhibition may be affecting microglial and astrocyte function in the brain by preventing their polarization to the M1 phenotype and enhancing anti-inflammatory regulatory T-cells, respectively (Li, Li et al., 2015, Xie, Sun et al., 2014). In the periphery, it is well established that inflammatory cells such as neutrophils can mobilize and damage the BBB, and it is feasible that rapamycin is inhibiting this process (Gomez-Cambronero, 2003). Rapamycin is also known to disrupt neutrophil extracellular trap (NET) formation, and NETs are known to impede revascularization after stroke (Kang, Yu et al., 2020, McInturff, Cody et al., 2012). While the findings of this thesis and others suggest that the positive immunomodulatory effects of rapamycin treatment are primarily impacting the hyperacute stroke phase, a deeper understanding of the timing of mTOR activity in the different cells involved in the ischemic cascade is needed (Wang, Lin et al., 2019). Experiments characterizing mTOR activity between organ systems, tissues, and cells during ischemia and the different post-stroke phases would provide a greater understanding of the metabolic functioning and whole-body effect of localized hypoperfusion and, therefore, the potential to inhibit this process using rapamycin.

5.3 Fasting as a rapamycin mimetic

Alfred J. Meijer described in 1995 that amino acids activated the S6 kinase of the mTOR pathway in cultured hepatocytes, demonstrating for the first time that the mTOR pathway discerns cellular energy levels (Blommaart, Luiken et al., 1995). Now, mTOR is recognized as the master regulator of energy metabolism by sensing nutrients, growth factors, and oxygen levels and responding

through anabolic or catabolic signaling for optimal cellular health and function (Liu and Sabatini, 2020). The largest body of literature concerning the comparison of rapamycin treatment and dietary restriction comes from anti-aging research (de Cabo, Carmona-Gutierrez et al., 2014, de Cabo and Mattson, 2019, Mattison, Colman et al., 2017, Pak, Haws et al., 2021), and it is widely accepted that mTORC1 plays a central role in response to dietary interventions (Unnikrishnan, Kurup et al., 2020). This is further supported by studies describing no further beneficial mTORC1-dependent effects, such as lifespan-extension, in dietary-restricted yeast lacking the TOR1 gene (Kaeberlein, Powers et al., 2005, Unnikrishnan, Kurup et al., 2020).

There has been significant interest in rapamycin as a potential DR-mimetic, but the side effects reported when using rapamycin have precluded its wider distribution (Blagosklonny, 2019a, Blagosklonny, 2019b, Leontieva, Paszkiewicz et al., 2014, Salmon, 2015). However, DR itself might be a promising therapeutic option, it is widely accessible and cheap and avoids the risk of pharmacological side effects (Ciobanu, Elena Sandu et al., 2017, Ran, Li et al., 2015, Varendi, Airavaara et al., 2014, Yu and Mattson, 1999). Still, for DR, as with rapamycin, the effective treatment strategy and interventional timing are yet to be established, and studies so far have varied wildly (Bruce-Keller, Umberger et al., 1999, Ciobanu, Elena Sandu et al., 2017, de Carvalho, Sanchez-Mendoza et al., 2021, Ran, Li et al., 2015, Varendi, Airavaara et al., 2014). To date, there are two clinical trials registered to investigate the effects of time-restricted feeding on stroke recovery, and results are currently pending.

Despite the similarities and shared mTORC1 target, the effects of DR and rapamycin treatment are not identical and work in this thesis, and other studies highlight different effects on some of the cellular processes and molecular pathways (Unnikrishnan, Kurup et al., 2020). Studies using *C. elegans*, a roundworm extensively used for gerontology research, identified longevity

mechanisms activated by DR independent of mTOR (Hansen, Taubert et al., 2007), while metabolomic and transcriptomic studies in mammals examining blood, liver, and adipose tissue suggest that rapamycin and DR have distinct, largely non-overlapping effects (Choi, Hong et al., 2017, Fok, Bokov et al., 2014, Fok, Livi et al., 2014, Karunadharma, Basisty et al., 2015, Unnikrishnan, Kurup et al., 2020, Yu, Wang et al., 2015). For example, only DR, but not rapamycin, has shown to impact gene expression, fatty acid biosynthesis, and circadian rhythm signaling while severely reducing energy storage molecules such as glycogen and lipid droplets (Choi, Hong et al., 2017, Fok, Livi et al., 2014). Further, while both DR and rapamycin have been shown to extend lifespan in part by improving protein quality and reducing the synthetic burden and damage, their impact on protein turnover and abundance significantly differs in mitochondrial and immune system signaling pathways (Karunadharma, Basisty et al., 2015). In the stroke setting, data from this thesis and elsewhere have shown that the two interventions also impact the post-stroke environment in distinct ways, with DR exhibiting mostly acute immune-modulatory effects and rapamycin acutely affecting the microcirculation and impacting the inflammatory response at a more chronic time point.

As we advance, a logical next step would be to combine fasting and rapamycin treatment to investigate whether, together, they improve stroke outcomes synergistically even more than alone, by, for example, administering a single dose of rapamycin immediately followed by a 24-hour fasting period. With this, to take the immune-modulatory effect of both interventions as an example, fasting would target post-stroke inflammation in the acute and rapamycin in the more chronic phase, while either treatment is kept to a minimum to avoid unwanted side effects.

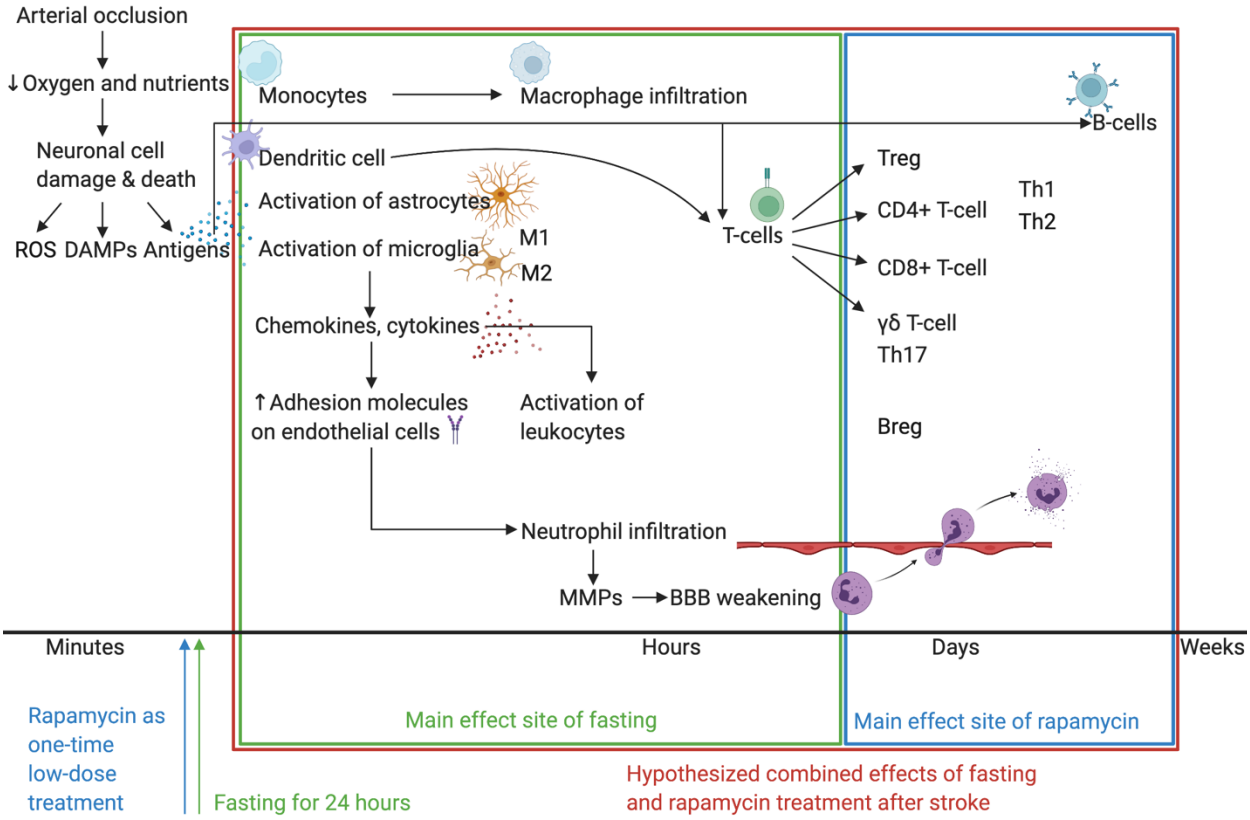

Figure 5.2 Hypothesized treatment effect of fasting and rapamycin combination therapy on post-ischemic inflammation. Fasting predominantly positively affects inflammation in the acute phase after stroke. Rapamycin has been shown to positively alter the inflammatory milieu at a more chronic time point. Combination therapy of one-time low-dose rapamycin treatment given at reperfusion, together with fasting starting also at reperfusion for 24 hours, might yield additional benefits for ameliorating inflammation after cerebral ischemia. Created with Biorender.

5.4 Stroke models

While a systematic review provided evidence for rapamycin's overall dose- and time-dependent efficacy, there has been contradictory evidence for its impact across different stroke models and outcomes analyzed (Beard, Hadley et al., 2019) (also see **Chapter 1.2.1** on preclinical models of stroke). For studying the BBB, for example, the effect of mTOR inhibition varies depending on the model used, which has also become apparent in this thesis with rapamycin effectively improving BBB integrity in the MCAo model while failing to show such an effect in the ET-1 model (Hadley, Beard et al., 2019).

In vitro models are advantageous for investigating the effect of mTOR inhibition on a particular cell type or confined cellular interactions, such as the previously discussed endothelial cell-pericyte crosstalk and BBB stabilization (Holloway and Gavins, 2016). For example, data from this thesis and elsewhere, although limited in number, suggest that rapamycin improves endothelial cell adhesion, tight junction integrity, and BBB stability when given as a one-time treatment following OGD (Li, Gao et al., 2014) (**Chapter 4**). However, *in vitro* models are limited to a certain degree of complexity, and more physiologically convoluted processes, such as CBF regulation, are harder to devise (Holloway and Gavins, 2016). Similarly, to study aspects of whole-body physiological relevance, such as fasting, using *in vitro* models becomes a challenge. Many immortalized lines use proprietary media which often contains extremely high, physiologically irrelevant levels of glucose (Holloway and Gavins, 2016). As such, data from these models should be considered carefully and in context.

In vivo models, on the other hand, being inherently more complex, better represent physiological conditions under which mTOR inhibition with rapamycin, for example, would also need to prove its efficacy before considerations for clinical translation (Diwakar, Gowaikar et al.,

2021, Macrae, 2011). Local application of ET-1 induces strong vasoconstriction leading to reduced regional blood flow and subsequent ischemia, and has the advantage of closely resembling gradual reperfusion of the hypoperfused artery and negligible whole-body effects of the surgery thanks to its minimal invasiveness (Abeysinghe and Roulston, 2018, Diwakar, Gowaikar et al., 2021). The ET-1 model lends itself to mTOR-related studies illustrating effects on whole-body phenomena such as reduced inflammation, but in light of the previously discussed eNOS-independency, it prohibits more extensive studies on the impact of mTOR inhibition on the cerebrovasculature post-stroke (Abeysinghe and Roulston, 2018, Macrae, 2011) (**Chapter 4**). In contrast, work from this thesis and beyond has shown that when using the pervasive MCAo model, low-dose one-time rapamycin treatment inhibiting mTORC1 improves CBF and BBB integrity, thereby reducing brain damage improved functional outcome (Beard, Couch et al., 2022, Beard, Hadley et al., 2021) (**Chapter 2**).

Ultimately, the appropriateness of the chosen stroke model is dependent on what effects of mTOR inhibition are central to the research question and which model is best suited to study a perceived mechanism of action on CBF, BBB integrity, inflammation, and the post-stroke pathophysiologic cascade overall (Holloway and Gavins, 2016, Macrae, 2011). However, reconsidering the chosen stroke models in my thesis, using the MCAo instead of the ET-1 model to investigate and compare the effect of DR and rapamycin treatment, would have potentially allowed more insights into the intervention's effects on stroke recovery, especially considering the previously discussed mTOR independence of the ET-1 model on the microcirculation.

5.5 Concluding remarks

This thesis made several novel observations concerning neuroprotective therapy following cerebral ischemia. Inhibition of mTORC1 in the hyperacute phase of stroke appears beneficial. Rapamycin enhances CBF, mitigates BBB breakdown, reduces stroke volume, and improves functional outcomes. This supports the literature on rapamycin being a promising pharmacological agent as an adjunct treatment to recanalization therapy. Comparing post-ischemic fasting, a non-pharmacological way to reduce mTOR, found that it successfully reduces stroke volume and inflammation. However, both interventions affect the whole body, and, precisely, the distinct effects on the brain and individual brain cells have not yet been fully elucidated. In addition to that, a better understanding of the time-dependent effects of stroke and treatment on various cells of the brain and other organ systems is missing. More pre-clinical studies should build on this work and expand this knowledge to find the optimal time and dose of treatment in the presence and absence of recanalization therapy.

While further work is required to refine the potential of the proposed neuroprotective agents as additional treatment options for ischemic stroke therapy, this thesis nonetheless highlights the potential of therapeutic possibilities that go beyond reperfusion and suggests that targeting ubiquitous systems such as mTOR might be effective adjunct therapy options alongside reperfusion for patients suffering from an ischemic stroke.

Bibliography

Abbott, N. J., et al. (2010). Structure and function of the blood-brain barrier. *Neurobiol Dis* 37(1) 13-25.

Abeysinghe, H. C. S. and C. L. Roulston (2018). A Complete Guide to Using the Endothelin-1 Model of Stroke in Conscious Rats for Acute and Long-Term Recovery Studies. *Methods Mol Biol* 1717 115-133.

Abraham, M. and R.-C. P. l. s. P. A. M. (2016). Noninvasive Brain Imaging in Small Animal Stroke Models: MRI, PET, and SPECT. New York, NY, Humana Press. 157-186.

Adamczak, J. and M. Hoehn (2015). Poststroke angiogenesis, con: dark side of angiogenesis. *Stroke* 46(5) e103-104.

Al Ahmad, A., et al. (2011). Astrocytes and pericytes differentially modulate blood-brain barrier characteristics during development and hypoxic insult. *J Cereb Blood Flow Metab* 31(2) 693-705.

Albers, G. W., et al. (2018). Thrombectomy for Stroke at 6 to 16 Hours with Selection by Perfusion Imaging. *N Engl J Med* 378(8) 708-718.

Andjelkovic, A. V., et al. (2019). Endothelial Targets in Stroke: Translating Animal Models to Human. *Arterioscler Thromb Vasc Biol* 39(11) 2240-2247.

Antonic, A., et al. (2018). NXY-059, a Failed Stroke Neuroprotectant, Offers No Protection to Stem Cell-Derived Human Neurons. *J Stroke Cerebrovasc Dis* 27(8) 2158-2165.

Aoyagi, T., et al. (2012). Cardiac mTOR protects the heart against ischemia-reperfusion injury. *Am J Physiol Heart Circ Physiol* 303(1) H75-85.

Arai, K., et al. (2011). Cellular mechanisms of neurovascular damage and repair after stroke. *J Child Neurol* 26(9) 1193-1198.

Arba, F., et al. (2020). Blood-Brain Barrier Disruption and Hemorrhagic Transformation in Acute Ischemic Stroke: Systematic Review and Meta-Analysis. *Front Neurol* 11 594613.

Armulik, A., A. Abramsson and C. Betsholtz (2005). Endothelial/pericyte interactions. *Circ Res* 97(6) 512-523.

Arriola Apelo, S. I., et al. (2016). Alternative rapamycin treatment regimens mitigate the impact of rapamycin on glucose homeostasis and the immune system. *Aging Cell* 15(1) 28-38.

Arumugam, T. V., et al. (2010). Age and energy intake interact to modify cell stress pathways and stroke outcome. *Ann Neurol* 67(1) 41-52.

Asaithambi, G., et al. (2020). Current trends in the acute treatment of ischemic stroke: analysis from the Paul Coverdell National Acute Stroke Program. *J Neurointerv Surg* 12(6) 574-578.

Asani, B., et al. (2022). Anti-angiogenic properties of rapamycin on human retinal pericytes in an in vitro model of neovascular AMD via inhibition of the mTOR pathway. *BMC Ophthalmol* 22(1) 138.

Balami, J. S., et al. (2018). Complications of endovascular treatment for acute ischemic stroke: Prevention and management. *Int J Stroke* 13(4) 348-361.

Bang, O. Y., M. Goyal and D. S. Liebeskind (2015). Collateral Circulation in Ischemic Stroke: Assessment Tools and Therapeutic Strategies. *Stroke* 46(11) 3302-3309.

Bardutzky, J., et al. (2005). Differences in ischemic lesion evolution in different rat strains using diffusion and perfusion imaging. *Stroke* 36(9) 2000-2005.

Baron, J. C. (2018). Protecting the ischaemic penumbra as an adjunct to thrombectomy for acute stroke. *Nat Rev Neurol* 14(6) 325-337.

Beard, D. J., L. S. Brown and B. A. Sutherland (2020). The rise of pericytes in neurovascular research. *J Cereb Blood Flow Metab* 40(12) 2366-2373.

Beard, D. J., et al. (2022). Rapamycin Treatment Reduces Brain Pericyte Contraction by Reducing RhoA Pathway Activity in an In Vitro Model of Ischemia *Unpublished*.

Beard, D. J., et al. (2021). Commentary: Rapalink-1 Increased Infarct Size in Early Cerebral Ischemia-Reperfusion With Increased Blood-Brain Barrier Disruption. *Front Physiol* 12 761556.

Beard, D. J., et al. (2019). The effect of rapamycin treatment on cerebral ischemia: A systematic review and meta-analysis of animal model studies. *Int J Stroke* 14(2) 137-145.

Beard, D. J., et al. (2020). Rapamycin Induces an eNOS (Endothelial Nitric Oxide Synthase) Dependent Increase in Brain Collateral Perfusion in Wistar and Spontaneously Hypertensive Rats. *Stroke* 51(9) 2834-2843.

Bederson, J. B., et al. (1986). Rat middle cerebral artery occlusion: evaluation of the model and development of a neurologic examination. *Stroke* 17(3) 472-476.

Bernardo-Castro, S., et al. (2020). Pathophysiology of Blood-Brain Barrier Permeability Throughout the Different Stages of Ischemic Stroke and Its Implication on Hemorrhagic Transformation and Recovery. *Front Neurol* 11 594672.

Blagosklonny, M. V. (2019a). Fasting and rapamycin: diabetes versus benevolent glucose intolerance. *Cell Death Dis* 10(8) 607.

Blagosklonny, M. V. (2019b). Rapamycin for longevity: opinion article. *Aging (Albany NY)* 11(19) 8048-8067.

Blommaart, E. F., et al. (1995). Phosphorylation of ribosomal protein S6 is inhibitory for autophagy in isolated rat hepatocytes. *J Biol Chem* 270(5) 2320-2326.

Bochelen, D., M. Rudin and A. Sauter (1999). Calcineurin inhibitors FK506 and SDZ ASM 981 alleviate the outcome of focal cerebral ischemic/reperfusion injury. *J Pharmacol Exp Ther* 288(2) 653-659.

Boehme, C., et al. (2019). The dimension of preventable stroke in a large representative patient cohort. *Neurology* 93(23) e2121-e2132.

Brandhorst, S., et al. (2017). Protective effects of short-term dietary restriction in surgical stress and chemotherapy. *Ageing Res Rev* 39 68-77.

Bright, R. (1827). *Reports of Medical Cases*. London: Richard Taylor for Longman, Rees, Orme, Brown, and Green.

Brott, et al. (1995). Tissue plasminogen activator for acute ischemic stroke. *N Engl J Med* 333(24) 1581-1587.

Bruce-Keller, A. J., et al. (1999). Food restriction reduces brain damage and improves behavioral outcome following excitotoxic and metabolic insults. *Ann Neurol* 45(1) 8-15.

Brugnara, G., et al. (2022). Dynamics of cerebral perfusion and oxygenation parameters following endovascular treatment of acute ischemic stroke. *J Neurointerv Surg* 14(1).

Brunet, A., et al. (2004). Stress-dependent regulation of FOXO transcription factors by the SIRT1 deacetylase. *Science* 303(5666) 2011-2015.

Bruno, A., et al. (2002). Admission glucose level and clinical outcomes in the NINDS rt-PA Stroke Trial. *Neurology* 59(5) 669-674.

Buchan, A. and W. A. Pulsinelli (1990). Hypothermia but not the N-methyl-D-aspartate antagonist, MK-801, attenuates neuronal damage in gerbils subjected to transient global ischemia. *J Neurosci* 10(1) 311-316.

Buchan, A. M., A. Slivka and D. Xue (1992). The effect of the NMDA receptor antagonist MK-801 on cerebral blood flow and infarct volume in experimental focal stroke. *Brain Res* 574(1-2) 171-177.

Buckley, K. M., et al. (2014). Rapamycin up-regulation of autophagy reduces infarct size and improves outcomes in both permanent MCAL, and embolic MCAO, murine models of stroke. *Exp Transl Stroke Med* 6 8.

Böttiger, Y., et al. (2001). Pharmacokinetic interaction between single oral doses of diltiazem and sirolimus in healthy volunteers. *Clin Pharmacol Ther* 69(1) 32-40.

Campbell, B. C., et al. (2013). CT perfusion improves diagnostic accuracy and confidence in acute ischaemic stroke. *J Neurol Neurosurg Psychiatry* 84(6) 613-618.

Campbell, B. C. V., et al. (2019). Ischaemic stroke. *Nat Rev Dis Primers* 5(1) 70.

Canazza, A., et al. (2014). Experimental models of brain ischemia: a review of techniques, magnetic resonance imaging, and investigational cell-based therapies. *Front Neurol* 5 19.

Cao, S. and H. Dong (2021). Predictive value of DWI-FLAIR Mismatch in patients with Ischemic Stroke and receiving Endovascular treatment beyond Time Window. *Pak J Med Sci* 37(2) 466-471.

Caplan, L. R. (2016). *Caplan's Stroke A Clinical Approach*: Cambridge University Press.

Chamorro, Á., et al. (2021). The future of neuroprotection in stroke. *J Neurol Neurosurg Psychiatry* 92(2) 129-135.

Chauhan, A., et al. (2015). Rapamycin ameliorates brain metabolites alterations after transient focal ischemia in rats. *Eur J Pharmacol* 757 28-33.

Chauhan, A., et al. (2011). Rapamycin protects against middle cerebral artery occlusion induced focal cerebral ischemia in rats. *Behav Brain Res* 225(2) 603-609.

Chen, J., et al. (2019). Oxygen-Glucose Deprivation/Reoxygenation Induces Human Brain Microvascular Endothelial Cell Hyperpermeability Via VE-Cadherin Internalization: Roles of RhoA/ROCK2. *J Mol Neurosci* 69(1) 49-59.

Chen, S. and N. Sang (2016). Hypoxia-Inducible Factor-1: A Critical Player in the Survival Strategy of Stressed Cells. *J Cell Biochem* 117(2) 267-278.

Chen, Y., et al. (2021). Intermittent Fasting Inhibits High-Fat Diet-Induced Atherosclerosis by Ameliorating Hypercholesterolemia and Reducing Monocyte Chemoattraction. *Front Pharmacol* 12 719750.

Chi, O. Z., et al. (2016). Effects of rapamycin on cerebral oxygen supply and consumption during reperfusion after cerebral ischemia. *Neuroscience* 316 321-327.

Chi, O. Z., et al. (2017). Rapamycin decreased blood-brain barrier permeability in control but not in diabetic rats in early cerebral ischemia. *Neurosci Lett* 654 17-22.

Chi, O. Z., et al. (2016). Effects of rapamycin pretreatment on blood-brain barrier disruption in cerebral ischemia-reperfusion. *Neurosci Lett* 620 132-136.

Choi, K. M., et al. (2017). Caloric Restriction and Rapamycin Differentially Alter Energy Metabolism in Yeast. *J Gerontol A Biol Sci Med Sci* 73(1) 29-38.

Ciobanu, O., et al. (2017). Caloric restriction stabilizes body weight and accelerates behavioral recovery in aged rats after focal ischemia. *Aging Cell* 16(6) 1394-1403.

Cipolla, M. J., et al. (2014). Postischemic reperfusion causes smooth muscle calcium sensitization and vasoconstriction of parenchymal arterioles. *Stroke* 45(8) 2425-2430.

Connolly, E. S., Jr., et al. (1996). Cerebral protection in homozygous null ICAM-1 mice after middle cerebral artery occlusion. Role of neutrophil adhesion in the pathogenesis of stroke. *J Clin Invest* 97(1) 209-216.

Cruveilhier, J. (1829). *ANATOMIE PATHOLOGIQUE DU CORPS HUMAIN*: J. B. Baillière.

Cuccione, E., et al. (2017). Multi-site laser Doppler flowmetry for assessing collateral flow in experimental ischemic stroke: Validation of outcome prediction with acute MRI. *J Cereb Blood Flow Metab* 37(6) 2159-2170.

Cui, Q., et al. (2013). Rho kinase: A new target for treatment of cerebral ischemia/reperfusion injury. *Neural Regen Res* 8(13) 1180-1189.

da Luz Sousa Fialho, M., et al. (2021). Activation of HIF1α Rescues the Hypoxic Response and Reverses Metabolic Dysfunction in the Diabetic Heart. *Diabetes*.

Dalkara, T. (2019). Pericytes: A Novel Target to Improve Success of Recanalization Therapies. *Stroke* 50(10) 2985-2991.

Dalkara, T., L. Alarcon-Martinez and M. Yemisci (2019). Pericytes in Ischemic Stroke. *Adv Exp Med Biol* 1147 189-213.

Daniel, J. M., et al. (2017). Systemic application of sirolimus prevents neointima formation not via a direct anti-proliferative effect but via its anti-inflammatory properties. *Int J Cardiol* 238 79-91.

Daniele, S. G., et al. (2021). Brain vulnerability and viability after ischaemia. *Nat Rev Neurosci* 22(9) 553-572.

de Cabo, R., et al. (2014). The search for antiaging interventions: from elixirs to fasting regimens. *Cell* 157(7) 1515-1526.

de Cabo, R. and M. P. Mattson (2019). Effects of Intermittent Fasting on Health, Aging, and Disease. *N Engl J Med* 381(26) 2541-2551.

de Carvalho, T. S., et al. (2021). Hypocaloric Diet Initiated Post-Ischemia Provides Long-Term Neuroprotection and Promotes Peri-Infarct Brain Remodeling by Regulating Metabolic and Survival-Promoting Proteins. *Mol Neurobiol* 58(4) 1491-1503.

Dekter, H. E., et al. (2010). A spectrophotometric assay for routine measurement of mammalian target of rapamycin activity in cell lysates. *Anal Biochem* 403(1-2) 79-87.

del Zoppo, G. J. (2010). The neurovascular unit in the setting of stroke. *J Intern Med* 267(2) 156-171.

del Zoppo, G. J. and J. M. Hallenbeck (2000). Advances in the vascular pathophysiology of ischemic stroke. *Thromb Res* 98(3) 73-81.

Delgoffe, G. M. and J. D. Powell (2009). mTOR: taking cues from the immune microenvironment. *Immunology* 127(4) 459-465.

Denic, A., et al. (2011). MRI in rodent models of brain disorders. *Neurotherapeutics* 8(1) 3-18.

Dijkhuizen, R. M. and K. Nicolay (2003). Magnetic resonance imaging in experimental models of brain disorders. *J Cereb Blood Flow Metab* 23(12) 1383-1402.

Dirnagl, U., C. Iadecola and M. A. Moskowitz (1999). Pathobiology of ischaemic stroke: an integrated view. *Trends Neurosci* 22(9) 391-397.

Diwakar, L., et al. (2021). Endothelin-1 mediated vasoconstriction leads to memory impairment and synaptic dysfunction. *Sci Rep* 11(1) 4868.

Dohgu, S., et al. (2005). Brain pericytes contribute to the induction and up-regulation of blood-brain barrier functions through transforming growth factor-beta production. *Brain Res* 1038(2) 208-215.

Dostovic, Z., et al. (2016). Brain Edema After Ischaemic Stroke. *Med Arch* 70(5) 339-341.

Duong, T. Q. and M. Fisher (2004). Applications of diffusion/perfusion magnetic resonance imaging in experimental and clinical aspects of stroke. *Curr Atheroscler Rep* 6(4) 267-273.

Duregon, E., et al. (2021). Intermittent fasting: from calories to time restriction. *Geroscience* 43(3) 1083-1092.

Durukan, A. and T. Tatlisumak (2007). Acute ischemic stroke: overview of major experimental rodent models, pathophysiology, and therapy of focal cerebral ischemia. *Pharmacol Biochem Behav* 87(1) 179-197.

Dutta, S., et al. (2015). The mechanistic target of rapamycin (mTOR) pathway and S6 Kinase mediate diazoxide preconditioning in primary rat cortical neurons. *J Neurochem* 134(5) 845-856.

Dyer, D. P. (2020). Understanding the mechanisms that facilitate specificity, not redundancy, of chemokine-mediated leukocyte recruitment. *Immunology* 160(4) 336-344.

EA, H., et al. (2018). Biphasic Blood-Brain Barrier Openings after Stroke. Neurol Disord Stroke Int.

Emberson, J., et al. (2014). Effect of treatment delay, age, and stroke severity on the effects of intravenous thrombolysis with alteplase for acute ischaemic stroke: a meta-analysis of individual patient data from randomised trials. *Lancet* 384(9958) 1929-1935.

Emerich, D. F., R. L. Dean, 3rd and R. T. Bartus (2002). The role of leukocytes following cerebral ischemia: pathogenic variable or bystander reaction to emerging infarct? *Exp Neurol* 173(1) 168-181.

Engelhardt, S., et al. (2014). Hypoxia selectively disrupts brain microvascular endothelial tight junction complexes through a hypoxia-inducible factor-1 (HIF-1) dependent mechanism. *J Cell Physiol* 229(8) 1096-1105.

Evans, M. R. B., et al. (2017). Revolution in acute ischaemic stroke care: a practical guide to mechanical thrombectomy. *Pract Neurol* 17(4) 252-265.

Faes, S., et al. (2017). Evolving Significance and Future Relevance of Anti-Angiogenic Activity of mTOR Inhibitors in Cancer Therapy. *Cancers (Basel)* 9(11).

Fang, M., et al. (2019). Effect of Inflammation on the Process of Stroke Rehabilitation and Poststroke Depression. *Front Psychiatry* 10 184.

Farkas, E. and P. G. Luiten (2001). Cerebral microvascular pathology in aging and Alzheimer's disease. *Prog Neurobiol* 64(6) 575-611.

Fields, W. S. (1989). A History of Stroke: Its Recognition and Treatment. Oxford University Press Inc, USA.

Fletcher, L., et al. (2013). Rapamycin treatment improves neuron viability in an in vitro model of stroke. *PLoS One* 8(7) e68281.

Fok, W. C., et al. (2014). Combined treatment of rapamycin and dietary restriction has a larger effect on the transcriptome and metabolome of liver. *Aging Cell* 13(2) 311-319.

Fok, W. C., et al. (2014). Short-term rapamycin treatment in mice has few effects on the transcriptome of white adipose tissue compared to dietary restriction. *Mech Ageing Dev* 140 23-29.

Fontana, L., L. Partridge and V. D. Longo (2010). Extending healthy life span--from yeast to humans. *Science* 328(5976) 321-326.

Fransen, P. S., et al. (2014). MR CLEAN, a multicenter randomized clinical trial of endovascular treatment for acute ischemic stroke in the Netherlands: study protocol for a randomized controlled trial. *Trials* 15 343.

Frijns, C. J. and L. J. Kappelle (2002). Inflammatory cell adhesion molecules in ischemic cerebrovascular disease. *Stroke* 33(8) 2115-2122.

Gabandé-Rodríguez, E., M. M. Gómez de Las Heras and M. Mittelbrunn (2019). Control of Inflammation by Calorie Restriction Mimetics: On the Crossroad of Autophagy and Mitochondria. *Cells* 9(1).

Gao, J., et al. (2020). Hepatic stellate cell autophagy inhibits extracellular vesicle release to attenuate liver fibrosis. *J Hepatol* 73(5) 1144-1154.

Garcia, J. H., et al. (1995). Neurological deficit and extent of neuronal necrosis attributable to middle cerebral artery occlusion in rats. Statistical validation. *Stroke* 26(4) 627-634; discussion 635.

Gautam, J. and Y. Yao (2018). Roles of Pericytes in Stroke Pathogenesis. *Cell Transplant* 27(12) 1798-1808.

Geevarghese, A. and I. M. Herman (2014). Pericyte-endothelial crosstalk: implications and opportunities for advanced cellular therapies. *Transl Res* 163(4) 296-306.

Geiseler, S. J. and C. Morland (2018). The Janus Face of VEGF in Stroke. *Int J Mol Sci* 19(5).

Ginsberg, M. D. (2018). The cerebral collateral circulation: Relevance to pathophysiology and treatment of stroke. *Neuropharmacology* 134(Pt B) 280-292.

Gomez-Cambronero, J. (2003). Rapamycin inhibits GM-CSF-induced neutrophil migration. *FEBS Lett* 550(1-3) 94-100.

Goyal, M., et al. (2016). Endovascular thrombectomy after large-vessel ischaemic stroke: a meta-analysis of individual patient data from five randomised trials. *Lancet* 387(10029) 1723-1731.

Greene, A. E., et al. (2001). Caloric restriction inhibits seizure susceptibility in epileptic EL mice by reducing blood glucose. *Epilepsia* 42(11) 1371-1378.

Grunewald, Z. I., et al. (2019). Chronic Elevation of Endothelin-1 Alone May Not Be Sufficient to Impair Endothelium-Dependent Relaxation. *Hypertension* 74(6) 1409-1419.

Guo, W., et al. (2014). Rapamycin alleviates brain edema after focal cerebral ischemia reperfusion in rats. *Immunopharmacol Immunotoxicol* 36(3) 211-223.

Guo, Z., et al. (2014). A combination of four active compounds alleviates cerebral ischemia-reperfusion injury in correlation with inhibition of autophagy and modulation of AMPK/mTOR and JNK pathways. *J Neurosci Res* 92(10) 1295-1306.

Hacke, W., et al. (2008). Thrombolysis with alteplase 3 to 4.5 hours after acute ischemic stroke. *N Engl J Med* 359(13) 1317-1329.

Hacke, W., et al. (1998). Randomised double-blind placebo-controlled trial of thrombolytic therapy with intravenous alteplase in acute ischaemic stroke (ECASS II). Second European-Australasian Acute Stroke Study Investigators. *Lancet* 352(9136) 1245-1251.

Hadley, G., et al. (2019). Rapamycin in ischemic stroke: Old drug, new tricks? *J Cereb Blood Flow Metab* 39(1) 20-35.

Hakimelahi, R., et al. (2012). Rapid identification of a major diffusion/perfusion mismatch in distal internal carotid artery or middle cerebral artery ischemic stroke. *BMC Neurol* 12 132.

Haley, M. J. and C. B. Lawrence (2017). The blood-brain barrier after stroke: Structural studies and the role of transcytotic vesicles. *J Cereb Blood Flow Metab* 37(2) 456-470.

Hall, C. N., et al. (2014). Capillary pericytes regulate cerebral blood flow in health and disease. *Nature* 508(7494) 55-60.

Halterman, M. W. and H. J. Federoff (1999). HIF-1alpha and p53 promote hypoxia-induced delayed neuronal death in models of CNS ischemia. *Exp Neurol* 159(1) 65-72.

Hancock, A. A., et al. (2004). Antiobesity effects of A-331440, a novel non-imidazole histamine H-3 receptor antagonist. *European Journal of Pharmacology* 487(1-3) 183-197.

Hansen, M., et al. (2007). Lifespan extension by conditions that inhibit translation in Caenorhabditis elegans. *Aging Cell* 6(1) 95-110.

Headland, M. L., P. M. Clifton and J. B. Keogh (2018). Effect of Intermittent Energy Restriction on Flow Mediated Dilatation, a Measure of Endothelial Function: A Short Report. *Int J Environ Res Public Health* 15(6).

Hill, M. D., et al. (2020). Efficacy and safety of nerinetide for the treatment of acute ischaemic stroke (ESCAPE-NA1): a multicentre, double-blind, randomised controlled trial. *Lancet* 395(10227) 878-887.

Hollman, A. (1995). The paintings of pathological anatomy by
Sir Robert Carswell (1793-1 857). Heart. 566-570.

Holloway, P. M. and F. N. Gavins (2016). Modeling Ischemic Stroke In Vitro: Status Quo and Future Perspectives. *Stroke* 47(2) 561-569.

Hooper, R. (1828). *The morbid anatomy of the human brain*: London: Longman, Rees, Orme, Brown, and Green.

Hori, S., et al. (2004). A pericyte-derived angiopoietin-1 multimeric complex induces occludin gene expression in brain capillary endothelial cells through Tie-2 activation in vitro. *J Neurochem* 89(2) 503-513.

Huang, J. and B. D. Manning (2008). The TSC1-TSC2 complex: a molecular switchboard controlling cell growth. *Biochem J* 412(2) 179-190.

Huang, W. Y., et al. (2019). Multi-parameters of Magnetic Resonance Imaging to Estimate Ischemia-Reperfusion Injury after Stroke in Hyperglycemic Rats. *Sci Rep* 9(1) 2852.

Huang, Z. G., et al. (1999). Biphasic opening of the blood-brain barrier following transient focal ischemia: effects of hypothermia. *Can J Neurol Sci* 26(4) 298-304.

Hucklesby, J. J. W., et al. (2021). Comparison of Leading Biosensor Technologies to Detect Changes in Human Endothelial Barrier Properties in Response to Pro-Inflammatory TNFα and IL1β in Real-Time. *Biosensors (Basel)* 11(5).

Hurford, R., et al. (2020). Diagnosis and management of acute ischaemic stroke. *Pract Neurol* 20(4) 304-316.

Iadecola, C. (2017). The Neurovascular Unit Coming of Age: A Journey through Neurovascular Coupling in Health and Disease. *Neuron* 96(1) 17-42.

Iadecola, C., M. S. Buckwalter and J. Anrather (2020). Immune responses to stroke: mechanisms, modulation, and therapeutic potential. *J Clin Invest* 130(6) 2777-2788.

Jacewicz, M., J. Tanabe and W. A. Pulsinelli (1992). The CBF threshold and dynamics for focal cerebral infarction in spontaneously hypertensive rats. *J Cereb Blood Flow Metab* 12(3) 359-370.

Jamrozik, K., et al. (1994). The role of lifestyle factors in the etiology of stroke. A population-based case-control study in Perth, Western Australia. *Stroke* 25(1) 51-59.

Jaworski, J. and M. Sheng (2006). The growing role of mTOR in neuronal development and plasticity. *Mol Neurobiol* 34(3) 205-219.

Jeong, J. H., et al. (2016). Intermittent fasting is neuroprotective in focal cerebral ischemia by minimizing autophagic flux disturbance and inhibiting apoptosis. *Exp Ther Med* 12(5) 3021-3028.

Jin, R., G. Yang and G. Li (2010). Inflammatory mechanisms in ischemic stroke: role of inflammatory cells. *J Leukoc Biol* 87(5) 779-789.

Johnson, J. B., et al. (2007). Alternate day calorie restriction improves clinical findings and reduces markers of oxidative stress and inflammation in overweight adults with moderate asthma. *Free Radic Biol Med* 42(5) 665-674.

Johnson, R. H., et al. (2018). The functional and inflammatory response of brain endothelial cells to Toll-Like Receptor agonists. *Sci Rep* 8(1) 10102.

Jordan, S., et al. (2019). Dietary Intake Regulates the Circulating Inflammatory Monocyte Pool. *Cell* 178(5) 1102-1114.e1117.

Juergenson, I., S. Mazzucco and M. Tinazzi (2011). A typical example of cerebral watershed infarct. *Clin Pract*. e114.

Kaeberlein, M., et al. (2005). Regulation of yeast replicative life span by TOR and Sch9 in response to nutrients. *Science* 310(5751) 1193-1196.

Kang, L., et al. (2020). Neutrophil extracellular traps released by neutrophils impair revascularization and vascular remodeling after stroke. *Nat Commun* 11(1) 2488.

Kaplan, B., et al. (1991). Temporal thresholds for neocortical infarction in rats subjected to reversible focal cerebral ischemia. *Stroke* 22(8) 1032-1039.

Karunadharma, P. P., et al. (2015). Subacute calorie restriction and rapamycin discordantly alter mouse liver proteome homeostasis and reverse aging effects. *Aging Cell* 14(4) 547-557.

Kaur, J., et al. (2004). The neurotoxicity of tissue plasminogen activator? *J Cereb Blood Flow Metab* 24(9) 945-963.

Kawai, N., R. F. Keep and A. L. Betz (1997). Hyperglycemia and the vascular effects of cerebral ischemia. *Stroke* 28(1) 149-154.

Khalil, R. A. (2010). Integrated Systems Physiology: From Molecule to Function. *Regulation of Vascular Smooth Muscle Function*. San Rafael (CA), Morgan & Claypool Life Sciences
Copyright © 2010 by Morgan & Claypool Life Sciences.

Kilkenny, C., et al. (2010). Animal research: reporting in vivo experiments: the ARRIVE guidelines. *Br J Pharmacol* 160(7) 1577-1579.

Kim, K. A., et al. (2020). Autophagy-mediated occludin degradation contributes to blood-brain barrier disruption during ischemia in bEnd.3 brain endothelial cells and rat ischemic stroke models. *Fluids Barriers CNS* 17(1) 21.

Kim, K. H., et al. (2017). Intermittent fasting promotes adipose thermogenesis and metabolic homeostasis via VEGF-mediated alternative activation of macrophage. *Cell Res* 27(11) 1309-1326.

Kloner, R. A., K. S. King and M. G. Harrington (2018). No-reflow phenomenon in the heart and brain. *Am J Physiol Heart Circ Physiol* 315(3) H550-h562.

Knowland, D., et al. (2014). Stepwise recruitment of transcellular and paracellular pathways underlies blood-brain barrier breakdown in stroke. *Neuron* 82(3) 603-617.

Koziel, A., et al. (2012). The influence of high glucose on the aerobic metabolism of endothelial EA.hy926 cells. *Pflugers Arch* 464(6) 657-669.

Kume, S., et al. (2010). Calorie restriction enhances cell adaptation to hypoxia through Sirt1-dependent mitochondrial autophagy in mouse aged kidney. *J Clin Invest* 120(4) 1043-1055.

Kuriakose, D. and Z. Xiao (2020). Pathophysiology and Treatment of Stroke: Present Status and Future Perspectives. *Int J Mol Sci* 21(20).

Lakhan, S. E., A. Kirchgessner and M. Hofer (2009). Inflammatory mechanisms in ischemic stroke: therapeutic approaches. *J Transl Med* 7 97.

Lakhan, S. E., et al. (2013). Matrix metalloproteinases and blood-brain barrier disruption in acute ischemic stroke. *Front Neurol* 4 32.

Lambertsen, K. L., B. Finsen and B. H. Clausen (2019). Post-stroke inflammation-target or tool for therapy? *Acta Neuropathol* 137(5) 693-714.

Laplante, M. and D. M. Sabatini (2009). mTOR signaling at a glance. *J Cell Sci* 122(Pt 20) 3589-3594.

Larkin, J. R., et al. (2019). Quantitative blood flow measurement in rat brain with multiphase arterial spin labelling magnetic resonance imaging. *J Cereb Blood Flow Metab* 39(8) 1557-1569.

Lees, K. R., et al. (2016). Effects of Alteplase for Acute Stroke on the Distribution of Functional Outcomes: A Pooled Analysis of 9 Trials. *Stroke* 47(9) 2373-2379.

Lees, K. R., et al. (2006). NXY-059 for acute ischemic stroke. *N Engl J Med* 354(6) 588-600.

Leontieva, O. V., G. M. Paszkiewicz and M. V. Blagosklonny (2014). Weekly administration of rapamycin improves survival and biomarkers in obese male mice on high-fat diet. *Aging Cell* 13(4) 616-622.

Lescano de Souza, A., et al. (2015). Effect of fasting and refeeding on the consequences of myocardial infarction in rats.

Li, C. Y., et al. (2015). Inhibition of mTOR pathway restrains astrocyte proliferation, migration and production of inflammatory mediators after oxygen-glucose deprivation and reoxygenation. *Neurochem Int* 83-84 9-18.

Li, D., et al. (2016). mTORC1 pathway disruption ameliorates brain inflammation following stroke via a shift in microglia phenotype from M1 type to M2 type. *Faseb j* 30(10) 3388-3399.

Li, H., et al. (2014). Evaluation of the protective potential of brain microvascular endothelial cell autophagy on blood-brain barrier integrity during experimental cerebral ischemia-reperfusion injury. *Transl Stroke Res* 5(5) 618-626.

Li, Z., et al. (2017). mTOR activation protects liver from ischemia/reperfusion-induced injury through NF-κB pathway. *Faseb j* 31(7) 3018-3026.

Liebeskind, D. S., et al. (2019). Cerebral Edema Associated With Large Hemispheric Infarction. *Stroke* 50(9) 2619-2625.

Lin, A. L., et al. (2013). Chronic rapamycin restores brain vascular integrity and function through NO synthase activation and improves memory in symptomatic mice modeling Alzheimer's disease. *J Cereb Blood Flow Metab* 33(9) 1412-1421.

Lin, L., et al. (2018). bFGF Protects Against Oxygen Glucose Deprivation/Reoxygenation-Induced Endothelial Monolayer Permeability via S1PR1-Dependent Mechanisms. *Mol Neurobiol* 55(4) 3131-3142.

Lindsberg, P. J. and R. O. Roine (2004). Hyperglycemia in acute stroke. *Stroke*. United States. 363-364.

Lindvall, O., et al. (1992). Differential regulation of mRNAs for nerve growth factor, brain-derived neurotrophic factor, and neurotrophin 3 in the adult rat brain following cerebral ischemia and hypoglycemic coma. *Proc Natl Acad Sci U S A* 89(2) 648-652.

Liu, G. Y. and D. M. Sabatini (2020). mTOR at the nexus of nutrition, growth, ageing and disease. *Nat Rev Mol Cell Biol* 21(4) 183-203.

Liu, H., et al. (2010). Notch3 is critical for proper angiogenesis and mural cell investment. *Circ Res* 107(7) 860-870.

Liu, J., et al. (2012). Matrix metalloproteinase-2-mediated occludin degradation and caveolin-1-mediated claudin-5 redistribution contribute to blood-brain barrier damage in early ischemic stroke stage. *J Neurosci* 32(9) 3044-3057.

Liu, Z. and M. Chopp (2016). Astrocytes, therapeutic targets for neuroprotection and neurorestoration in ischemic stroke. *Prog Neurobiol* 144 103-120.

Lo, E. H. (2008). A new penumbra: transitioning from injury into repair after stroke. *Nat Med* 14(5) 497-500.

Lo, E. H., T. Dalkara and M. A. Moskowitz (2003). Mechanisms, challenges and opportunities in stroke. *Nat Rev Neurosci* 4(5) 399-415.

Loncarevic-Vasiljkovic, N., et al. (2012). Caloric restriction suppresses microglial activation and prevents neuroapoptosis following cortical injury in rats. *PLoS One* 7(5) e37215.

Longo, V. D. and M. P. Mattson (2014). Fasting: molecular mechanisms and clinical applications. *Cell Metab* 19(2) 181-192.

Lyden, P. D. (2021). Cerebroprotection for Acute Ischemic Stroke: Looking Ahead. *Stroke* 52(9) 3033-3044.

Lyden, P. D., et al. (2007). Safety and tolerability of NXY-059 for acute intracerebral hemorrhage: the CHANT Trial. *Stroke* 38(8) 2262-2269.

Ma, H., et al. (2019). Thrombolysis Guided by Perfusion Imaging up to 9 Hours after Onset of Stroke. *N Engl J Med* 380(19) 1795-1803.

Macrae, I. M. (2011). Preclinical stroke research--advantages and disadvantages of the most common rodent models of focal ischaemia. *Br J Pharmacol* 164(4) 1062-1078.

Manzanero, S., et al. (2011). Calorie restriction and stroke. *Exp Transl Stroke Med* 3 8.

Martin-Perez, M., et al. (2020). PKC downregulation upon rapamycin treatment attenuates mitochondrial disease. *Nat Metab* 2(12) 1472-1481.

Martino, R., et al. (2005). Dysphagia after stroke: incidence, diagnosis, and pulmonary complications. *Stroke* 36(12) 2756-2763.

Maswood, N., et al. (2004). Caloric restriction increases neurotrophic factor levels and attenuates neurochemical and behavioral deficits in a primate model of Parkinson's disease. *Proc Natl Acad Sci U S A* 101(52) 18171-18176.

Mateos, L., M. J. Perez-Alvarez and F. Wandosell (2016). Angiotensin II type-2 receptor stimulation induces neuronal VEGF synthesis after cerebral ischemia. *Biochim Biophys Acta* 1862(7) 1297-1308.

Mattison, J. A., et al. (2017). Caloric restriction improves health and survival of rhesus monkeys. *Nat Commun* 8 14063.

Mattson, M. P., V. D. Longo and M. Harvie (2017). Impact of intermittent fasting on health and disease processes. *Ageing Res Rev* 39 46-58.

McCay, C. M., et al. (1975). The Journal of Nutrition. Volume 18 July--December, 1939. Pages 1--13. Retarded growth, life span, ultimate body size and age changes in the albino rat after feeding diets restricted in calories. *Nutr Rev* 33(8) 241-243.

McDonald, R. B. and J. J. Ramsey (2010). Honoring Clive McCay and 75 years of calorie restriction research. *J Nutr* 140(7) 1205-1210.

McInturff, A. M., et al. (2012). Mammalian target of rapamycin regulates neutrophil extracellular trap formation via induction of hypoxia-inducible factor 1 α. *Blood* 120(15) 3118-3125.

McLeod, D. D., et al. (2013). Inadvertent occlusion of the anterior choroidal artery explains infarct variability in the middle cerebral artery thread occlusion stroke model. *PLoS One* 8(9) e75779.

Mejia, P., et al. (2017). A single rapamycin dose protects against late-stage experimental cerebral malaria via modulation of host immunity, endothelial activation and parasite sequestration. *Malar J* 16(1) 455.

Meng, X., et al. (2004). Characterizing the diffusion/perfusion mismatch in experimental focal cerebral ischemia. *Ann Neurol* 55(2) 207-212.

Merino, J. G. and S. Warach (2010). Imaging of acute stroke. *Nat Rev Neurol* 6(10) 560-571.

Michinaga, S. and Y. Koyama (2015). Pathogenesis of brain edema and investigation into anti-edema drugs. *Int J Mol Sci* 16(5) 9949-9975.

Milidonis, X., et al. (2015). Magnetic resonance imaging in experimental stroke and comparison with histology: systematic review and meta-analysis. *Stroke* 46(3) 843-851.

Momjian-Mayor, I. and J. C. Baron (2005). The pathophysiology of watershed infarction in internal carotid artery disease: review of cerebral perfusion studies. *Stroke* 36(3) 567-577.

Moro, T., et al. (2016). Effects of eight weeks of time-restricted feeding (16/8) on basal metabolism, maximal strength, body composition, inflammation, and cardiovascular risk factors in resistance-trained males. *J Transl Med* 14(1) 290.

Munafò, M., B. Nosek and D. Bishop (2017). A manifesto for reproducible science. *Nat Hum Behav* 1 0021.

Nagaraja, N., et al. (2020). Reversible diffusion-weighted imaging lesions in acute ischemic stroke: A systematic review. *Neurology* 94(13) 571-587.

Nalbandian, A., et al. (2015). Rapamycin and chloroquine: the in vitro and in vivo effects of autophagy-modifying drugs show promising results in valosin containing protein multisystem proteinopathy. *PLoS One* 10(4) e0122888.

Navaratna, D., et al. (2013). Cerebrovascular degradation of TRKB by MMP9 in the diabetic brain. *J Clin Invest* 123(8) 3373-3377.

Nemes, K., et al. (2013). Mammalian target of rapamycin (mTOR) activity dependent phospho-protein expression in childhood acute lymphoblastic leukemia (ALL). *PLoS One* 8(4) e59335.

Neuhaus, A. A., et al. (2017). Neuroprotection in stroke: the importance of collaboration and reproducibility. *Brain* 140(8) 2079-2092.

Neuhaus, A. A., et al. (2014). Importance of preclinical research in the development of neuroprotective strategies for ischemic stroke. *JAMA Neurol* 71(5) 634-639.

Nian, K., et al. (2020). Blood-Brain Barrier Damage in Ischemic Stroke and Its Regulation by Endothelial Mechanotransduction. *Front Physiol* 11 605398.

Nogueira, R. G., et al. (2018). Thrombectomy 6 to 24 Hours after Stroke with a Mismatch between Deficit and Infarct. *N Engl J Med* 378(1) 11-21.

Nuland, S. B. (1995). Doctors: The Bibliography of Medicine. Vintage Books.

Owens Johnson, C., M. Nguyen and G. A. Roth (2019). Global, regional, and national burden of stroke, 1990-2016: a systematic analysis for the Global Burden of Disease Study 2016. *Lancet Neurol* 18(5) 439-458.

Ozerdem, U. and W. B. Stallcup (2003). Early contribution of pericytes to angiogenic sprouting and tube formation. *Angiogenesis* 6(3) 241-249.

Pak, H. H., et al. (2021). Fasting drives the metabolic, molecular and geroprotective effects of a calorie-restricted diet in mice. *Nat Metab* 3(10) 1327-1341.

Paljärvi, L., et al. (1983). Brain lactic acidosis and ischemic cell damage: quantitative ultrastructural changes in capillaries of rat cerebral cortex. *Acta Neuropathol* 60(3-4) 232-240.

Palomares, S. M. and M. J. Cipolla (2011). Vascular Protection Following Cerebral Ischemia and Reperfusion. *J Neurol Neurophysiol* 2011.

Panahian, N., M. Yoshiura and M. D. Maines (1999). Overexpression of heme oxygenase-1 is neuroprotective in a model of permanent middle cerebral artery occlusion in transgenic mice. *J Neurochem* 72(3) 1187-1203.

Papadakis, M., et al. (2013). Tsc1 (hamartin) confers neuroprotection against ischemia by inducing autophagy. *Nat Med* 19(3) 351-357.

Percie du Sert, N., et al. (2017). The IMPROVE Guidelines (Ischaemia Models: Procedural Refinements Of in Vivo Experiments). *J Cereb Blood Flow Metab* 37(11) 3488-3517.

Perez-Alvarez, M. J., et al. (2018). Role of mTORC1 Controlling Proteostasis after Brain Ischemia. *Front Neurosci* 12 60.

Petővári, G., et al. (2018). Targeting cellular metabolism using rapamycin and/or doxycycline enhances anti-tumour effects in human glioma cells. *Cancer Cell Int* 18 211.

Qi, H., et al. (2014). The antiaging activity and cerebral protection of rapamycin at micro-doses. *CNS Neurosci Ther* 20(11) 991-998.

Qiu, Y. M., et al. (2021). Immune Cells in the BBB Disruption After Acute Ischemic Stroke: Targets for Immune Therapy? *Front Immunol* 12 678744.

Radler, M. E., M. W. Hale and S. Kent (2014). Calorie restriction attenuates lipopolysaccharide (LPS)-induced microglial activation in discrete regions of the hypothalamus and the subfornical organ. *Brain Behav Immun* 38 13-24.

Ran, M., et al. (2015). Calorie restriction attenuates cerebral ischemic injury via increasing SIRT1 synthesis in the rat. *Brain Res* 1610 61-68.

Reid, E., et al. (2012). Penumbra detection using PWI/DWI mismatch MRI in a rat stroke model with and without comorbidity: comparison of methods. *J Cereb Blood Flow Metab* 32(9) 1765-1777.

Ribeiro, L. C., et al. (2009). Caloric restriction increases hippocampal glutamate uptake and glutamine synthetase activity in Wistar rats. *Neurosci Res* 64(3) 330-334.

Rodriguez, K. A., et al. (2014). Divergent tissue and sex effects of rapamycin on the proteasome-chaperone network of old mice. *Front Mol Neurosci* 7 83.

Roh, J. S. and D. H. Sohn (2018). Damage-Associated Molecular Patterns in Inflammatory Diseases. *Immune Netw* 18(4) e27.

Rosenberg, G. A. (2012). Neurological diseases in relation to the blood-brain barrier. *J Cereb Blood Flow Metab* 32(7) 1139-1151.

Rosenberg, G. A., E. Y. Estrada and J. E. Dencoff (1998). Matrix metalloproteinases and TIMPs are associated with blood-brain barrier opening after reperfusion in rat brain. *Stroke* 29(10) 2189-2195.

Sabatini, D. M. (2017). Twenty-five years of mTOR: Uncovering the link from nutrients to growth. *Proc Natl Acad Sci U S A* 114(45) 11818-11825.

Sacco, R. L., et al. (2013). An updated definition of stroke for the 21st century: a statement for healthcare professionals from the American Heart Association/American Stroke Association. *Stroke* 44(7) 2064-2089.

Salmon, A. B. (2015). About-face on the metabolic side effects of rapamycin. *Oncotarget*. 2585-2586.

Sandoval, K. E. and K. A. Witt (2008). Blood-brain barrier tight junction permeability and ischemic stroke. *Neurobiol Dis* 32(2) 200-219.

Savitz, S. I., et al. (2017). Reconsidering Neuroprotection in the Reperfusion Era. *Stroke* 48(12) 3413-3419.

Schaar, K. L., M. M. Brenneman and S. I. Savitz (2010). Functional assessments in the rodent stroke model. *Exp Transl Stroke Med* 2(1) 13.

Schreuder, F. and M. Cliteur (2021). Anakinra in Cerebral Haemorrhage to Target Secondary Injury Resulting From Neuroinflammation - a Phase II Clinical Trial.

Shang, E., et al. (2006). Retraction: The Influence of Early Supplementation of Parenteral Nutrition on Quality of Life and Body Composition in Patients With Advanced Cancer. *JPEN J Parenter Enteral Nutr* 30(3) 222-230.

Sharif, Y., et al. (2018). Blood brain barrier: A review of its anatomy and physiology in health and disease. *Clin Anat* 31(6) 812-823.

Sharkey, J. and S. P. Butcher (1994). Immunophilins mediate the neuroprotective effects of FK506 in focal cerebral ischaemia. *Nature* 371(6495) 336-339.

Sheng, R., et al. (2010). Autophagy activation is associated with neuroprotection in a rat model of focal cerebral ischemic preconditioning. *Autophagy* 6(4) 482-494.

Shi, Y., et al. (2016). Rapid endothelial cytoskeletal reorganization enables early blood-brain barrier disruption and long-term ischaemic reperfusion brain injury. *Nat Commun* 7 10523.

Shuaib, A., et al. (2007). NXY-059 for the treatment of acute ischemic stroke. *N Engl J Med* 357(6) 562-571.

Sims, N. R. and H. Muyderman (2010). Mitochondria, oxidative metabolism and cell death in stroke. *Biochim Biophys Acta* 1802(1) 80-91.

Sohal, R. S. and R. Weindruch (1996). Oxidative stress, caloric restriction, and aging. *Science* 273(5271) 59-63.

Sommer, C., et al. (2003). Exogenous brain-derived neurotrophic factor prevents postischemic downregulation of [3H]muscimol binding to GABA(A) receptors in the cortical penumbra. *Brain Res Mol Brain Res* 111(1-2) 24-30.

Song, E. C., et al. (2003). Hyperglycemia exacerbates brain edema and perihematomal cell death after intracerebral hemorrhage. *Stroke* 34(9) 2215-2220.

Spratt, N. J., et al. (2006). Modification of the method of thread manufacture improves stroke induction rate and reduces mortality after thread-occlusion of the middle cerebral artery in young or aged rats. *J Neurosci Methods* 155(2) 285-290.

Stahl, A., et al. (2008). Rapamycin reduces VEGF expression in retinal pigment epithelium (RPE) and inhibits RPE-induced sprouting angiogenesis in vitro. *FEBS Lett* 582(20) 3097-3102.

Stamatovic, S. M., et al. (2016). Junctional proteins of the blood-brain barrier: New insights into function and dysfunction. *Tissue Barriers* 4(1) e1154641.

Steinhagen, V., et al. (2009). Swallowing disturbance pattern relates to brain lesion location in acute stroke patients. *Stroke* 40(5) 1903-1906.

Su, J., et al. (2014). Autophagy activation contributes to the neuroprotection of remote ischemic perconditioning against focal cerebral ischemia in rats. *Neurochem Res* 39(11) 2068-2077.

Sukriti, S., et al. (2014). Mechanisms regulating endothelial permeability. *Pulm Circ* 4(4) 535-551.

Sun, J. J., et al. (2018). Rapamycin inhibits ox-LDL-induced inflammation in human endothelial cells in vitro by inhibiting the mTORC2/PKC/c-Fos pathway. *Acta Pharmacol Sin* 39(3) 336-344.

Sutherland, B. A., et al. (2016). The transient intraluminal filament middle cerebral artery occlusion model as a model of endovascular thrombectomy in stroke. *J Cereb Blood Flow Metab* 36(2) 363-369.

Sweeney, M. and G. Foldes (2018). It Takes Two: Endothelial-Perivascular Cell Cross-Talk in Vascular Development and Disease. *Front Cardiovasc Med* 5 154.

Szalay, G., et al. (2016). Microglia protect against brain injury and their selective elimination dysregulates neuronal network activity after stroke. *Nat Commun* 7 11499.

Tan, P. L., et al. (2006). Diffusion weighted magnetic resonance imaging for acute stroke: practical and popular. *Postgrad Med J* 82(966) 289-292.

Teunissen-Beekman, K. F., et al. (2015). Dietary proteins improve endothelial function under fasting conditions but not in the postprandial state, with no effects on markers of low-grade inflammation. *Br J Nutr* 114(11) 1819-1828.

Thrippleton, M. J., et al. (2019). Quantifying blood-brain barrier leakage in small vessel disease: Review and consensus recommendations. *Alzheimers Dement* 15(6) 840-858.

Tsao, C. C., et al. (2021). Pericyte hypoxia-inducible factor-1 (HIF-1) drives blood-brain barrier disruption and impacts acute ischemic stroke outcome. *Angiogenesis* 24(4) 823-842.

Tubbs, R. S., et al. (2011). The bishop and anatomist Niels Stensen (1638-1686) and his contributions to our early understanding of the brain. *Childs Nerv Syst* 27(1) 1-6.

Tymianski, M. (2017). Combining Neuroprotection With Endovascular Treatment of Acute Stroke: Is There Hope? *Stroke* 48(6) 1700-1705.

Unnikrishnan, A., et al. (2020). Is Rapamycin a Dietary Restriction Mimetic? *J Gerontol A Biol Sci Med Sci* 75(1) 4-13.

van Kranendonk, K. R., et al. (2019). Hemorrhagic transformation is associated with poor functional outcome in patients with acute ischemic stroke due to a large vessel occlusion. *J Neurointerv Surg* 11(5) 464-468.

Van Skike, C. E., et al. (2018). Inhibition of mTOR protects the blood-brain barrier in models of Alzheimer's disease and vascular cognitive impairment. *Am J Physiol Heart Circ Physiol* 314(4) H693-h703.

Varendi, K., et al. (2014). Short-term preoperative dietary restriction is neuroprotective in a rat focal stroke model. *PLoS One* 9(4) e93911.

Vasconcelos, A. R., et al. (2014). Intermittent fasting attenuates lipopolysaccharide-induced neuroinflammation and memory impairment. *J Neuroinflammation* 11 85.

Vesalius, A. (1543). *De humani corporis fabrica libri septem* School of Medicine, Padua.

Virani, S. S., et al. (2021). Heart Disease and Stroke Statistics-2021 Update: A Report From the American Heart Association. *Circulation* 143(8) e254-e743.

Wang, C., et al. (2014). Rapamycin antagonizes TNF induction of VCAM-1 on endothelial cells by inhibiting mTORC2. *J Exp Med* 211(3) 395-404.

Wang, J., et al. (2016). A Combination of Remote Ischemic Perconditioning and Cerebral Ischemic Postconditioning Inhibits Autophagy to Attenuate Plasma HMGB1 and Induce Neuroprotection Against Stroke in Rat. *J Mol Neurosci* 58(4) 424-431.

Wang, J., et al. (2019). Rapamycin Increases Collateral Circulation in Rodent Brain after Focal Ischemia as detected by Multiple Modality Dynamic Imaging. *Theranostics* 9(17) 4923-4934.

Wang, X., et al. (2004). Mechanisms of hemorrhagic transformation after tissue plasminogen activator reperfusion therapy for ischemic stroke. *Stroke* 35(11 Suppl 1) 2726-2730.

Wang, X., et al. (2020). Effects of intermittent fasting diets on plasma concentrations of inflammatory biomarkers: A systematic review and meta-analysis of randomized controlled trials. *Nutrition* 79-80 110974.

Warner, J. J., et al. (2019). Guidelines for the Early Management of Patients With Acute Ischemic Stroke: 2019 Update to the 2018 Guidelines for the Early Management of Acute Ischemic Stroke. *Stroke* 50(12) 3331-3332.

Webb, R. C. (2003). Smooth muscle contraction and relaxation. *Adv Physiol Educ* 27(1-4) 201-206.

Wei, M., et al. (2017). Fasting-mimicking diet and markers/risk factors for aging, diabetes, cancer, and cardiovascular disease. *Sci Transl Med* 9(377).

Weksler, B., I. A. Romero and P. O. Couraud (2013). The hCMEC/D3 cell line as a model of the human blood brain barrier. *Fluids Barriers CNS* 10(1) 16.

Wepfer, J. J. (1658). *Observationes Anatomicae Ex Cadaveribus Eorum, Quos Sustulit Apoplexia Cum Exercitatione de Eius Loco Affecto*: Schaffhausen: Onophrii A Waldkirch.

Weston, R. M., et al. (2007). Inflammatory cell infiltration after endothelin-1-induced cerebral ischemia: histochemical and myeloperoxidase correlation with temporal changes in brain injury. *J Cereb Blood Flow Metab* 27(1) 100-114.

Wu, M., et al. (2018). Rapamycin prevents cerebral stroke by modulating apoptosis and autophagy in penumbra in rats. *Ann Clin Transl Neurol* 5(2) 138-146.

Xian, Y., et al. (2011). Association between stroke center hospitalization for acute ischemic stroke and mortality. *Jama* 305(4) 373-380.

Xie, L., et al. (2014). mTOR signaling inhibition modulates macrophage/microglia-mediated neuroinflammation and secondary injury via regulatory T cells after focal ischemia. *J Immunol* 192(12) 6009-6019.

Xie, R., et al. (2014). Mammalian target of rapamycin cell signaling pathway contributes to the protective effects of ischemic postconditioning against stroke. *Stroke* 45(9) 2769-2776.

Xin, X., et al. (2013). Hypoxic retinal Muller cells promote vascular permeability by HIF-1-dependent up-regulation of angiopoietin-like 4. *Proc Natl Acad Sci U S A* 110(36) E3425-3434.

Xu, L., A. Nirwane and Y. Yao (2019). Basement membrane and blood-brain barrier. *Stroke Vasc Neurol* 4(2) 78-82.

Xu, W., C. Gao and J. Wu (2021). CD151 Alleviates Early Blood-Brain Barrier Dysfunction After Experimental Focal Brain Ischemia in Rats. *Cell Mol Neurobiol* 41(1) 151-162.

Yaghi, S., et al. (2017). Treatment and Outcome of Hemorrhagic Transformation After Intravenous Alteplase in Acute Ischemic Stroke: A Scientific Statement for Healthcare Professionals From the American Heart Association/American Stroke Association. *Stroke* 48(12) e343-e361.

Yan, J., Z. Zhang and H. Shi (2012). HIF-1 is involved in high glucose-induced paracellular permeability of brain endothelial cells. *Cell Mol Life Sci* 69(1) 115-128.

Yan, J., et al. (2011). Differential effects of HIF-1 inhibition by YC-1 on the overall outcome and blood-brain barrier damage in a rat model of ischemic stroke. *PLoS One* 6(11) e27798.

Yan, W., et al. (2011). Autophagy activation is involved in neuroprotection induced by hyperbaric oxygen preconditioning against focal cerebral ischemia in rats. *Brain Res* 1402 109-121.

Yang, C., et al. (2019). Neuroinflammatory mechanisms of blood-brain barrier damage in ischemic stroke. *Am J Physiol Cell Physiol* 316(2) C135-c153.

Yang, Q., et al. (2019). Potential Neuroprotective Treatment of Stroke: Targeting Excitotoxicity, Oxidative Stress, and Inflammation. *Front Neurosci* 13 1036.

Yang, Z., et al. (2015). Hypoxia induces microglia autophagy and neural inflammation injury in focal cerebral ischemia model. *Exp Mol Pathol* 98(2) 219-224.

Yao, Y., et al. (2020). Potential Therapies for Cerebral Edema After Ischemic Stroke: A Mini Review. *Front Aging Neurosci* 12 618819.

Yemisci, M., et al. (2009). Pericyte contraction induced by oxidative-nitrative stress impairs capillary reflow despite successful opening of an occluded cerebral artery. *Nat Med* 15(9) 1031-1037.

Yilmaz, G. and D. N. Granger (2008). Cell adhesion molecules and ischemic stroke. *Neurol Res* 30(8) 783-793.

Yilmaz, G. and D. N. Granger (2010). Leukocyte recruitment and ischemic brain injury. *Neuromolecular Med* 12(2) 193-204.

Yin, L., et al. (2012). Rapamycin preconditioning attenuates transient focal cerebral ischemia/reperfusion injury in mice. *Int J Neurosci* 122(12) 748-756.

Yu, Z., et al. (2015). Rapamycin and dietary restriction induce metabolically distinctive changes in mouse liver. *J Gerontol A Biol Sci Med Sci* 70(4) 410-420.

Yu, Z. F. and M. P. Mattson (1999). Dietary restriction and 2-deoxyglucose administration reduce focal ischemic brain damage and improve behavioral outcome: evidence for a preconditioning mechanism. *J Neurosci Res* 57(6) 830-839.

Yushkevich, P. A., et al. (2019). User-Guided Segmentation of Multi-modality Medical Imaging Datasets with ITK-SNAP. *Neuroinformatics* 17(1) 83-102.

Zatroch, K. K., et al. (2017). Refinement of intraperitoneal injection of sodium pentobarbital for euthanasia in laboratory rats (Rattus norvegicus). *BMC Vet Res* 13(1) 60.

Zhang, Y., et al. (2014). Rapamycin extends life and health in C57BL/6 mice. *J Gerontol A Biol Sci Med Sci* 69(2) 119-130.

Zheng, Z., J. E. Lee and M. A. Yenari (2003). Stroke: molecular mechanisms and potential targets for treatment. *Curr Mol Med* 3(4) 361-372.

Zhou, B., et al. (2019). Mitochondrial Permeability Uncouples Elevated Autophagy and Lifespan Extension. *Cell* 177(2) 299-314.e216.

Zimmer, C. (2005). *Soul Made Flesh: The Discovery of the Brain-and How it Changed the World*: Free Press.